OPTICAL PROPERTIES OF DENTAL HARD TISSUES

Jaap R. Zijp

Promotiecommissie: Prof. Dr. Ir. M.J.C. van Gemert
Prof. Dr. R. Hibst
Prof. Dr. H.A. de Raedt

Paranimfen: Roos van Goudoever
Hanneke de Man

PDF - version by J.R. Zijp,

This thesis was sponsored by and has been prepared within the Instute for Biomedical Materials Science and Application (BMSA).

Front cover: Slabs of bovine enamel in liquids. Top row sound, bottom row carious. Left column immersed in water, right column immersed in a solution with a refractive index of 1.62. It is clearly seen that the carious slab becomes transparent in the refractive index matchig solution. This happens because carious enamel is porous and the solution easily penetrates the carious enamel. The differences in the refractive indices are reduced and so the scattering is decreased.

Back cover: False colour image of the most beautiful Fraunhofer diffraction pattern measured with the set-up as shown in Figure 6.1 (page 65). The colours represent different intensities in logarithmic scale, ranging from 1 (black) to 550 000 (red) in arbitrary units.

Voorkant: Plakjes rundglazuur in vloeistof. Bovenste rij gezond, onderste rij carieus. Linker kolom ondergedompeld in water, rechter kolom ondergedompeld in oplossing met een brekingsindex van 1.62. Het is duidelijk te zien dat het carieuze plakje transparant wordt in de brekingsindex matching vloeistof. Dit komt doordat deze vloeistof gemakkelijk in de porïen van het carieuze glazuur doordringt. De brekingsindex verschillen in het plakje worden kleiner en daardoor neemt de lichtverstrooiing af.

Achterkant: Vals kleuren plaatje van het mooiste Fraunhofer diffractie patroon gemeten met de opstelling die is weergegeven in Figuur 6.1 (pagina 65). De kleuren representeren verschillende intensiteiten, lopend van 1 (zwart) tot 550 000 (rood) in willekeurige eenheden.

Rijks*universiteit* Groningen

OPTICAL PROPERTIES OF DENTAL HARD TISSUES

Proefschrift ter verkrijging van het doctoraat in de Wiskunde en Natuurwetenschappen aan de Rijksuniversiteit Groningen op gezag van de Rector Magnificus, dr. D.F.J. Bosscher, in het openbaar te verdedigen op vrijdag 11 mei 2001 om 14.15 uur

door

J.R. Zijp

Promotores: Prof. Dr. J.J. ten Bosch
Prof. Dr. M.C.D.N.J.M. Huysmans

Voorwoord

Op deze plaats kan ik vooral mijn vreugde uiten over het feit dat mijn proefschrift af is. Het is één van de resultaten van 14 jaar onderzoek. Gedurende die tijd is er veel veranderd vooral door de voortgang van computer-technologie. Toen ik in 1986 in dienst kwam had onze vakgroep twee XT computers en een paar Apple IIe's voor zo'n 30 medewerkers. Nu zijn er meer computers dan medewerkers, die het werken ermee niet bepaald eenvoudiger hebben gemaakt. Dit komt vooral doordat er meer met de computer kan, en we er daardoor ook meer mee willen. Uit mijn begintijd herinner ik me discussies over of rekenen op de computers voorrang moest hebben boven tekstverwerking. Dit soort discussies zijn nu niet meer denkbaar. De rekenkracht van computers is enorm toegenomen. Mijn eerste berekeningen van hoekafhankelijke intensiteits functies, die in Hoofdstuk 2 beschreven worden, duurden drie kwartier. Nu gebeurt dat in een paar seconden. Schrijven zonder computer, bijvoorbeeld op een schrijfmachine gebeurt nog zelden. De komst van iimeel en internet heeft ons computer gebruik drastisch veranderd. Communicatie met vakgenoten, vooral wanneer deze in andere tijdzone's werken, is door die faciliteiten veel sneller en gemakkelijker geworden. Voor mijn onderzoek hebben computer ontwikkelingen als gevolg gehad dat het uitvoeren van metingen over het algemeen veel minder tijd kost, maar dat het proces van dataverwerking tot publicatie meer van mijn tijd in beslag neemt. Ik vind het leuk dat ik al deze ontwikkelingen meegemaakt heb.
Vaak probeer ik geïnteresseerde mensen uit te leggen wat ik onderzoek, en waarom ik dat doe. Ik vind dat alle onderzoekers bij openbare instellingen verplicht zijn dat te doen. Het meeste onderzoek wordt immers door de belastingbetalers gefinancierd en die hebben daarom ook het recht te weten wat er met hun geld gebeurt. Voor die geïnteresseerden heb ik Hoofdstuk 10 geschreven.
Vele collega's hebben mij bij mijn onderzoek en bij de productie van mijn proefschrift geholpen. Ik wil hen allen bedanken voor hun werk en de gezelligheid daarnaast. Slechts een aantal van hen kan ik met toenaam bedanken. Frans Hofsteenge, Henk Leydsman, Jan Nieborg, Bert Schreuder en Bernard Wolfs en anderen van de mechanische werkplaats wil ik bedanken voor de prachtige werkstukken die ze gemaakt hebben voor het bouwen van meetopstellingen en het repareren van instrumenten. Zonder zo'n goed bemande en geoutilleerde werkplaats is experimenteel onderzoek bijna niet mogelijk. Jaap Noordmans wil ik bedanken voor zijn hulp bij computer soft- en hardware problemen. Dankzij zijn software heb ik vele grafieken op beeldschermen en op papier kunnen maken. Ellen van Drooge, Ina Heidema, Jaap Lubbers, Marjon Schakenraad en Joop de Vries ben ik dankbaar voor het helpen bij en instrueren van de bediening van diverse software pakketten. Jan Ruben bedank ik vooral voor zijn hulp bij de bereiding van samples en demineralisatie gels. Reindert Graaff bedankt voor de interressante bijdragen bij het uitwerken van resultaten en het lezen van manuscripten. Mijn nieuwe baas, Gerhard Rakhorst, bedankt voor de ruimte die je mij hebt gegeven om het geheel af te maken.
Van het Grafisch Centrum hebben Jan de Wit en Marcel Zinger, die het omslag ontwierpvan de boek uitgave, mij in de laatste fase geholpen, bedankt daarvoor.
Op deze plaats wil ik ook mijn inmiddels overleden (oud)collega's prof. dr. J. Arends en dr. Pieter L. Cuperus gedenken en postuum bedanken voor hun betrokkenheid en het plezier dat we hebben gedeeld.

Mijn vroegere docent, dr. A.J. Postma, van de lerarenopleiding Ubbo Emmius wil ik bedanken voor het feit dat hij mij geleerd heeft de moed niet te gauw op te geven wanneer een vergelijking meerdere regels of zelfs een hele bladzijde beslaat.
Mijn eerste promotor Jaap ten Bosch bedankt voor je bijna grenzeloze optimisme over het onderzoek. Onze wetenschappelijke discussies hebben ons soms tot diep nadenken gezet, en zijn daardoor een stimulans geweest om kwalitatief goed werk af te leveren.
Mijn tweede promotor Marie-Charlotte Huysmans bedankt voor je kritische blik, daarmee heb je ervoor gezorgd dat er een betere relatie tussen mijn laboratorium gegevens en de tandheelkundige praktijk is gelegd.
Mijn familie, vrienden en vriendinnen wil ik bedanken voor hun interesse en betrokkenheid.
Mijn vrouw Resie, en mijn kinderen Teun en Janneke wil ik bedanken voor hun warmte, en genegenheid voor wie ik ben.

Jaap, 2 april 2001

TABLE OF CONTENTS

Chapter 1 **Introduction**

1.1 INTRODUCTION

In the present western society the role of the individual is important. People want to become independent and want to distinguish themselves from others. This is in contradiction with some tendencies to become uniform and perfect. One of the most striking examples of this phenomenon is the enormous increase in the number of adolescents visiting orthodontists and wearing orthodontic appliances to obtain the perfect smile. It also seems to be unacceptable that one has discoloured teeth, or a dental restoration whose colour is different from the surrounding teeth. Our attention is attracted to colour differences, like the colour difference between teeth, when we are talking to someone whose dentition is restored after loss of a tooth *e.g.* with an accident or during a not solely verbal debate. Non obtrusive restoration or replacement is desired, especially in the anterior region. The total appearance of the restoration is important. This appearance is determined by numerous factors like colour, transparency, form and smoothness of the surface. Development of materials to be used for invisible restorations necessitates the knowledge of the optical properties of natural materials.

When we are looking at objects, we mostly see the result of a combination of light scattering and absorption. Scattering is the phenomenon that light changes its direction. A glass of milk is seen as white because light incident on the milk is scattered in all directions, and leaving the milk without absorption. A glass of tea is seen as transparent because it does not scatter light, but it looks brown because much light, especially green and blue, is absorbed by the tea. Pooring milk in to the tea will cause an increase of the scattering in the tea, and so a change in its colour, depending on how much milk is used. In physical terms we distinguish scattering and absorption as two material properties. Properties that are responsible for the way we see things, and so properties that are essential for the way we see our teeth.

Fluorescence is another optical phenomenon that we see daily. Fluorescence is the phenomenon that *e.g.* ultraviolet light is transformed to violet-blue light. This phenomenon is easily seen in discotheques where 'blacklights' light up white shirts, the shirts are seen as sources of violet light. Also teeth are fluorescing and the dentition lights up in a dark-yellow colour under black light illumination. Daylight contains ultraviolet light and so fluorescence of teeth contributes to their colour.

Why do young children commonly have whiter teeth than adults? It is known that deciduous teeth have a lower mineral content than permanent teeth. Probably pores present in the enamel increase the scattering in the teeth, and so the teeth appear whiter. The appearance of anterior teeth will change in time. After eruption the incisal edge is very transparent, and so looks dark with the dark mouth behind it. After abrasion of this edge a lighter, thicker edge is seen. More abrasion may remove the entire enamel layer at the edge and uncover the dentine. As dentine is more porous dyes from food, drinks, and the use of tobacco may diffuse in to the dentine causing discolouration of the teeth.

Tooth discolouration is a common esthetical problem in dentistry. Numerous origins of discolouration are known, like bacterial growth, retention of dyes from food or beverages, and the use of antibacterial agents like chlorhexidine and stannous fluoride. The use of tetracycline (*i.e.* a specific antibiotic) during tooth formation may result in grey to black discolourations.

Accidents may also cause discolouration of teeth. After an accident teeth may become necrotic. Remains of blood present in the pulp chamber will desintegrate and form black

ironsulfide, this diffuses in to the dentine and the tooth will have a grey colour. Non-vital bleaching of the pulp chamber with sodium perborate can be very effective. A small trauma, or a lesion in the vicinity of the dentine, may start growth of dentine in the pulp chamber *i.e.* obliteration. This obliteration causes an increase of scattering in the tooth crown, and so a decrease of translucency. Brown to yellow discolourations may arise.
Some discolourations can partially be restored by application of vital bleaching. For professional bleaching the enamel is etched and a bleaching gel containing hydrogenperoxide is applied. The gingiva has to be protected for the high concentration of hydrogenperoxide and so it is not possible to bleach near the gingiva. At these sites it is possible to cover the teeth with opaque composite material to increase the brightness of the teeth. For home bleaching a milder carbamideperoxide containing gel can be used. It is not exactly known how these bleaching processes work.
When teeth become older they become more yellow. Probably the enamel becomes more translucent, so, the light scattering decreases with time. The observed reflected light penetrates deeper into the tooth and so a larger fraction may be absorbed. This causes a darker colour, but also a change in the appearance.
Teeth present in the mouth are continuously exposed to a changing chemical environment. During a meal consumption of acidic food and drinks will raise acidity in the mouth. This causes dissolution of some mineral at the very outside of the tooth (*i.e.* demineralisation). Chemical resting conditions in the mouth are such that redeposition of mineral within demineralised tooth tissue can occur (*i.e.* remineralisation). These processes of de- and remineralisation go on and on, day in day out.
Acid conditions on the tooth surfaces may also occur at those places where a plaque-biofilm is attached to the tooth. This local acidity is caused by acid producing bacteria present in the plaque. At these places dental caries, which is a net mineral loss from the tooth, may develop. The very early stages of dental caries are characterized by the development of subsurface lesions in enamel presenting as white spots. Ever since there are dentists this optical property has been used to detect and estimate the severity of these carious lesions. It is believed that the increased whiteness is caused by increased scattering of light. The causes of the increased scattering are not fully understood.
The carious spot may also be examined by shining light through the entire tooth, this is called transillumination. Transillumination of teeth is a promising technique for the detection of caries and measuring its severity. At a white spot lesion the light is more scattered and so this lesion is less transparent, and can be detected by decreased light transmission. Understanding of these effects requires the knowledge of the entire light scattering processes in sound and carious dental tissues.
Many colour differences and colour changes exist and appear in the dentition present in the mouth. Most of these effects are not fully understood. Why is there a systematic difference between the colour of teeth? Cuspids, for instance, appear more yellow than the other anterior teeth. This is probably caused by the fact that their dentine layer is thicker than the dentine layer in other teeth. Why is the colour of teeth deepening and yellowing with increasing age?
Possibly the continuous de- and remineralisation makes the enamel more homogeneous, decreasing the light scattering and so deepening the colour. Why do older teeth sometimes show transparent root dentine, especially near the apex? Probably the continuous deposition of mineral in the tubules reduces their size and so their contribution to light scattering. Why does fluorosis cause discolouration of teeth? Fluorosis is seen as white stripes. People living in areas where drinking water contains high concentrations of fluoride, and people using too much fluoride containing dental care products, may develop fluorosis.

Some of these questions can be answered when we know more of the optical properties of dental tissues.

1.2 REVIEW ON THE OPTICAL PROPERTIES OF DENTAL TISSUES

1.2.1 Dental hard tissues

The outer part of a tooth crown consists of dental enamel. The enamel layer (thickness 1-3 mm) is the only part of the sound tooth that is in direct contact with the oral cavity. And so dental caries mostly starts in the enamel. Enamel is the hardest tissue grown in nature. It consists for about 87 vol% of hydroxyapatite-like crystalline material, 2 vol% organic material and 11 vol% water (Jenkins, 1978). These values were accepted during several decades, however some investigators (Elliott *et al*., 1998) proposed a higher mineral content of about 95 vol%. Sound enamel is rather transparent, carious enamel is opaque.
The body of teeth consists of dentine, which is a bone like material containing about 48 vol% of mineral, 28 vol% of organic material and 24 vol% of water. In dentine tubules are present, extending from the dentine enamel junction to the pulp. Their size and number depend on the location within the dentine.
The root is covered with cementum. When retraction of the gingiva occurs the cementum will be exposed to the oral milieu and root caries can develop.

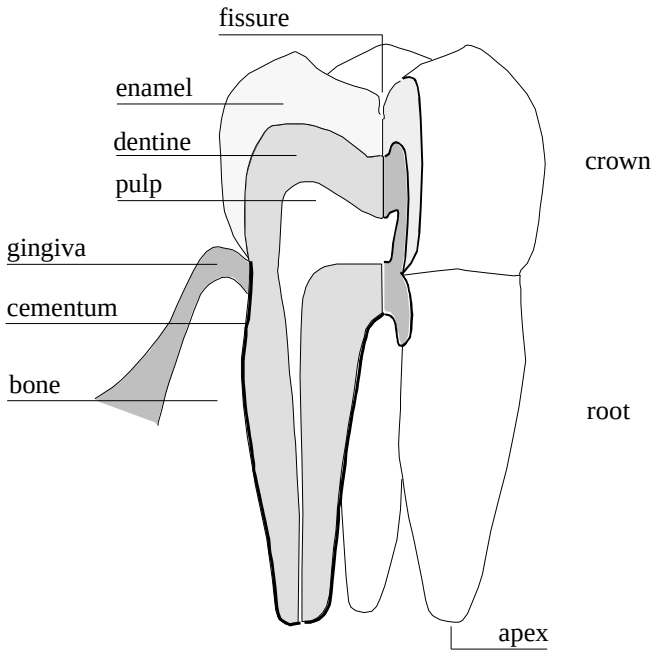

Figure 1.1 Human molar. The tissues dentine and enamel are the dental hard tissues considered in this thesis.

1.2.2 Previous work

At the time we started the investigations presented in this thesis, some work dealing with the optical properties of dental tissues had already been published.

Angmar *et al.* (1963) measured the birefringence of human dental enamel. Wet superficial parts of enamel showed a negative birefringence of 0.0024 with a general tendency to decrease to values of 0.0017 towards the inner parts. They found no correlation between birefringence and the mineral content.

Luminescence (*i.e.* fluorescence and phosphorescence) of human dental enamel and dentine were studied by Hefferren *et al.* (1971). They found phosphorescence excitation maxima at 310 nm (human enamel) and 300 nm (human dentine), and emission maxima at 455 nm (human enamel) and 445 nm (human dentine). For human enamel fluorescence excitation maxima at 280 and 370 nm, and an emission maximum at 450 nm were measured.

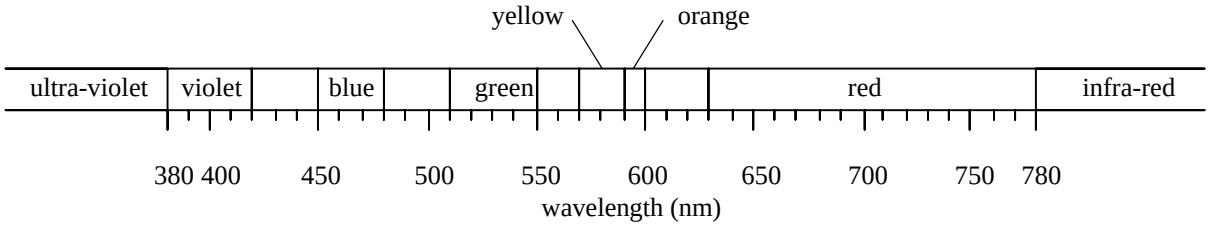

Figure 1.2 The visible light spectrum and colours of light.

The light transmission and reflection spectra of bovine and human dental enamel slabs were measured with an integrating sphere set-up by Spitzer and ten Bosch (1975). They also measured the refractive index of dental enamel as a function of the wavelength ranging from 220 to 700 nm, for wavelengths from 400 nm to 700 nm they found the refractive index equal to $n = 1.62$. Using these data they calculated the linear absorption a and scattering coefficients s. For human enamel they found a decreasing from 1.2 mm^{-1} (at 220 nm) to 0.15 mm^{-1} (at 400 nm), and $a \cong 0.12$ mm^{-1} (from 400 to 700 nm). For the linear scattering coefficient they found $s = 37$ mm^{-1} (at 220 nm) decreasing to 2.3 mm^{-1} (at 700 nm). Spitzer and ten Bosch (1976) also determined the fluorescence and phosphorescence spectra of bovine and human enamel and of the organic components of these materials. They concluded that the organic component is the major contributor to the total luminescence.

The translucency of human dental enamel was measured by Brodbelt *et al.*(1981). They used a spectrophotometer with an integrating sphere and found that the total transmission of 1 mm thick slabs increased from 0.34 at 400 nm to 0.74 at 700 nm. They did not perform the necessary corrections like accounting for light that was transmitted by the sample first and reentering the sample from the integrating sphere. They ascribed the measured strong wavelength dependence of the scattering coefficient to the Rayleigh effect. This effect is caused by scattering particles with typical dimensions much smaller than the wavelength used. The mineral crystals present in the enamel meet this property.

Groenhuis *et al.* (1981) investigated the scattering of light by dental enamel by measuring the angular dependent radiance for scattering angles up to $\pi/6$. They observed first order maxima which they attributed to diffraction by the enamel prisms. From collimated transmission measurements of enamel samples they calculated the linear scattering coefficient as $s = 5$ mm^{-1} (at 500 nm) decreasing to 3 mm^{-1} (at 700 nm). Some of their work was used to complete Chapter 6 in this thesis.

1.2.3 Simultaneous work

During our research also other investigators explored the optical properties of dental tissues.
Observations of Fraunhofer diffraction of light by human dental enamel were published by O'Brien (1988). He expected a first order peak at 7° 20', and measured 6° 48'. We did further investigations on this phenomenon as presented in Chapter 6.
The colour of whole teeth was investigated by Solheim (1988), he found an increase of the reflection of yellow light versus age.
Altshuler and Grisimov (1989) cut plane-parallel cross sectional slabs of human teeth and illuminated them with a small laser beam incident on the original outer surface. The angle of incidence of the laser beam with respect to the surface normal was varied. They observed wave guiding of light by the enamel prisms and by the dentine tubules.
The birefringence of the body of caries-like lesions immersed in Thoulet's solution was shown to be linearly dependent on the mineral content (Theuns *et al*., 1993). This birefringence was not related to mineral content in sound superficial enamel immersed in Thoulet's solution or in the body of the lesion immersed in water.
Ten Bosch and Coops (1995) measured the colour of whole human anterior teeth. After removing the enamel, they measured the colour of the remaining dentine. From comparisons of these measurements they concluded that tooth colour is mainly determined by colour of the dentine. Removing the enamel causes on average a decrease of the a* values (*i.e.* a shift from red to green) and an increase of the b* values (*i.e.* a shift from blue to yellow), the latter being the largest. So the presence of the enamel causes a higher reflection of blue light, and so blue light has a higher scattering coefficient than light of longer wavelengths.
Vaarkamp *et al.*(1995) measured the light propagation through square 0.85 mm thick human enamel and dentine bars in four perpendicular directions, forward, backward and at 90° (left and right). From these measurements they determined the scattering asymmetry parameter of enamel as $g = 0.68 \pm 0.09$.
Fried *et al.*(1995) measured the light scattering properties of human enamel and dentine at 543, 632 and 1053 nm. For enamel they found linear scattering coefficients s ranging from 10.5 mm^{-1} (at 543 nm), 6 mm^{-1} (at 632 nm) to 1.5 mm^{-1} (at 1053 nm). The asymmetry parameters at these wavelengths were about $g = 0.46$ (enamel at 1053 and 632 nm), $g = 0.24$ (enamel at 543 nm) and $g = 0.91$ (dentine at 1053, 632 and 543 nm).
Van der Veen and ten Bosch (1995) measured the auto-fluorescence excitation and emission spectra of sound and carious human root dentine. For both the sound and demineralised samples excited at 488 nm they found a shoulder-like emission maximum at about 520 nm, this peak was more pronounced for the demineralised dentin. Detecting the emission at 520 nm they recorded excitation spectra with maxima around 405 nm. They also measured the influence of mineral loss on the auto-fluorescent behaviour of in vitro demineralised dentine (van der Veen and ten Bosch, 1996). With excitation at 515 nm and emission at 529 nm, the auto-fluorescence increased when the dentine was demineralised.
Monitoring de- and remineralisation of human enamel in vitro was investigated by Anderson *et al.* (1996) using an infrared reflectance meter operating at 935 nm. They reported decrease of the surface reflection during demineralisation. Remineralisation caused increase of the reflection. The device used had two optical axes, those of the illuminating LED and the sensor, these made an equal angle with respect to the surface normal. It could be expected that this device also measures some volume reflection, which should increase during demineralisation, but this was not observed.
Grisimov (1999a) observed slabs of human teeth under different illuminations. He found that the backscattering decreased with the age of the teeth. He also observed that the location of

the Hunter-Schreger bands is dependent on the direction of the incident light (Grisimov 1999b).
The optical scattering power of slabs of enamel was measured as a function of the decrease of mineral content by Ko *et al*. (2000). They found that caries increases the scattering coefficient by a factor of about 3.
Analoui *et al.* (2000) measured reflectance spectra of human enamel samples against white and black backgrounds. They reduced the measured spectra, each containing 81 points, by principal component analysis. At least 4 principal components were needed to represent the spectra. A similar method was used by ten Bosch (to be published). He measured the reflectance spectra of 102 whole teeth and performed factor analysis. He showed that the reflectance spectra of teeth for the wavelength range 390 - 730 nm could be calculated from its CIELAB colour coordinates a*, b* and L* using three factors.

1.3 DISCUSSION

Birefringence of dental enamel plays no role in the appearance of teeth as an untrained observer sees them. Luminescence plays a small role in the colour determining process, this is due to the low quantum efficiency. Rare illumination conditions however, like *e.g.* blacklights in a discotheque, will cause extreme influence of the luminescence on the observed tooth colour. Under daily conditions the colour of teeth is mainly determined by the colour of the dentine. But enamel plays a role in the total appearance of teeth. This appearance changes with age due to increase of transparency. The optical properties of enamel change very much at carious sites, particularly the scattering.
The linear light scattering coefficients for human enamel as calculated by Spitzer and ten Bosch (1975), s = 4.7 mm^{-1} (at 543 nm) and s = 2.3 mm^{-1} (at 632 nm) are about half the values found by Fried *et al.* (1995) at these wavelengths.
Using an asymmetry parameter value g = 0.68, refractive index n = 1.62 and scattering coefficients s = 4.7 mm^{-1} and s = 2.3 mm^{-1} as input parameters, we estimated the total transmission of 1 mm thick slabs of enamel by Monte Carlo simulations as 0.49 (at 543 nm) and 0.62 (at 632 nm). These values are somewhat lower than those found by Brodbelt *et al.* (1981) (0.58 and 0.68 respectively). This indicates that the scattering coefficients used in the Monte Carlo simulation should be higher, this is confirmed by the higher values of s shown in Table 7.1 and the values found by Fried *et al*. (1995).

1.4 AIM OF THE STUDY

The aim of the work presented in this thesis is to determine the optical properties of dental tissues, and to explain the relations between the optical properties of dental tissues and the structures present. Changes of these structures will cause changes in the optical properties. Modelling these structures will enable us to explain optical effects caused by structural changes.

1.5 REFERENCES

Altshuler GB, Grisimov VN (1989) New optical effects in the human hard tooth tissues. In: *Lasers and Medicine*, Konov VI, Müller GJ, Prokhorov AM, eds. SPIE 1353:97-102.

Analoui M, Ando M, Stookey GK (2000) Comparison of reflectance spectra of sound and carious enamel. In: *Lasers in Dentistry VI*, Featherstone JDB, Rechmann P, Fried D, eds. SPIE 3910:227-234.

Anderson P, Davis GR, Ahluwalia MH (1996) Monitoring de- and remineralisation of enamel *in vitro* using an infrared reflectance meter. *Caries Res* 30: 394-399

Angmar B, Carlström D, Glas J-E (1963) Studies on the ultrastructure of dental enamel IV. The mineralization of normal human enamel. *J Ultrastruct Res* 8:12-23.

Brodbelt RHW, O'Brien WJ, Fan PL, Frazer-Dib JG, Yu R (1981) Translucency of human dental enamel. *J Dent Res* 60:1749-1753.

Elliott JC, Wong FSL, Anderson P, Davis GR, Dowker SEP (1998) Determination of mineral concentration in dental enamel from X-ray attenuation measurements. *Connective Tiss Res* 39:61-72.

Fried D, Glena RE, Featherstone JDB, Seka W (1995) Nature of light scattering in dental enamel and dentin in the visible and near-infrared wavelengths. *Appl Opt* 34:1278-1285.

Groenhuis RAJ, ten Bosch JJ, Ferwerda HA (1981) Scattering of light by dental enamel: theoretical model compared with experiments. In: *Scattering and absorption of light in turbid materials, especially dental enamel*, thesis University of Groningen, pp. 25-42.

Grisimov VN (1999a), Backscattered HeNe laser light intensity and distribution of the light scattered inside dental tissues. In: *Medical Applications of Lasers in Dermatology, Cardiology, Ophthalmology, and Dentistry II*, Altshuler GB, Andersson-Engels S, Birngruber R, Bjerring P, Fercher AF, Geschwind HJ, Hibst R, Hoenigsmann H, Laffitte F, Sterenborg HJ, eds. SPIE 3564:231-236.

Grisimov VN (1999b) Optical model of Hunter-Schreger bands phenomenon in human dental enamel. In: *Medical Applications of Lasers in Dermatology, Cardiology, Ophthalmology, and Dentistry II*, Altshuler GB, Andersson-Engels S, Birngruber R, Bjerring, P, Fercher AF, Geschwind HJ, Hibst R, Hoenigsmann H, Laffitte F, Sterenborg HJ, eds. SPIE 3564:237-242.

Hefferren JJ, Hall JB, Bennett E (1971) Luminescence as a tool to study enamel interactions. In: *Tooth enamel II* ,Fearnhead RW, Stack MV, eds. (John Wright, Bristol) pp. 161-165.

Jenkins GN (1978) *The physiology and biochemistry of the mouth*. (Blackwell Scientific, Oxford) pp. 54-112.

Ko CC, Tantbirojn D, Wang T, Douglas WH (2000) Optical scattering power for characterization of mineral loss. *J Dent Res* 79:1584-1589.

O'Brien WJ (1988) Fraunhofer diffraction of light by human enamel. *J Dent Res* 67:484-486.

Solheim T (1988) Dental color as an indicator of age. *Gerodontics* 4:114-118.

Spitzer D, ten Bosch JJ (1974) The absorption and scattering of light in bovine and human dental enamel. *Calcif Tiss Res* 17:129-137

ten Bosch JJ, Coops JC (1995). Tooth color and reflectance as related to light scattering and enamel hardness. *J Dent Res* 74:374-380.

ten Bosch (*to be published*) Tooth reflectance spectra derived from color coordinates by regression analysis.

Theuns HM, Shellis RP, Groeneveld A, van Dijk JWE, Poole DFG (1993) Relationships between birefringence and mineral content in artificial caries lesions of enamel. *Caries Res* 27:9-14

Vaarkamp J, ten Bosch JJ, Verdonschot EH (1995) Propagation of light through human dental enamel and dentine. *Caries Res* 29:8-13.

van der Veen MH, ten Bosch JJ (1995) Autofluorescence of bulk sound and *in vitro* demineralized human root dentin. *Eur J Oral Sci* 103:375-381

van der Veen MH, ten Bosch JJ (1996) The influence of mineral loss on the auto-fluorescent behaviour of in vitro demineralised dentine. *Caries Res* 30:93-99

Chapter 2 Light scattering measurement set-ups and theoretical models

2.1 MEASURING SET-UPS

2.1.1 Introduction

The measurements described in this thesis are carried out with a few of different instruments and set-ups. These instruments and set-ups are described in this chapter with their ins and outs.
The most frequently used units are:

a as the linear absorption coefficient in mm^{-1},
s as the linear scattering coefficient in mm^{-1},
K as the Kubelka-Munk absorption coefficient in mm^{-1} (Kortüm, 1969),
S as the Kubelka-Munk scattering coefficient in mm^{-1},
g as the asymmetry parameter for scattering, *i.e.* the mean cosine of the scattering angle,
q as the scattering angle, *i.e.* the angle between incident and scattering direction, and
j as the azimuthal angle of the scattering process.

2.1.2 Integrating sphere for diffuse reflection and transmission measurements

An integrating sphere is a spherical cavity, which has a white wall. In the ideal case the wall is ideally white and diffusely reflecting, and so it absorbs no light. Light, once present in such a sphere, will be present there forever. It will propagate to the wall, where it is reflected. After that it will propagate in another direction, reflect at the wall again. After each reflection the new direction of propagation is independent on the previous direction. And so the light will propagate from wall to wall forever, but it will not be observed, because observation needs absorption of at least a small part.

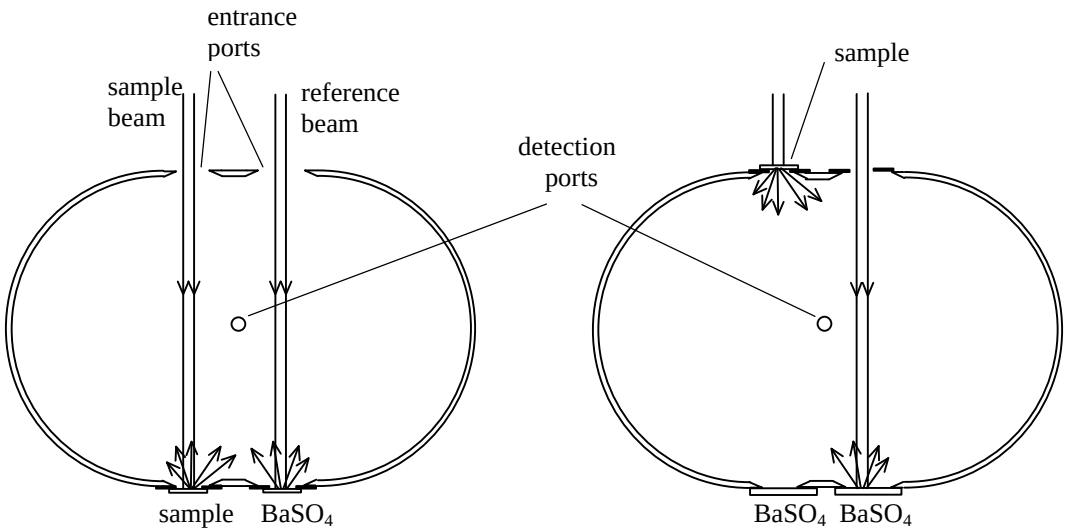

Figure 2.1 Geometry for diffuse reflectance and diffuse transmittance measurement with integrating sphere set-up.

Integrating spheres, as used in measuring instruments, are not ideal. They are losing light because their wall is a little bit absorbing, although wall material with reflection coefficients above 0.99 for visible light may be used. Also light is lost through some ports present in the wall, they are used as light entrance port, sample port, reference port and/or detection port. The number of ports and their function depends on the way the integrating sphere is used.
The set-up that we used in Chapter 3 is shown in Figure 2.1. This integrating sphere contains 5 ports: the detection port, the sample entrance port, the sample exit port, the reference entrance port and the reference exit port. The light used is alternating in such a way that it enters either the sample entrance port or the reference entrance port. Phase-sensitive amplification of the measured signal provides correction for fluctuations, *e.g.* of the lamp output.
Because our samples are much smaller than the ports we applied equally sized black diaphragms during all reflection measurements to reduce the exit ports sizes. During these measurements both entrance ports are fully open. The reference exit port faces a diaphragm with a white standard. For 0% reflection the sample exit port 's diaphragm was open, for 100% reflection the sample exit port 's diaphragm was covered with a white standard. While measuring the samples, the sample exit port 's diaphragm was covered by a sample.
The same diaphragms were applied during all transmission measurements. Transmission measurements were all made with the exit ports covered with white standards, and the reference entrance port open. For 0% transmission the sample entrance port was covered with a black sheet, for 100% transmission measurement this port was open. While measuring the samples the samples were covering the sample entrance port.
The reflection and transmission values measured in this way were considered as the real reflection and transmission values. We did not perform the corrections like those proposed by Pickering (1992, 1993), of which changes in the amplification of the sphere by presence of the sample is the most important.
The measured reflection values r and transmission values t were used in the following equations given by Klein (1965):

$$r = \frac{[(1-r_i)^2 - b^2(1-r_i-2r_0)(1+r_i)]\sinh sD + 2b(r_0+r_i)(1-r_i)\cosh sD}{[b^2(1+r_i)^2+(1-r_i)^2]\sinh sD + 2b(1-r_i^2)\cosh sD}$$

$$t = \frac{2b(1-r_0)(1-r_i)}{[b^2(1+r_i)^2+(1-r_i)^2]\sinh sD + 2b(1-r_i^2)\cosh sD} \qquad (2.1)$$

with:
r as the transmittance of the slab (dimensionless),
t as the reflectance of the slab (dimensionless),
$b = \sqrt{K/(K+2S)}$ (dimensionless),
$s = \sqrt{K(K+2S)}$ in mm^{-1},
D as the thickness of the slab in mm,
r_0 as the reflection coefficient for the light incident from air on the front surface:

$$r_0 \cong -0.4399 + 0.7099n - 0.3319n^2 + 0.0636n^3 ,$$

r_i as the reflection coefficient for diffuse light inside the sample that is reflected at the backside of the sample :

$$r_i = 1 - \frac{1 - r_0}{n^2},$$

and n as the refractive index of the sample.
With an iterating computer program that uses values of r and t as input parameters, the proper values of K and S (both in mm^{-1}) are found.

2.1.3 Integrating hemisphere for diffuse reflection with different backgrounds

For the measurements performed in Chapter 7 we use the set-up as shown in Figure 2.2. Five halogen lamps mounted in a box illuminate a frosted glass lid. The inside of the box is covered with aluminium sheet acting as a reflecting layer. The lid of the box acts as a rather

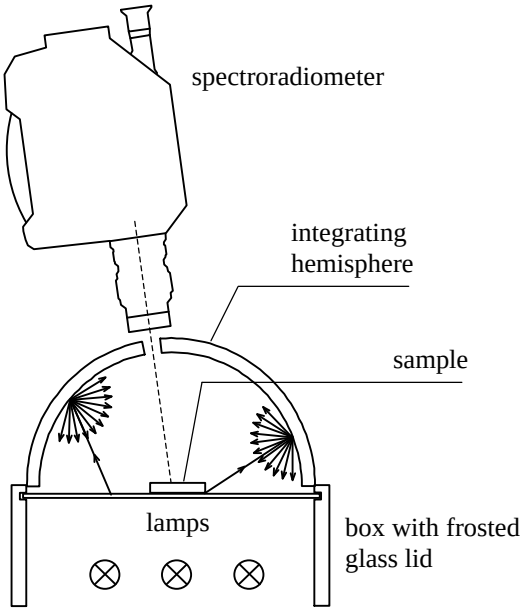

Figure 2.2 Set-up for reflectance measurement.

diffuse light source that illuminates the inner side of a white styrofoam hemisphere. The hemisphere, with a diameter of 240 mm, provides illumination of the sample from all spatial directions. In the centre of the lid a 25 × 60 mm black sample holder is fixed to enable repositioning of the samples and to prevent light entering the sample from below. The bottom of the sample holder can be shifted to provide a black or a white background. At 8° from the apex of the hemisphere a circular hole with a diameter of 25 mm enables measurement of the sample with a spectroradiometer. The samples used have to be translucent, so that the background of the sample influences the measured reflectance. From measurements with a black and with a white background the transmission and reflection of the sample without a background can be calculated. Corrections, like subtraction of specular reflection of the incident light and reflections from the boundaries, have to be made before the Kubelka-Munk

scattering and absorption coefficients, S and K, respectively, can be calculated. The corrections and calculations are well described by Molenaar (1999). In Chapter 7 we used this set-up to measure the reflection and transmission of samples consisting of two layers, *i.e.* sound and carious enamel. We assumed that the coefficients of one layer (sound enamel) were known.

2.1.4 Collimated transmission

For the collimated transmission measurements described in Chapter 6 we used the set-up as shown in Figure 2.3. The collimated light transmitted trough a thin layer is attenuated due to absorption and scattering in the layer. In case of absorption the light energy is converted into heat or excited states of molecules present in this layer. Scattering is conversion of collimated light into light that is not collimated anymore, but propagating in all spatial directions. Collimated transmission measurements may be used to measure the extinction coefficient of thin samples.

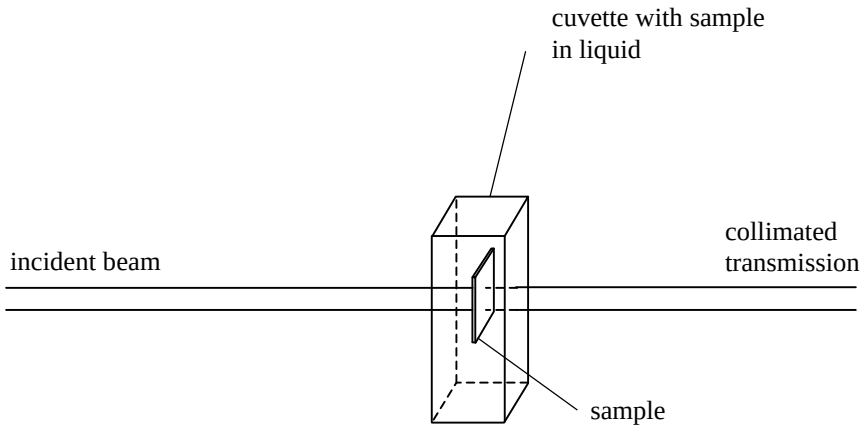

Figure 2.3 Geometry for measurement of collimated transmission

Biological tissue samples mostly have to be placed in a liquid to prevent drying. Samples that contain living cells have to be placed in a saline solution, which prevents osmotic swelling of the samples. Mostly the transmittance of a cuvette containing the liquid is measured and considered as 100% transmission. The transmission of the same set-up but with a sample present measures T_c , *i.e.* the collimated transmission of the sample. According to the Lambert-Beer law:

$$T_c = e^{-m_t D} \tag{2.2}$$

inverting leads to:

$$m_t = a + s = -\tfrac{1}{D}\ln(T_c) \tag{2.3}$$

with D as the thickness of the sample in mm,
m_t as the extinction coefficient in mm^{-1},
T_c as the collimated transmission.

The thickness of the sample has to be smaller than $1/s$, otherwise the calculated s value is not the true value for single scattering. The measured transmission may be too low, due to the fact that the roughness of the surface of the sample causes some extra scattering. This may lead to values of m_t which are too high. The influence of surface roughness can be lowered by applying refractive index matching liquid in the cuvette, because this causes an optical connection between the samples and its environment. But, in case of soft biological tissues, this refractive index matching liquid may cause osmotic shrinkage. That is why this technique is not very suitable for measuring soft tissue samples (Zijp and ten Bosch, 1998). In case of hard tissues, like dental enamel, we apply a refractive index matching liquid containing high ion concentrations (Chapter 6), this however does not alter the structures present.

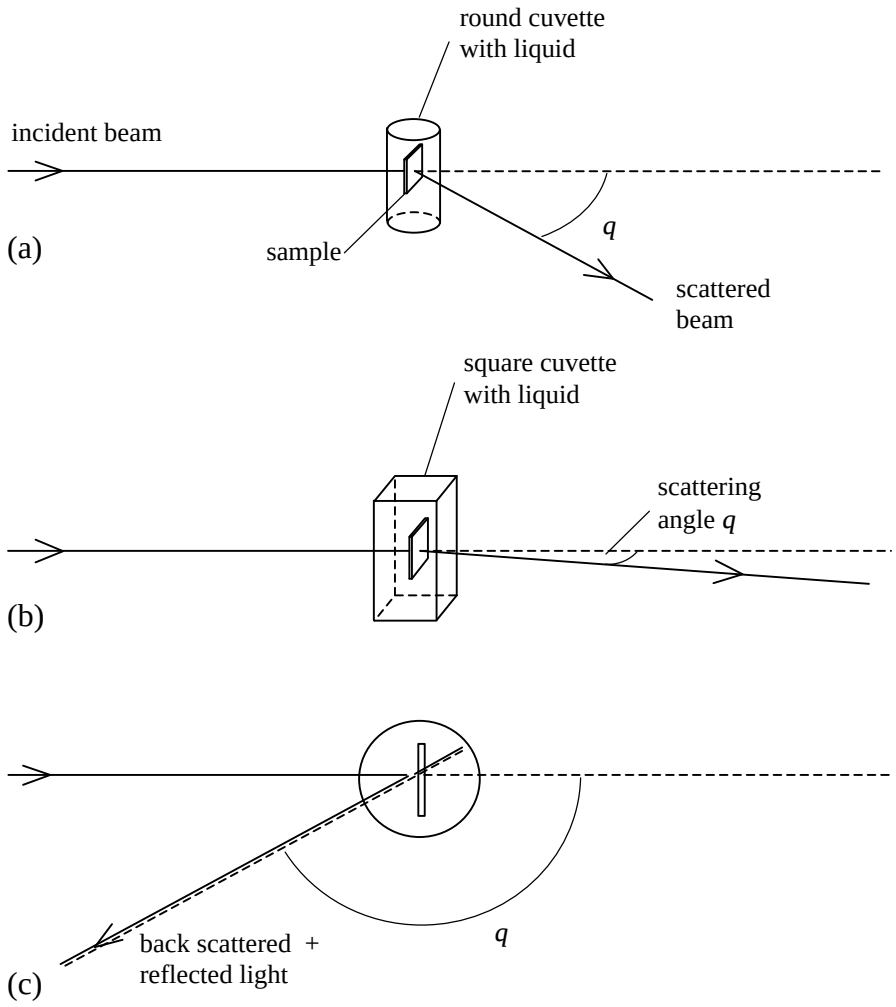

Figure 2.4 Geometries for measurement of angular intensity function.
a. Measurement at large angles
b. Measurement at small angles
c. Light, measured at large angles, contains reflected forwardly scattered light

2.1.5 Angular intensity functions

Angular intensity functions describe the intensity of the scattered light as a function of the scattering angle. In this case also the sample has to be optically thin: $D << 1/s$. For the same reasons as in the case of collimated transmission measurements (2.1.4), we can apply saline or refractive index matching liquid, but we will also face the same problems. Using a cylindrical cuvette (Figure 2.4a) will limit surface reflections at the cuvette wall. A disadvantage of measuring with a cylindrical cuvette is the fact that it acts as a lens. The diameter of the cuvette that we used was 25 mm, and the diameter of the incident beam was about 1 mm, resulting in a focus at about 250 mm behind the cuvette. This focus mainly disturbs the light distribution at small angles. That is why we applied a square cuvette for small angle measurements (Figure 2.4b).

Another problem of measuring these intensity functions arises at scattering angles close to 0°. Here it is impossible to measure the angular intensity function (Figure 2.4c), as the shadow of the sample holder disturbs the measurements. Also the fact that the sample is observed at a very large angle with respect to the optical axis causes that light scattered from a larger apparent thickness is observed. Measuring with the sample present in a cylinder cuvette may also cause reflection of light scattered in the forward direction to be detected in a backward direction. The opposite light path is not a problem because only a small fraction of the light is scattered backwardly, and reflected backscattered light will disappear in the noise.

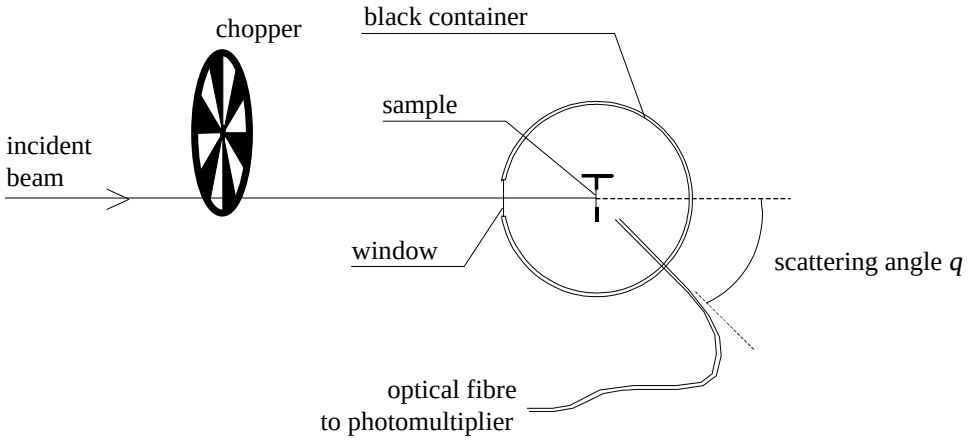

Figure 2.5 Improved set-up to measured angular intensity functions.

For later measurements (Zijp and ten Bosch, 1998) we improved the set-up for measuring angular intensity functions based on ideas of Jacques *et al.* (1987), to solve the problems caused by the use of cuvettes. This set-up is shown in Figure 2.5. It was used when we tried to measure the angular intensity functions of carious enamel (*c.f.* Chapter 7). During these measurements the enamel slabs were hanging in the centre of a black cylindrical container of 120 mm diameter. At the place where the incident beam entered the container, a microscope cover slip was placed in the wall. The container was filled with refractive matching liquid. An optical fibre hanging in the liquid was used to feed the scattered light to the detector. The fibre was connected to a revolving bar whose axis of rotation was coincident with the centre of the container.

2.2 THEORY OF SCATTERING BY PARTICLES

2.2.1 Introduction

Electromagnetic radiation propagating through a medium will be scattered when it passes areas with different permeabilities and/or susceptibilities. For visible light we can observe this phenomenon when we dissolve sugar. Streaks of lighter and darker regions can be seen when a lump of sugar is dropped in a glass cup of tea, regions with higher sugar concentrations have a higher refractive index, these differences in refractive indices cause light scattering. After stirring the liquid becomes homogeneous again and so the streaks will disappear. The streaks are irregularly formed, and so it is hard to predict how the light is scattered. When we are dealing with regular forms, like spheres or cylinders, the behaviour of light can be predicted by calculations. In this chapter these calculations will be shown.

As a reference for the calculations we define the scattering plane (Figure 2.6) as the plane containing the incident and the scattering directions. A plane electromagnetic wave propagates from the negative X-axis towards the positive direction. To simplify the calculations, the electrical vector of the incident radiation is split up in components parallel to and perpendicular to the scattering plane, $F_{0,l}$ and $F_{0,r}$ respectively (N.B. here we use F for electrical field to prevent confusion with the irradiance E). In the calculations these components can be treated independently. Because we will only deal with linear processes, the scattered radiation can be calculated by (van de Hulst, 1981):

$$\begin{pmatrix} F_r \\ F_l \end{pmatrix} = \frac{e^{-ikr}}{ikr} \begin{pmatrix} S_1 & S_4 \\ S_3 & S_2 \end{pmatrix} \begin{pmatrix} F_{0,r} \\ F_{0,l} \end{pmatrix} \tag{2.4}$$

with F_l and F_r as the scattered electrical field in V/m

k as the wavenumber in m^{-1}

r as the distance from the centre of the scatterer in m.

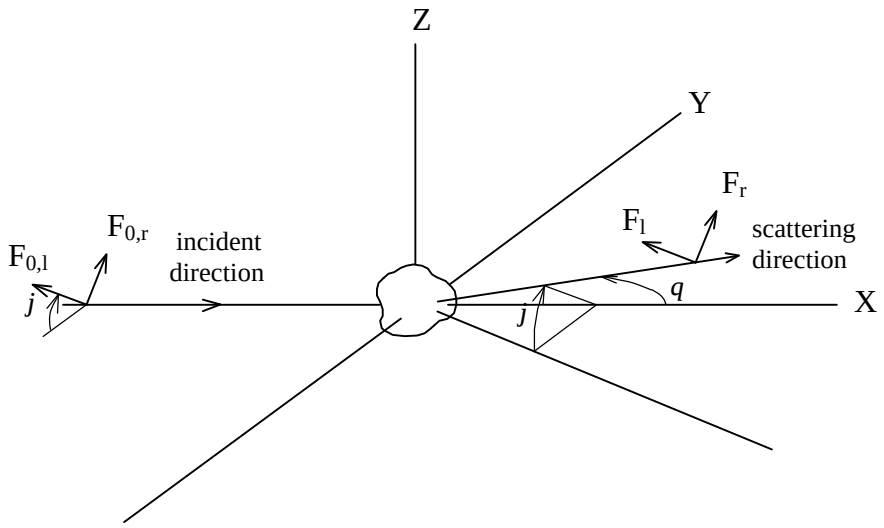

Figure 2.6 Scattering plane for scattering by an arbitrary particle, with incident and scattering direction and definitions of the angles q and j.

In general the amplitude functions S_1, S_2, S_3, and S_4 depend on the direction, represented by the angles q and j as defined in Figure 2.5.
If the particle is axially symmetric and oriented parallel to F_r, then no cross polarisation will occur, *i.e.* the functions S_3 and S_4 are equal to 0. Examples of such particles are spheres and circular straight cylinders at perpendicular incidence. The calculations of the functions describing the scattering of such particles are shown, because they are used in this thesis. In this chapter we are calculating for scattering in vacuum or air, if we are measuring in other media like liquids we have to perform corrections which account for the different refractive index.
The irradiance incident on the particle E_0 (in W/m^2) can be calculated from the incident electrical field by:

$$E_0 = ce_0F_0^2 \tag{2.5}$$

with c as the speed of light in vacuum, which equals 3×10^8 m/s,
e_0 as the vacuum permittivity, equal to 8.85×10^{-12} C^2 N^{-1} m^{-2}.
The scattered irradiance $E(q,j)$ of linearly polarized incident light in any direction can be calculated by:

$$E(q,j) = \frac{E_0}{k^2r^2}[i_1(q)\sin^2 j + i_2(q)\cos^2 j] \tag{2.6}$$

with q is the scattering direction,
j is the angle between the polarisation direction and the scattering plane.

The functions $i_1(q)$ and $i_2(q)$ describe the angular dependency of the perpendicular and parallel polarised components, respectively, these functions are given by:

$$i_1(q) = |S_1(q)|^2 \quad \text{and} \quad i_2(q) = |S_2(q)|^2 \tag{2.7}$$

The functions S are the amplitude functions.

For most applications the knowledge of the exact angular intensity functions is not necessary. In these cases it is sufficient to know the scattering cross section C_{sca} and the asymmetry parameter g of the scatterers present. The scattering cross section of a particle can be calculated as the ratio of the total amount of light scattered (in W) and the incident irradiance (in W/m^2). In some cases it is more common to use the scattering efficiency Q_{sca}, which is the ratio of the scattering cross section and the geometrical cross section (both in m^2), and so it is dimensionless.
The asymmetry parameter g is a condensed expression of the angular distribution of the scattered light. It is defined as the mean cosine of the angular distribution of the scattered light.

$$g = <\cos q> = \frac{\int_{j=0}^{2p} dj \int_{q=0}^{p} dq\ E(q,j)\sin q\cos q}{\int_{j=0}^{2p} dj \int_{q=0}^{p} dq\ E(q,j)\sin q} \tag{2.8}$$

In some light scattering calculations it is common to use fictitious 'isotropic scatterers', their asymmetry parameter equals $g = 0$. In biological tissues much particles or structures scatter with an asymmetry parameter in the range $0.7 < g < 1.0$ (Beek, 1997).

2.2.2 Rayleigh-Gans scattering

The amplitude functions of the scattered radiation can be approximated by the simple Rayleigh-Gans formulae (van de Hulst, 1981) in case that the scattering particles obey the following conditions:

- the refractive index m is close to 1: $|m-1| << 1$
- the phase shift is small: $2ka|m-1| << 1$ (2.9)

with a as a length (in m) of the order of the size of the scattering particle, and
m as the refractive index of the particle n_p with respect to its surrounding n_s:
$m = n_p/n_s$.
Some special types, as are spheres and thin rods, will be treated.

Spheres
The amplitude functions for Rayleigh-Gans scattering by spheres are given by:

$$S_1(q) = ik^3a^3(m-1)\frac{2}{u^2}\left(\frac{\sin u}{u} - \cos u\right)$$

$$S_2(q) = ik^3a^3(m-1)\frac{2}{u^2}\left(\frac{\sin u}{u} - \cos u\right)\cos q \qquad (2.10)$$

$$S_3(q) = 0 \qquad S_4(q) = 0$$

with $u = 2ka\sin\frac{1}{2}q$ and a as the radius of the sphere in m.

Thin rods
The thin rods, in the Rayleigh-Gans approximation, are circular cylinders with a radius a much smaller than the wavelength, expressed as $ka << 1$. They have a finite length l. The amplitude functions for this case are given by:

$$S_1(q) = \tfrac{1}{2}ik^3a^2l(m-1)R(q,j)$$

$$S_2(q) = \tfrac{1}{2}ik^3a^2l(m-1)\cos q\ R(q,j) \qquad (2.11)$$

$$S_3(q) = 0 \qquad S_4(q) = 0$$

with:

$$R(q,j) = \frac{\sin(kl\sin\frac{1}{2}q\ \cos b)}{kl\sin\frac{1}{2}q\cos b} \qquad \text{and} \qquad \cos b = -\cos a\ \sin\tfrac{1}{2}q + \sin a\ \cos\tfrac{1}{2}q\ \cos j\ .$$

With: a as the angle between the incident direction and the axis of the cylinder.

2.2.3 Mie-scattering

The scattering amplitude functions for scattering by spherical particles of any size were calculated for the first time by Mie (Mie, 1908). Here the more modern notation is shown (van de Hulst, 1981). The scattering properties of the spheres only depend on their size with respect to the wavelength used, and their refractive index with respect to their surrounding. The size is represented by the size parameter $x = ka$, the relative refractive index is represented by m. The amplitude functions for Mie scattering are given by:

$$S_1(q) = \sum_{n=1}^{\infty} \frac{2n+1}{n(n+1)} [a_n p_n(\cos q) + b_n t_n(\cos q)]$$

$$S_2(q) = \sum_{n=1}^{\infty} \frac{2n+1}{n(n+1)} [b_n p_n(\cos q) + a_n t_n(\cos q)] \qquad (2.12)$$

$$S_3(q) = 0 \qquad S_4(q) = 0$$

The coefficients a_n and b_n in Equation (2.12) depend on size and refractive index, and read:

$$a_n = \frac{y'_n(mx) y_n(x) - m y_n(mx) y'_n(x)}{y'_n(mx) z_n(x) - m y_n(mx) z'_n(x)}$$

$$b_n = \frac{m y'_n(mx) y_n(x) - y_n(mx) y'_n(x)}{m y'_n(mx) z_n(x) - y_n(mx) z'_n(x)} \qquad (2.13)$$

in which:

$$y_1(z) = \frac{\sin z}{z} - \cos z \qquad y_2(z) = \left(\frac{3}{z^2} - 1\right)\sin z - \frac{3\cos z}{z}$$

$$\text{for } n > 2: \quad y_n(z) = \frac{(2n-1)}{z} y_{n-1}(z) - y_{n-2}(z) \qquad (2.14)$$

$$y'_1(z) = \left(1 - \frac{1}{z^2}\right)\sin z + \frac{\cos z}{z} \qquad \text{for } n > 1: \qquad y'_n(z) = y_{n-1}(z) - \frac{n y_n(z)}{z} \qquad (2.15)$$

$$z_1(z) = \frac{\sin z}{z} - \cos z + i \sin z + \frac{i \cos z}{z}$$

$$z_2(z) = \left(\frac{3}{z^2} - 1\right)\sin z - \frac{3\cos z}{z} + \left(\frac{3}{z^2} - 1\right) i \cos z + \frac{3i \sin z}{z} \qquad (2.16)$$

$$z_n(z) = \frac{(2n-1)}{z} z_{n-1}(z) - z_{n-2}(z)$$

$$z'_n(z) = \frac{(n+1)}{z} z_n(z) - z_{n+1}(z). \qquad (2.17)$$

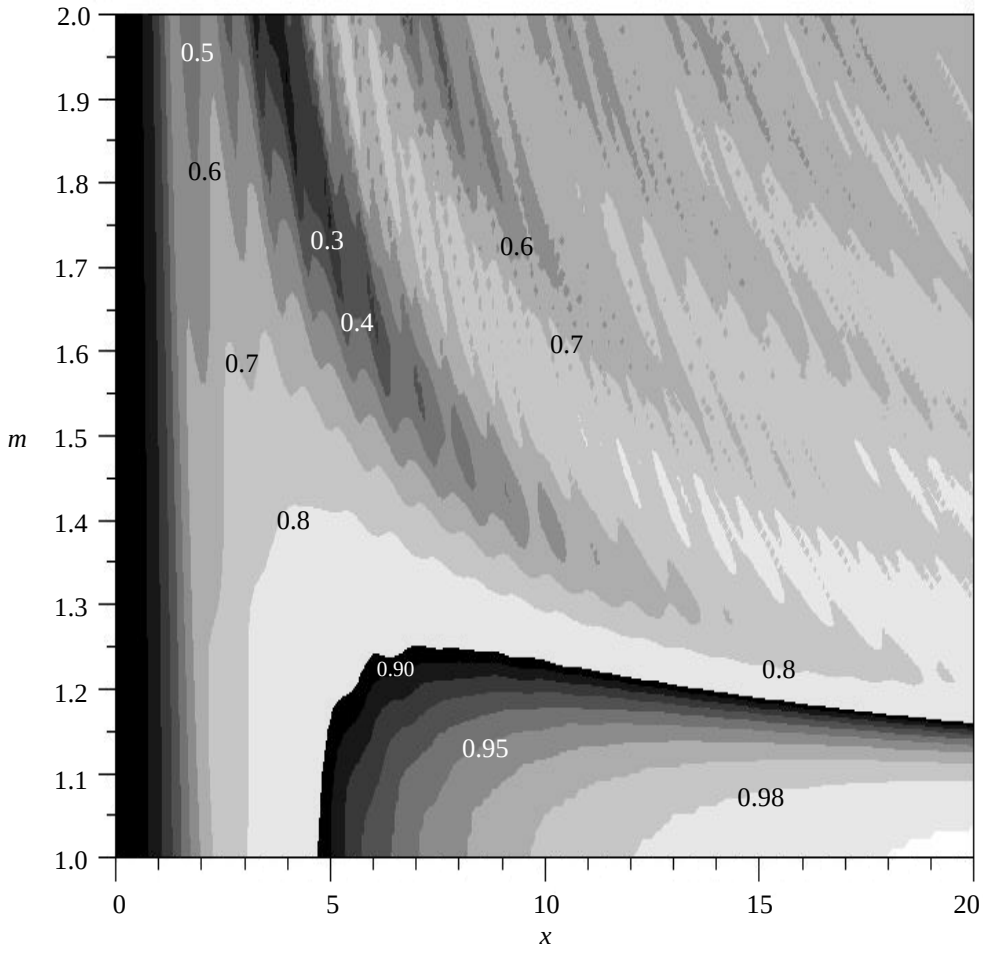

Figure 2.7 The asymmetry parameter g of scattering by spheres as a function of the size parameter x and the refractive index m. From 0.0 - 0.9 each altitude shade differs 0.1, from 0.9 - 1.0 differences of 0.01 are shown.

The functions p_n and t_n present in Equation (2.12) depend on the scattering angle q :

$$p_1(\cos q) = -1 \qquad p_2(\cos q) = -3\cos q$$
$$\text{for } n > 2: \quad p_n(\cos q) = \frac{(2n-1)\cos q\, p_{n-1}(\cos q) - n p_{n-2}(\cos q)}{(n-1)} \tag{2.18}$$

$$t_1(\cos q) = -\cos q \quad \text{for } n > 1: \quad t_n(\cos q) = n\cos q\, p_n(\cos q) - (n+1) p_{n-1}(\cos q) \tag{2.19}$$

The scattering efficiency for spheres is given by:

$$Q_{sca} = \frac{2}{x^2}\sum_{n=1}^{\infty}(2n+1)\left(|a_n|^2 + |b_n|^2\right). \tag{2.20}$$

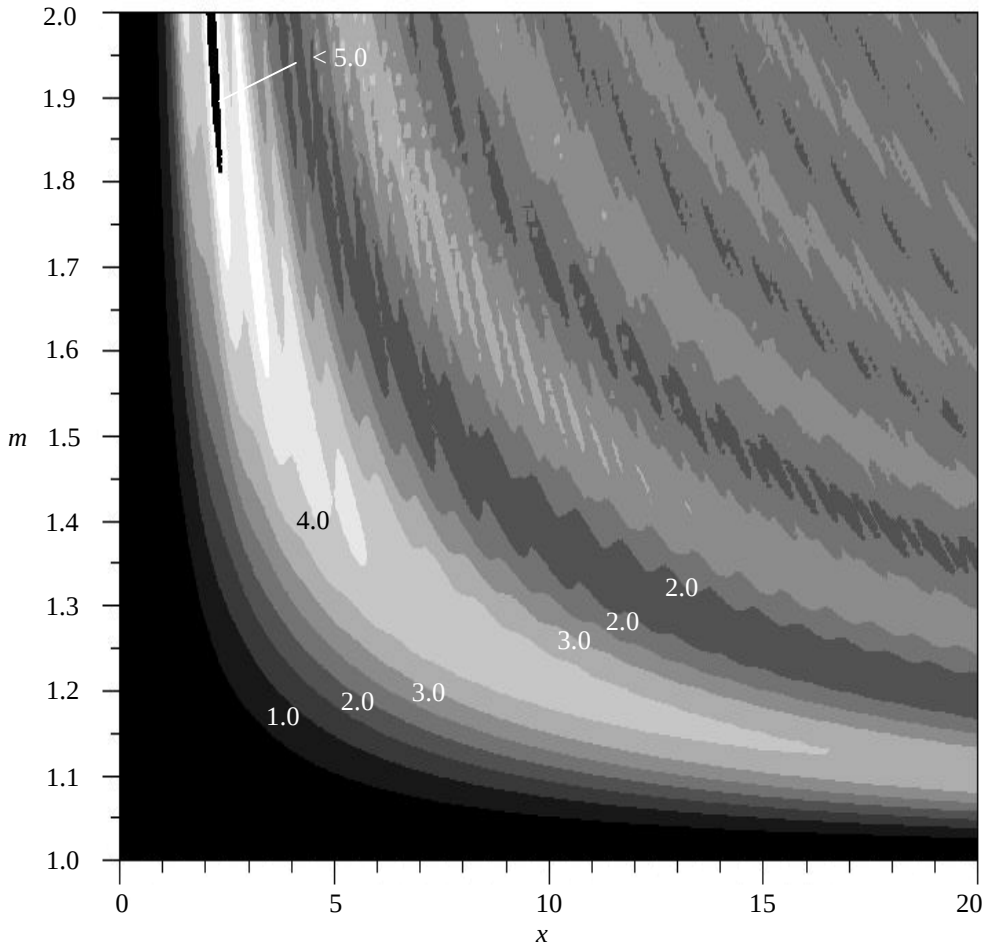

Figure 2.8 The scattering efficiency Q_{sca} of scattering by spheres as a function of the size parameter x and the refractive index m. Each altitude shade differs 0.5.

A computer program in standard ISO PASCAL (Jensen and Wirth, 1985) to perform these Mie-calculations has been published (Zijp and ten Bosch, 1993). The program was tested on personal computers (Graaff *et al*, 1992), and showed sufficient accuracy for most applications within the ranges $0.1 < x < 50$ and $1.025 < m < 1.20$.
The asymmetry parameter g and the scattering cross section Q_{sca} both plotted as functions of x and m are non-monotonic functions. Altitude maps of these functions are shown in Figure 2.7 for g and in Figure 2.8 for $Q_{sca.}$ The strange behaviour of these functions originates from resonances of the waves in the particles.

2.2.4 Scattering by circular cylinders

If radiation is incident on an infinitely long circular cylinder it will be scattered in directions along the surface of a cone, which contains the incident direction (Figure 2.9). The axis of the cone coincides with the axis of the cylinder. In general cross polarisation takes place. The equations for calculation of the scattered field are published by Wait (1955). We will treat

only the very special case that the incident direction is perpendicular to the cylinder axis, it was used in Chapter 5 to calculate the scattering from dentinal tubules. In this case the surface of the cone degenerates to a plane (Figure 2.10). Due to axial symmetry no cross polarisation takes place (van de Hulst, 1981). The scattering plane now is the plane perpendicular to the axis of the cylinder. To make calculations easy the incident radiation is dissected in transverse magnetic (TM-mode) and transverse electric components (TE-mode), representing the components the electrical field parallel and perpendicular to the axis of the cylinder respectively. The scattered field is calculated in components T_1 (TM-mode) and T_2 (TE-mode).

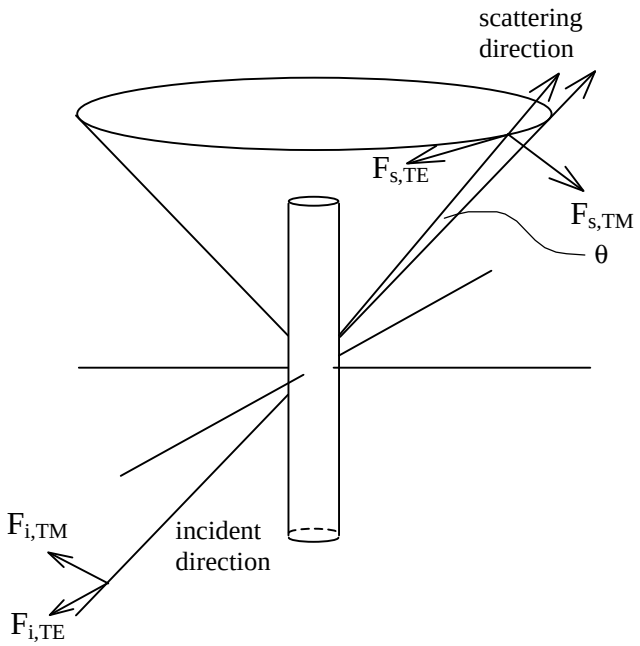

Figure 2.9 Light scattered by a cylinder, into a cone shell with arbitrary incidence direction.

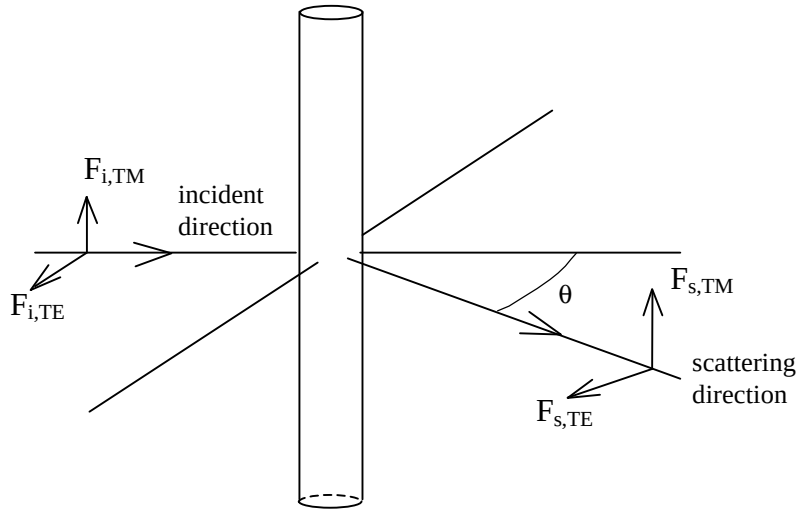

Figure 2.10 Light scattered by a cylinder, with perpendicular incidence (the cone degenerates into a plane).

The amplitude functions for scattering at perpendicular incidence are given by:

$$T_1(q) = b_0 + 2\sum_{n=1}^{\infty} b_n \cos nq$$
$$T_2(q) = a_0 + 2\sum_{n=1}^{\infty} a_n \cos nq \qquad (2.21)$$

The coefficients a_n and b_n in Equation (2.21) read:

$$a_n = \frac{J'_n(mx)\,J_n(x) - m\,J_n(mx)J'_n(x)}{J'_n(mx)H_n^{(2)}(x) - m\,J_n(mx)H'^{(2)}_n(x)}$$
$$b_n = \frac{mJ'_n(mx)\,J_n(x) - J_n(mx)\,J'_n(x)}{mJ'_n(mx)H_n^{(2)}(x) - J_n(mx)H'^{(2)}_n(x)} \qquad (2.22)$$

with $x = ka$ and a as the radius of the cylinder.

The Bessel functions of the first kind J_n and the Bessel functions of the third kind $H^{(2)}_n$ are given by (Abramowitz and Stegun, 1965):

$$J_n(z) = \sum_{r=0}^{\infty} \frac{(-1)^r\, z^{n+2r}}{2^{n+2r}\, r!\,(n+r)!} \quad \text{and} \quad J_{-n} = (-1)^n J_n(z) \qquad (2.23)$$

$$H_n^{(2)}(z) = J_n(z) - i\frac{J_n(z)\cos(np) - J_{-n}(z)}{\sin(np)} \qquad (2.24)$$

Their derivatives are given by:

$$J'_0(z) = -J_1(z) \quad \text{for n > 0:} \quad J'_n(z) = -J_{n+1}(z) + \frac{n}{z}J_n(z) \qquad (2.25)$$

$$H'^{(2)}_0(z) = -H_1^{(2)}(z) \quad \text{for n > 0:} \quad H'^{(2)}_{n+1}(z) = -H_{n+1}^{(2)}(z) + \frac{n}{z}H_n^{(2)}(z). \qquad (2.26)$$

In this case the scattering asymmetry parameter for non-polarised light is calculated by:

$$g = \frac{\int_{q=0}^{p} dq\ \ [T_1(q) + T_2(q)]\ \cos q}{\int_{q=0}^{p} dq\ \ [T_1(q) + T_2(q)]} \qquad (2.27)$$

Note that Equation (2.27) differs from Equation (2.8) because here light is only scattered in a plane. In the case of the spherical scatterers light is scattered in all spatial directions.

The scattering efficiency factor depends on the polarisation with respect to the axis of the cylinder,

for the TM-mode: $$Q_{sca} = \frac{2}{x}\sum_{n=-\infty}^{\infty} |b_n|^2$$

and for the TE-mode: $$Q_{sca} = \frac{2}{x}\sum_{n=-\infty}^{\infty} |a_n|^2 \ . \qquad (2.28)$$

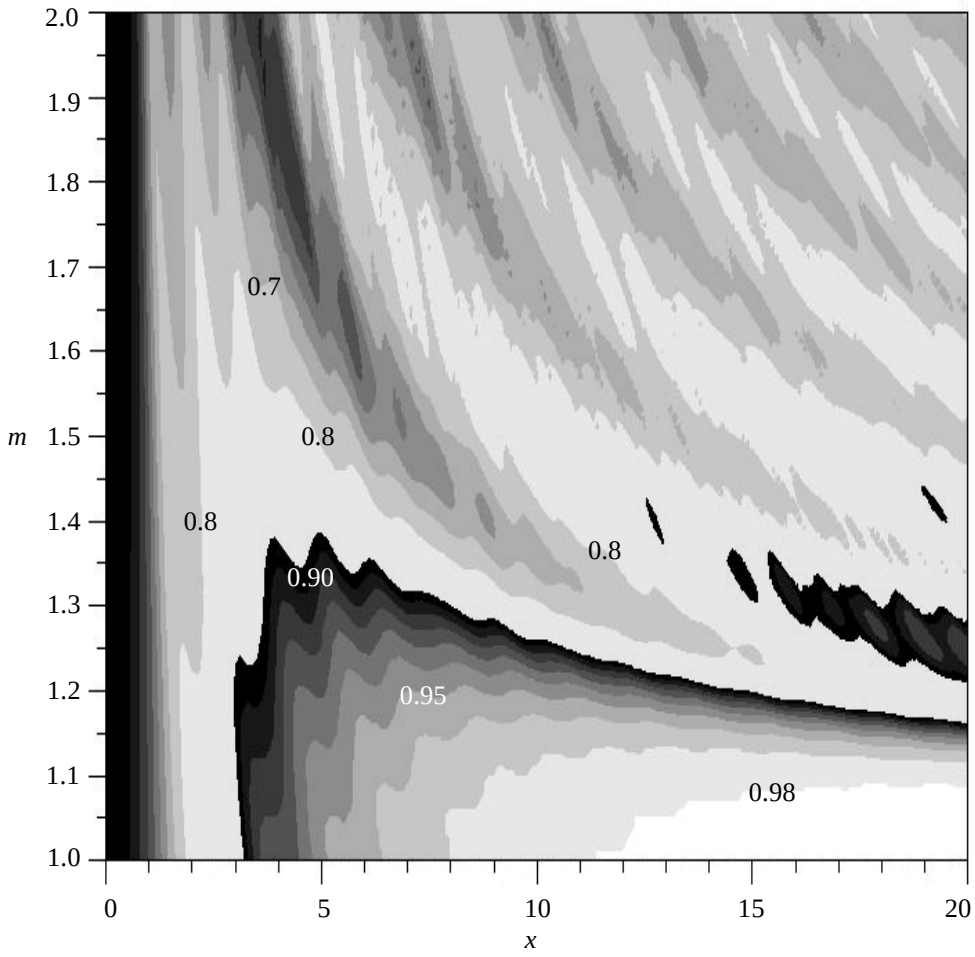

Figure 2.11 The asymmetry parameter g of scattering by cylinders as a function of the size parameter x and the refractive index m. From 0.0 - 0.9 each altitude shade differs 0.1, from 0.9 - 1.0 differences of 0.01 are shown.

The asymmetry parameter g and the scattering cross section Q_{sca} both plotted as functions of x and m are non-monotonic functions. Altitude maps of these functions are shown in Figure 2.11 for g and Figure 2.12 for Q_{sca}.

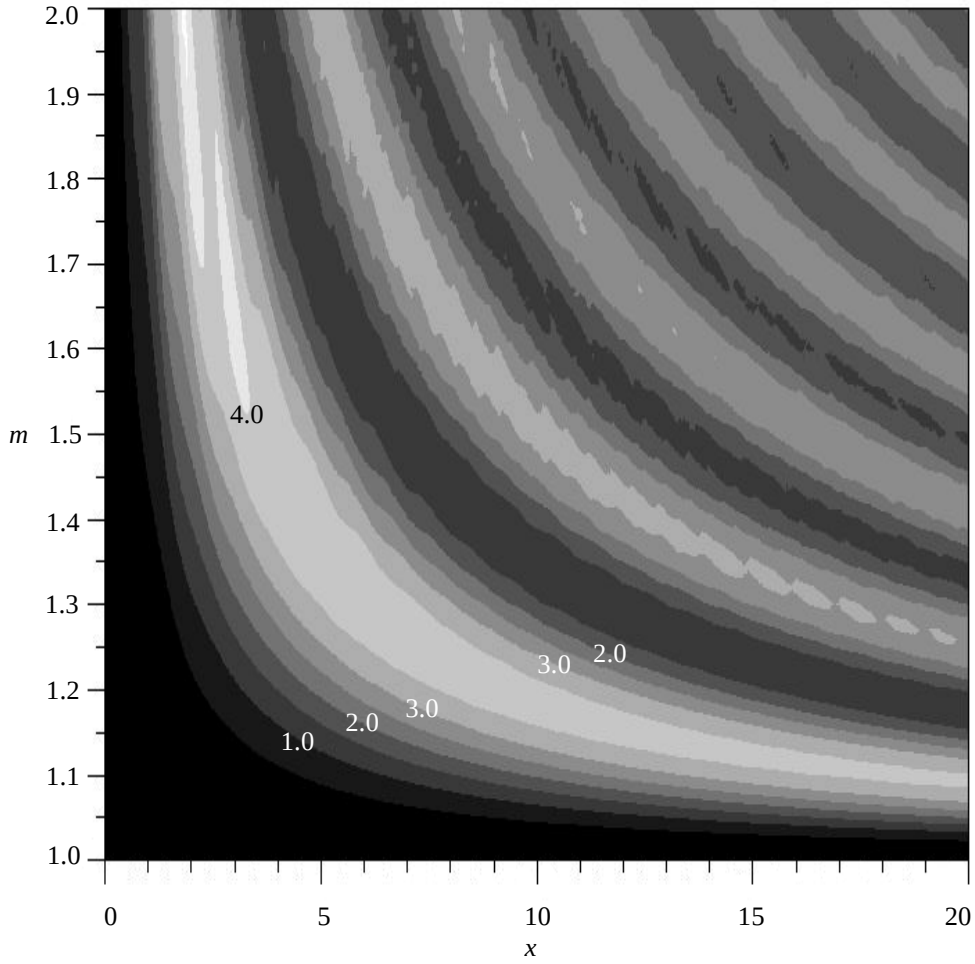

Figure 2.12 The scattering efficiency Q_{sca} of scattering by cylinders at perpendicular incidence as a function of the size parameter x and the refractive index m. Each altitude shade differs 0.5.

2.3 REFERENCES

Beek JF, Blokland P, Posthumus P, Aalders M, Pickering JW, Sterenborg HJCM, van Gemert MJC (1997) In vitro double-integrating-sphere optical properties of tissues between 630 and 1064 nm. *Phys Med Biol* 42:2255-2261

Mie G (1908) Beiträge zur Optik trüber Medien, speziell kolloidaler Metallösingen. *Annalen der Physik* 25:377-445

Molenaar R, ten Bosch JJ, Zijp JR (1999) Determination of Kubelka-Munk scattering and absorption coefficients by diffuse illumination. *Appl Opt* 38:2068-2077

Jacques SL, Alter CA, Prahl SA (1987) Angular dependence of HeNe laser light scattering by human dermis. *Lasers Life Sci* 1:309-333

Jensen KN, Wirth N (1985) *PASCAL user manual and report, ISO PASCAL standard*. 3rd ed. (Springer Verlag, New York)

Klein JD (1965) Radiation heat transfer through scattering and absorbing nonisothermal layers. *Techn Rept NASA* SP-55:73-81

Graaff R, Aarnoudse JG, Zijp JR, Sloot PMA, de Mul FFM, Greve J, Koelink MH (1992) Reduced light-scattering properties for mixtures of spherical particles: a simple approximation derived from Mie calculations. *Appl Opt* 31:1370-1376

Abramowitz M, Stegun IA (1965) *Handbook of mathematical functions*. (Dover Publications Inc., New York).

Pickering JW, Prahl SA, van Wieringen N, Beek JF, Sterenborg HJCM, van Gemert MJC (1993) Double-integrating-sphere system for measuring the optical properties of tissue. *Appl Opt* 32:399-410

Pickering JW, Moes CJM, Sterenborg HJCM, Prahl SA, van Gemert MJC (1992) Two integrating spheres with an intervening scattering sample. *J Opt Soc Am* A9:621-631

van de Hulst HC (1981) *Light scattering by small particles*. (Dover Publications Inc., New York).

Wait JR (1955) Scattering of a plane wave from a circular dielectric cylinder at oblique incidence. *Can J Phys* 33:189-195.

Zijp JR, ten Bosch JJ (1993) Pascal program to perform Mie calculations. *Opt Eng* 32:1691-1695

Zijp JR, ten Bosch JJ (1998) Optical properties of bovine muscle tissue *in vitro*; a comparison of methods. *Phys Med Biol* 43:3065-3081.

Chapter 3 **Optical properties of dentin**

[Previously published as: Optical properties of dentin - J.J. ten Bosch and J.R. Zijp. In: *Dentine and dentine reactions in the oral cavity*, A. Thylstrup, S.A. Leach and V. Qvist, eds. (IRL Press Ltd, Oxford, England, 1987) pp 59-65, by permission of Oxford University Press.]

3.1 ABSTRACT

Absorption, scattering and fluorescence together determine the color of dentin. These properties can probably be used as the basis of quantitative diagnostic methods for caries. It is useful therefore to quantitate these properties when possible. The absorption and scattering coefficient of bovine and human dentin were determined from 170 μm thick wet sections. Bovine incisors and human premolars were used. Several sections, parallel to the labial plane, were cut from the same tooth. Diffuse reflection and transmission of these sections was measured at visible wavelengths with a spectrophotometer equipped with an integrating sphere. Kubelka-Munk theory was used. Transversal microradiography was used to determine the mineral content of a section. The absorption coefficient for fluxes was found to be ~ 0.4 mm^{-1}, rather independent of wavelength, the scattering coefficient for fluxes was found as ~ 3 - 20 mm^{-1}, slowly decreasing with wavelength and hardly related to mineral content. The literature on fluorescence properties is reviewed and discussed. Four emission bands have been observed, at 350, 400, 450 and 520 nm. The chromophores of the first two bands have been identified, the others have not.

3.2 INTRODUCTION

In this paper we will consider some of the macroscopical optical properties of coronal dentin: absorption, scattering and fluorescence. These properties are of twofold relevance. First, they together determine the visual appearance, i.e. the color, of dentin which plays a large role in the color of the complete tooth crown. This aspect is of importance for visual dental diagnosis of dental problems and also for the matching of a prosthetic tooth crown to an adjacent natural crown. Quantitative data will be needed to improve these processes, which up to now are qualitative. Secondly, in enamel these properties have been successfully used to quantitate enamel caries. Development of a similar method for dentinal caries would be of relevance for caries research.

3.3 MATERIALS AND METHODS

3.3.1 Samples

Dentin samples were obtained from bovine incisors and human premolars by cutting slices with an inner hole diamond saw (Borsboom *et al.*, 1987). Slices were cut parallel to the buccal surface of the tooth, from the buccal dentin-enamel junction inward. Slices were roughened on 1200 mesh abrasive paper to increase diffusivity of the light. As many slices as possible were cut from a single tooth, the separation (saw blade thickness) being ~ 220 μm. Slice thickness was of the order of 170 μm. Samples were kept wet until their insertion in the spectrophotometer. Effects of drying during spectrophotometric measurement (~ 15 min) could not be observed.

3.3.2 Absorption and scattering coefficients

For determination of these coefficients we measured the diffuse reflection and diffuse transmission of dentin slices with a dual-beam integrating sphere-attachment (type 124-49) to a Perkin-Elmer type 124 UV-Vis spectrophotometer. Since the samples were smaller than the regular port holes of the sphere, both sample and reference hole were decreased in size with black diaphragms with a 2 x 5 mm opening. In reflection measurements a $BaSO_4$-pill prepared according to standard procedures (DIN 5033, part 9) was used in the reference port hole of the sphere. In transmission measurements, the reference port hole was open.
The Kubelka-Munk theory was used as was done previously for enamel (Spitzer and ten Bosch, 1975). A refractive index value, necessary to estimate surface reflections, was estimated at n = 1.45 based on an estimate of mineral content of 40 volume% and an apatite refractive index of hydroxyapatite of 1.64 (Perloff and Posner, 1956).

3.3.3 Luminescence Spectra

Luminescence data were all taken from the literature.

3.3.4. Mineral Content Determination

Mineral content was determined by traditional Transversal Micro Radiography with a semi-automated densitometer recently described (de Josselin de Jong *et al*., 1987). A single scan was made across the area that was measured optically.

3.4 RESULTS

3.4.1 Absorption and scattering

In between 8 and 11 slices per tooth of 2 bovine incisors and 2 human premolars were measured. Figure 3.1 shows examples of the spectral dependence of absorption and scattering. This spectral dependence is similar for all samples.
Figure 3.2 shows examples of averages of values at wavelengths of 535, 550 and 565 nm as a function of position in the tooth. From the other teeth similar curve shapes were obtained. The height of these curves varies from tooth to tooth, values at the tooth center are given in Table 3.1. Another impression of the distribution of scattering coefficients can be obtained from Figure 3.3, which depicts the scattering coefficients of all slices versus the mineral content of these slices.

Table 3.1 Absorption and scattering coefficients in mm^{-1} for the center part of the coronal dentin (with estimated s.e.).

		A	S
bovine samples	1	0.45 (0.1)	14 (2)
	2	0.25 (0.1)	26 (4)
human samples	3	0.4 (0.1)	3 (0.5)
	4	0.8 (0.1)	8 (1)

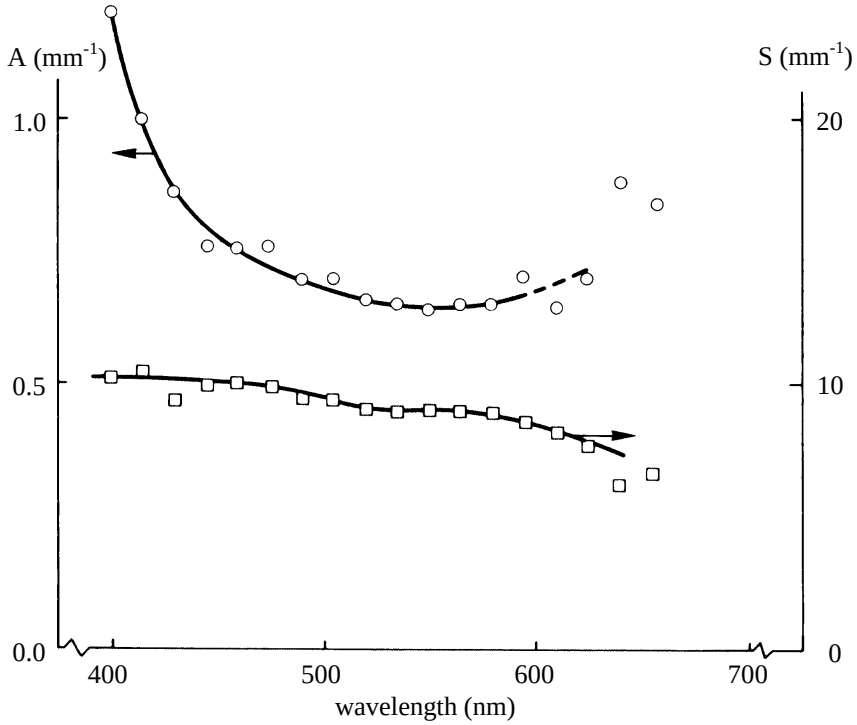

Figure 3.1 Examples of spectral dependence of absorption (○) and scattering (□).

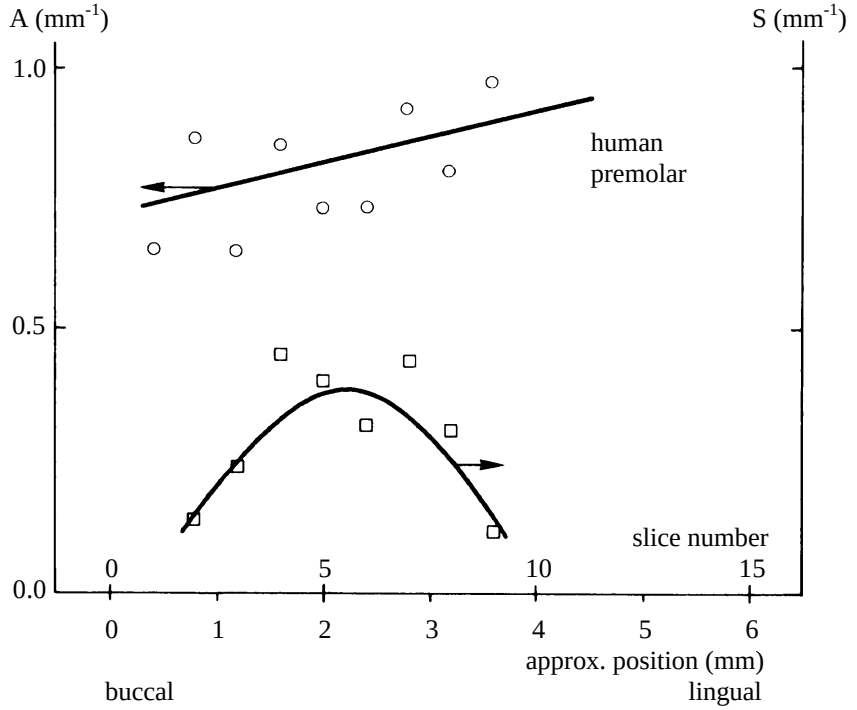

Figure 3.2 Dependence of absorption (○) and scattering coefficients (□) at 500 nm on the position of the slice in the tooth. Other teeth showed similar dependences.

Table 3.2 Fluorescence peak positions.

Optimum excitation	Maximum emission	Chromophore
< 300 nm	~ 350 nm	traces of trypthophan
325 nm	~ 400 nm	hydroxypyridinium
380 nm	450 nm	unknown
410 nm	520 nm	unknown

3.4.2 Luminescence

Numerous publications deal with luminescence of dentin, most consider fluorescence at room temperature only. Such fluorescence occurs at 4 bands. A summary is given in Table 3.2.
Excitation around and below 300 nm leads to emission around 350 nm (Hoerman and Mancewicz, 1964; Perry *et al*., 1969), which has been ascribed tentatively to traces of tryptophan (0.5 residue/1000). The next emission band shows a maximum around 400 nm. It has been investigated by several research groups (Perry *et al.*, 1969; Armstrong and Horsley, 1966). The origin of this emission is a collagen crosslink: hydroxypyridinium, of which there exist two forms (Fujimoto *et al*., 1977; Walters and Eyre, 1983). The fluorescence of this chromophore is excited optimally at 325 nm in neutral or alkaline conditions and at 300 nm in acid conditions (Fujimoto *et al*., 1977).
Fluorescence emission with a peak around 450 nm has been reported by Scharf (1971) and by Alfano and Yao (1981). Optimum excitation seems to be around 380 nm. Finally, a broad peak, often appearing as a shoulder on the 450 nm peak, is present at 520 nm but slowly decreases at higher wavelengths. This emission is excited optimally at 410 nm (ten Bosch *et al*., 1986). It is also caused by the organic component of the tissue but the chromophore is unknown. The color coordinates of these emissions, when excited by 365 nm radiation, have been given by Scharf (1971).
Other types of luminescence have been studied scarcely. Hefferren et al. (1971) report phosphorescence at liquid nitrogen temperature with an emission around 445 nm. Kolberg *et al.* (1974) report X-ray induced thermoluminescence peaking at 480 nm, which is ascribed to the dentin mineral.

3.5 DISCUSSION

3.5.1 Absorption and scattering

The scattering results show first of all that the scattering coefficient is not related to mineral content (Figure 3.3). This implies that the mineral crystals are not the predominant cause of scattering of light in dentin. Accordingly, larger structures such as the dentinal tubules, must be the cause.
This is confirmed by the results which show the wavelength dependence of the scattering (Figure 3.1), which is somewhat but not much higher at shorter wavelengths than at longer wavelengths. This rather small wavelength dependence points at large scatterers. Also, near the enamel-dentinal junction the scattering is low (low tubule density and small tubuler size)

compared to in the dentin directly adjacent to or above the pulp (high tubule density and large tubule size) (Figure 3.2).

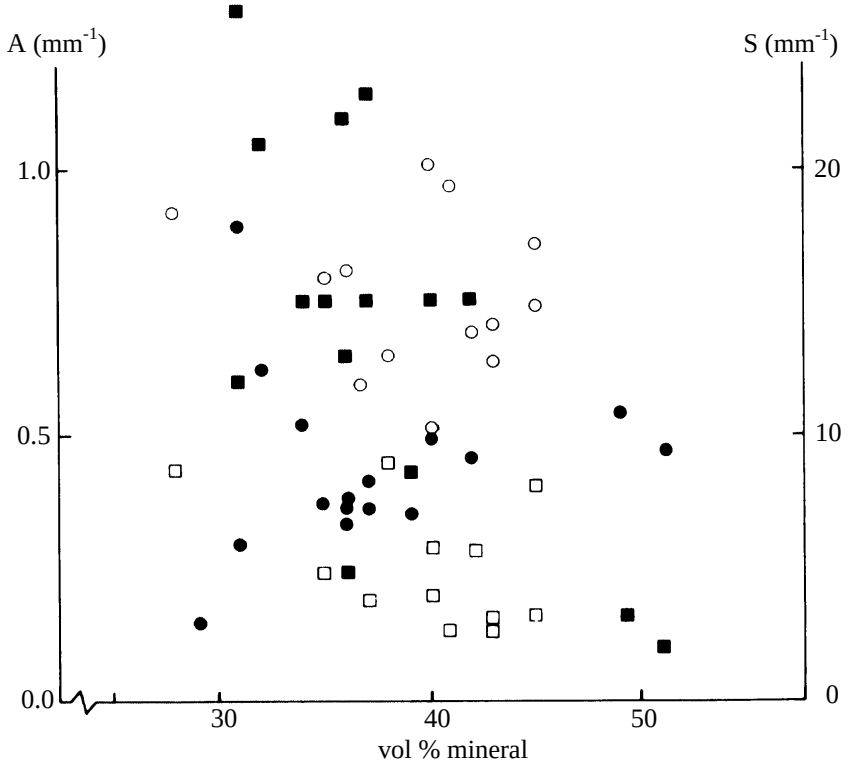

Figure 3.3 Scattering and absorption coefficients of all samples at 500 nm versus mineral content of these samples in volume percent mineral.
(□ ,○): human premolar samples, (■ ,●): bovine incisor samples.

The absorption results also are not strongly wavelength dependent. At 400 nm the beginning of a rise of the coefficient in the ultraviolet can be seen, possibly due to collagen crosslinks (viz. fluorescence). In the visible the absorption spectrum is rather flat. Although this is consistent with the greyish-yellowish color, it does not give any clue to the cause of the absorption. There is no systematic change of absorption with position in the tooth.
The scattering coefficients in human premolars found are of the order of 3 mm^{-1} near the EDJ, of the order of 8 mm^{-1} near the pulp. Values for bovine incisors are higher by a factor 2 - 3. These values can be compared with those of sound enamel: ~ 3 mm^{-1} for scattering, ~ 0.1 mm^{-1} for absorption (Spitzer and ten Bosch, 1975). Since the penetration depth of light in a material is roughly the inverse of the sum of both coefficients it can be understood quantitatively that the dentin only, and even the inner part of the dentin predominantly, determines the opacity of a non-carious tooth. Specifically, scattering is the dominating process, as it is in dental enamel (Spitzer and ten Bosch, 1975).

3.5.2 Fluorescence

The fluorescence bands of dentin can be compared with those of dental enamel. The 400 nm emission in enamel was rather carefully investigated by Booy and ten Bosch (1982) and ascribed to a compound very similar to dityrosine. This conclusion was based on a

comparison of emission and excitation spectra and their pH-dependence and on Biogel P2- and thin-layer-chromatography. Although the positions of the emissions and excitation maxima of the corresponding band in dentin are very similar, the emission has been ascribed to an entirely different chromophore on the basis of many different techniques.
The fluorescence emissions in the visible have also been observed in enamel (ten Bosch *et al.*, 1986, Sundström *et al.* 1985). They show the same spectral characteristics. Biochemical analysis of either chromophore has, as far as we know, not yet been performed. In view of the demonstrated possibility to use these emissions for caries diagnosis (Bjelkhagen, 1982), such research seems useful.

3.6 CONCLUSION

In conclusion, the visual appearance of dentin can semi-quantitatively be ascribed to the rather flat wavelength dependence of absorption and scattering, the latter specifically being due to the high density of tubules in the inner dentin layers. The fluorescence bands of dentin and enamel are very similar, but the 400 nm emissions band of both tissues are nevertheless due to different chromophores. The cause of emissions at higher wavelengths is unknown.

3.7 REFERENCES

Alfano RR, Yao SS (1981) Human teeth with and without dental caries studied by visible luminescent spectroscopy. *J Dent Res* 60:120-122.

Armstrong WG, Horsley HJ (1966) Isolation of fluorescent components from ox-bone, human dentine, and gelatin. *Nature* 211:981.

Bjelkhagen H, Sundström F, Angmar-Månsson B, Rydén H (1982) Early detection of enamel caries by luminescence excited by visible laser light. *Swed Dent J* 6:1-7.

Booij M, ten Bosch JJ (1982) A fluorescent compound in bovine dental enamel matrix compared with synthetic dityrosine. *Archs Oral Biol* 27:417-421.

Borsboom PCF, Wolfs BHJ, Leydsman H, Doorn N, ten Bosch JJ, Liem KG (1987) A machine for sawing 80-micrometer slices of carious enamel. *Stain Technol* 62:119-125.

Fujimoto D, Akiba K, Nakamura N (1977) Isolation and characterization of a fluorescent material in bovine achilles tendon collagen. *Biochem Biophys Res Comm* 76:1124-1129.

Hefferren JJ, Hall JB, Bennet E (1971) Luminescence as a tool to study enamel interactions. In: *Tooth enamel II*. RW Fearnhead and MV Stack, eds., (Wright, Bristol, England) pp.161-165

Hoerman KC, Mancewicz SA (1964) Fluorimetric demonstration of tryptophan in dentin and bone protein. *J Dent Res* 43:276-280.

de Josselin de Jong E, ten Bosch JJ, Noordmans J (1987) Optimized microcomputer-guided quantitative microradiography on dental mineralised tissue slices. *Phys Med Biol* 32:887-899.

Kolberg S, Prydz S, Dahm S (1974) Thermally stimulated luminescence in dental hard tissues and bone. *Calcif Tiss Res* 17:9-23.

Perloff A, Posner AS (1956) Preparation of pure hydroxyapatite crystals. *Science* 124:583-584.

Perry A, Biel M, DeJongh O, Hefferren J (1969) A comparative study of the native fluorescence of human dentine and bovine skin collagens. *Archs Oral Biol* 14:1193-1211.

Scharf F (1971) Uber die naturliche Lumineszenz der Zahnhartgewebe "Schmeltz und Dentin". *Stoma* 1:10-25

Spitzer D, ten Bosch JJ (1975) The absorption and scattering of light in bovine and human dental enamel. *Calcif Tiss Res* 17:129-137.

Sundström F, Frederiksson K, Montán S, Hafström-Björkman U, Ström J (1985) Laser-induced fluorescence from sound and carious tooth substance: spectroscopic studies. *Swed Dent J* 9:71-80

ten Bosch JJ, Angmar-Månsson B, Booij M, Sundström F (1986) Long-wavelength fluorescence of bovine tooth components (abstract). *Caries Res* 20:286-287

Walters C, Eyre DR (1983) Collagen crosslinks in human dentin: increasing content of hydroxypyridinium residues with age. *Calcif Tissue Int* 35:401-405.

Chapter 4 Angular dependence of HeNe-laser light scattering by bovine and human dentine

[Previously published as: Angular dependence of HeNe-laser light scattering by bovine and human dentine - J.R. Zijp and J.J. ten Bosch, Archives of Oral Biology, Vol. 36, 283-289, Copyright 1991, by permission of Elsevier Science]

4.1 SUMMARY

The scattering phase functions for HeNe-laser light of dentine sections 10 - 20 μm thick were measured. The functions perpendicular to the tubules had first-order maxima at angles of 4° for bovine dentine and 5° for human dentine; those parallel to the tubules showed no first order maxima. Several corrections were made before the asymmetry factors g for intertubular dentine were determined; the average values are for bovine dentine g = 0.37 and for human dentine g = 0.44.

4.2 INTRODUCTION

The behaviour of light in dentine may be examined in order to match prosthetic materials to natural dentine, and to assess if optical measurements can provide an indirect measure of dentine caries.

The optical matching of restorative and prosthetic materials has been by trial, error and experience, with both very good and very bad results (van der Burgt *et. al*., 1985). Better matching may be achieved by a better understanding of the optical processes in natural tissues. In both dental enamel and dentine, light scattering is the most important determinant of colour and appearance. In enamel the hydroxyapatite crystals are mainly responsible for this (Spitzer and ten Bosch, 1975). It is already possible to quantify enamel caries by measuring light scattering (ten Bosch *et al*., 1984). In dentine the tubules are the most important scatterers (ten Bosch and Zijp, 1987). When dentine is decalcified by caries, the cross-section of the dentinal tubules is increased (Arends *et al.*, 1989). This causes a change in the scattering properties, which in future might be used to quantify dentine caries.

The absorption (K) and scattering (S) coefficients for diffuse light in dentine have been recorded by ten Bosch and Zijp (1987). We have now measured the angular dependence of the light scattering and the anisotropy factor g.

4.3 THEORY

The colour of all materials is determined by the diffuse absorption coefficient K, the diffuse scattering coefficient S and the phase function $I(q)$ of the scatterers. In translucent materials, like dental enamel and dentine, the light penetrates the material before it re-emerges. The absorption, and therefore the colour is exponentially dependent on the penetration path. The thickness of teeth at the edges is about the same order of length as the real free path of the photons. So the phase functions, which describe the intensity of the scattered light as a function of the scattering angle, have to be known for good colour matching. In general the phase functions depend on the directions of polarization of both the incident and the scattered light. In most calculations the

asymmetry factor *g*, the mean cosine of the scattering angle of all photons, is used to estimate the penetration path length. *g* can be determined by:

$$g \equiv \frac{\int_{0°}^{180°} dq \int_{0°}^{360°} dj \; I(q,j) \cos q}{\int_{0°}^{180°} dq \int_{0°}^{360°} dj \; I(q,j)} \tag{4.1}$$

When the scattering phase function is circularly symmetrical round the axis of the incident beam:

$$g = \frac{\int_{0°}^{180°} dq \; I(q) \cos q \sin q}{\int_{0°}^{180°} dq \; I(q) \sin q} \tag{4.2}$$

For low *g* values ($g \approx 0$) the scattering process is isotropic and a photon re-emerges at the surface after a short path and contributes to volume reflection. For high *g* values ($g \approx 1$) the scattering is forward peaked, so that light paths are long and there is a relatively high probability of absorption. The linear absorption coefficient *a* will be neglected in this paper, because in dentine $a = K/2$ is small compared to *S*. *S* can be converted to the scattering coefficient for collimated beams *s*, by $s = (4S + a) / (1 - g) \approx 4S / 3(1 - g)$ for $a << 4S$ (Meador and Weaver, 1979). We define the effective mean free path S^{-1}, which is the mean distance covered by a photon before it is backscattered, and the real mean free path s^{-1}, which is the mean distance that a photon covers between two collisions with scatterers.

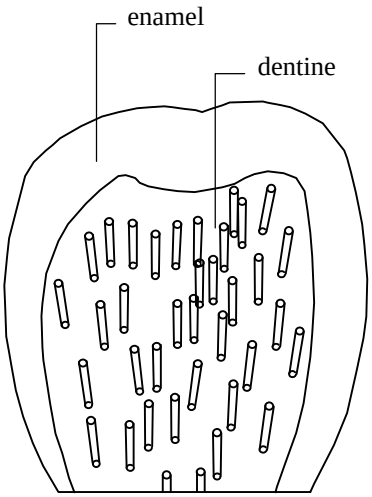

Figure 4.1 Schematic outline of a dentine section, tubules not to scale

In dentine sections, as schematically drawn in Figure 4.1, scattering can be split up in to three distinct processes. Firstly a rotation-symmetrical process (round the principal axis) caused by surface roughness of the sections. Secondly, a rotation-symmetrical process caused by stochastic inhomogeneities in density. Thirdly a rotation-asymmetrical process caused by the presence of the tubules which are oriented from the pulp to the dentine-enamel junction, and so are lying parallel when a small area is observed. If the tubules are considered as infinitely long, straight cylinders, they will scatter only in the plane perpendicular to their axes (van de Hulst, 1957).
When a thin section is observed in a transmission light microscope, it is apparent that it can be considered as a periodic grating of transparent intertubular dentine between oblique rods, *i.e.* the tubules surrounded by peritubular dentine. Such a grating will cause Fraunhofer diffraction, the spacing d between the tubules follows from $d = n\lambda/\sin\theta$, in which $n = 1.45$ (ten Bosch and Zijp, 1987) is the index of refraction of intertubular dentine. Fraunhofer diffraction was also observed in human dental enamel by O'Brien (1988), caused by the periodical presence of slits between the hydroxyapatite prisms.

4.4 MATERIALS AND METHODS

From the buccal side of two freshly extracted bovine incisors and six human third molars, 80 μm sections of dentine were cut, parallel to the buccal surface. These 10 and 34 sections, respectively, were stuck into a 10 μm deep groove in a metal disk, and sanded down to 20 μm on 1200-mesh sanding paper, and ultrasonically cleaned in water to reduce the smearlayer. The sections were stored on wetted tissues until measurement.
The measurement equipment is schematically outlined in Figure 4.2. An incident beam, supplied by a 5 mW HeNe-laser ($\lambda = 632.8$ nm) polarized 45° with respect to the vertical, enters a glass cell filled with millipore filtered water (Millex-GV 0.22μm, Millipore S.A., Molsheim, France). For scattering angles from 168° to 20° we used a round cell (type 540.114-OS 25 mm Hellma, Mullheim/Baden, Germany), because at all these angles the water-glass and the glass-air interface are perpendicular to the scattered light, and so the reflections at the interfaces are minimal. The incident beam is convergent after entering the round cell. This will mainly disturb the measurement at low scattering angles. Therefore at scattering angles 20° - 0° we used a square cell (type 101.062-OS 20 mm). At these angles a neutral density filter was placed in the incident beam to prevent saturation of the detection system. The measured phase functions at these angles were corrected for the index of refraction transition at the water-glass and the glass-air junctions, which cause enlarging of the observed scattering angle in air and the angle of acceptance of the detector with respect to these angles in water.
A T-shaped holder, painted black to prevent forward scattered light being reflected backward by the cylindrical cell wall, was placed in the centre of the scattering cell. The dentine section was mounted on this holder, and adjusted so that no scattering from scratches was observed. The section was placed in water, to achieve low surface reflections at the water-dentine junctions.
The centre of the section was focused with a single 57 mm lens on a photodiode mounted at a turnable bar 405 mm from the centre of the cell; the position of the bar and the measured intensity were read by a computer. A red filter was used to prevent the blue gas-discharging light from reaching the detector. The steric angle of observation was sufficiently large at 8×10^{-5} sr to smooth speckle patterns. Eight readings were taken for each sample: the polarization filter in front of the detector horizontal and vertical, at high and low scattering

angles (with the round and the square scattering cell, respectively) and in plane of and perpendicular to the tubule axes.

Like Jacques *et al.* (1987), we normalised the measured phase functions in the plane of the tubules to 2π. We further adopted their principle of plotting but did not adopt an isotropic scattering function to account for backward scattering. Thus, we plotted $I(q)^{-3/2}$ as a function of $\cos q$. In the interval $0.7 < \cos q < 0.92$ this plot appeared linear, indicating that $I(q)$ resembled a Henyey-Greenstein phase function (Henyey and Greenstein, 1941). We extrapolated the linearity towards $\cos q = 1.0$, which gave calculated $I(q)$ values in this q interval including $I(0°)$. In the interval of $q \approx 90°$ we assumed the phase functions to be linear and equal to the measured values at the borders of the interval, as indicated by the dotted lines in Figures 4.4(a) and 4.5(a). In the interval $q \approx 180°$ we assumed the phase functions to be constant and equal to the value at 168°. After these corrections we calculated the anisotropy factor g by Equation 4.2.

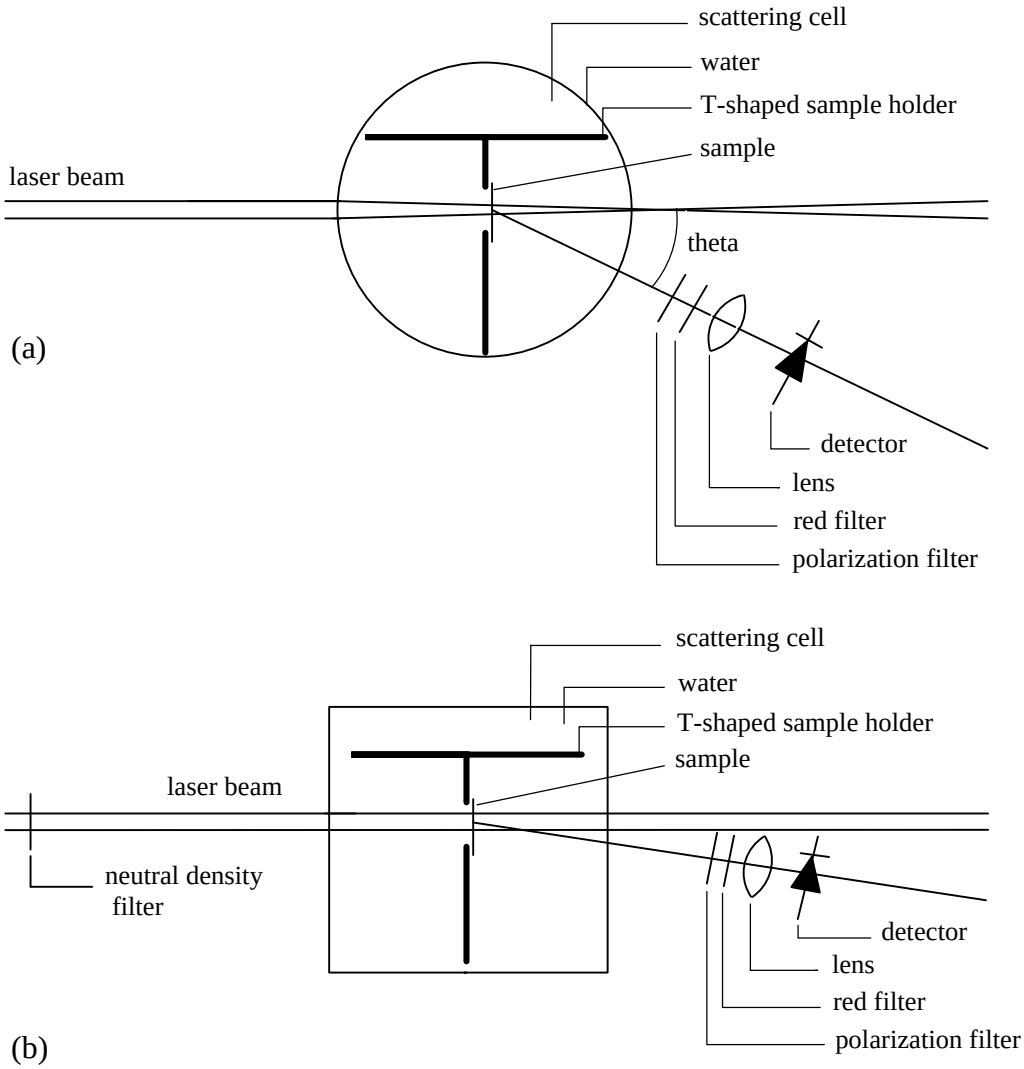

Figure 4.2 Schematic outline of the measurement equipment.
(a) For angles 168° - 20°.
(b) For angles 20° - 0°.

The transmission of the sections at $q = 0°$ was measured. The contribution of $I(0°)$ to this transmission was very small and neglected, as were reflections at the dentine-water interface. The mean thickness of each section was calculated from micrometer measurements at five different points.
The phase functions of two monodispersed polystyrene latex suspensions (∅ 688 nm and 2010 nm) were measured to check the sensitivity of the equipment. These suspensions were diluted to a mass concentration of 1.6×10^{-6} solid to guarantee single scattering in the cell (Harris *et al.*, 1967). All values shown are means with their standard deviation.

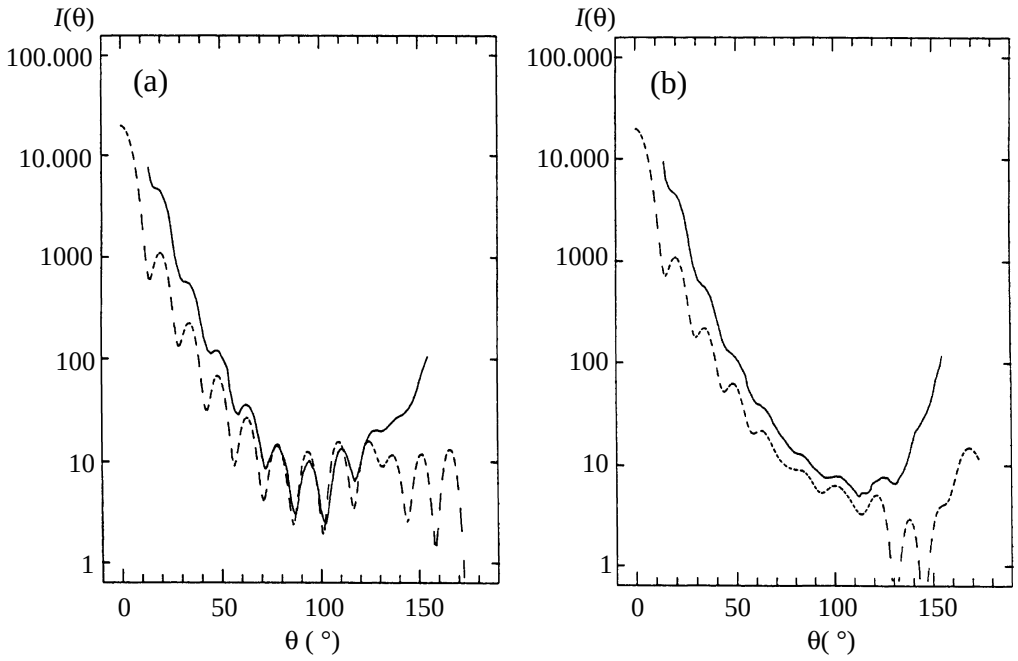

Figure 4.3 Comparison of calculated and measured phase functions of 2010 nm polystyrene latex spheres in water.
(a) Polarization perpendicular to plane of scattering.
(b) Polarization parallel to plane of scattering.
Full lines: measured; interrupted lines: theoretical.

4.5 RESULTS

The measured and theoretical single scattering phase functions of 2010 nm latex spheres in water are shown in Figure 4.3. In Figure 4.3(a) the light is polarized perpendicular to the plane of scattering (vertical); in Figure 4.3(b) the light is polarized in the plane of scattering (horizontal); in both figures the intensity axis is logarithmic.
In Figure 4.4 the measured phase functions of a typical bovine dentine sample are shown: in Figure 4.4(a) with the tubules oriented parallel to the plane of scattering; in Figure 4.4(b) with the tubules perpendicular to the plane of scattering. Figures 4.5(a) and 4.5(b) show the phase functions of a typical human sample. These do not depend on the orientation of the polarization filter in front of the detector. The functions are strongly forward-peaked. In the plane perpendicular to the tubules there is a first-order maximum; for bovine dentine at 4° (± 0.8°), and for human dentine at 5° (± 0.6°). The g values determined from the corrected

phase functions in the plane of the tubules are shown in Table 4.1. Table 4.2 gives an overview of the optical properties of dentine at 633 nm.

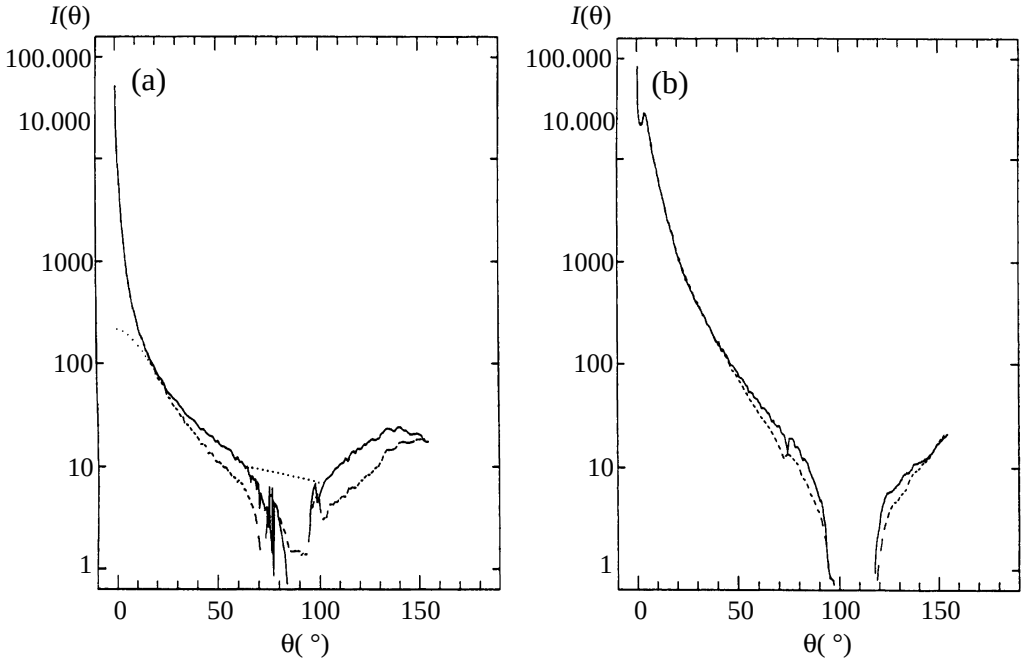

Figure 4.4 Measured (unnormalised) phase functions of bovine dentine with tubules parallel (a) and perpendicular (b) to plane of scattering. Full and interrupted lines: polarization perpendicular and parallel to this plane, respectively. Dotted lines: correction for sample holder (≈ 90°) and Henyey-Greenstein function approximation (≈ 0°)

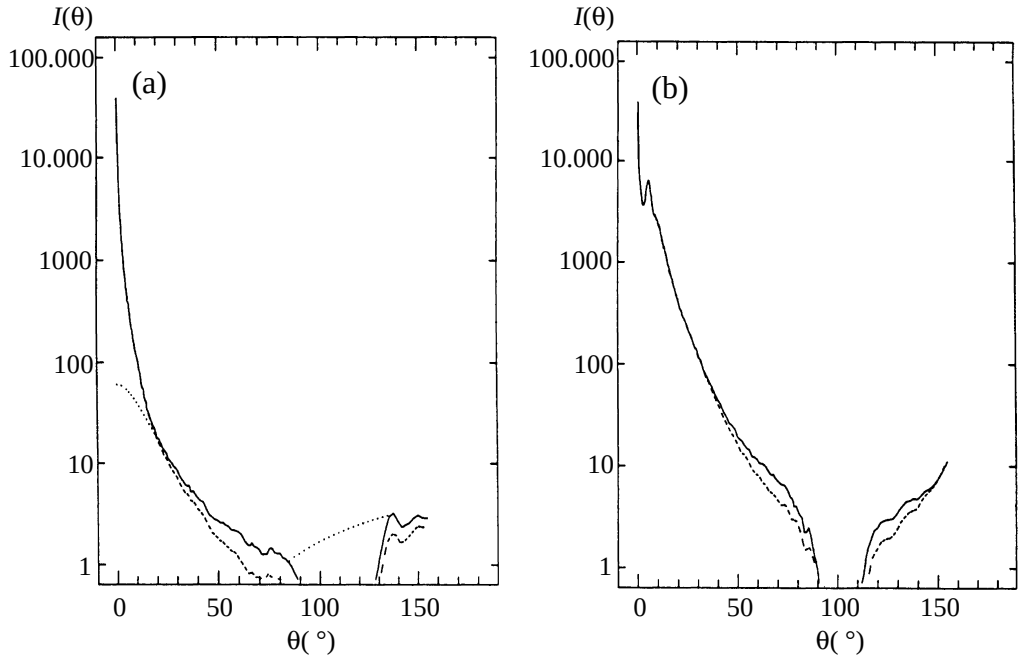

Figure 4.5 As Fig. 4.4, but for human dentine.

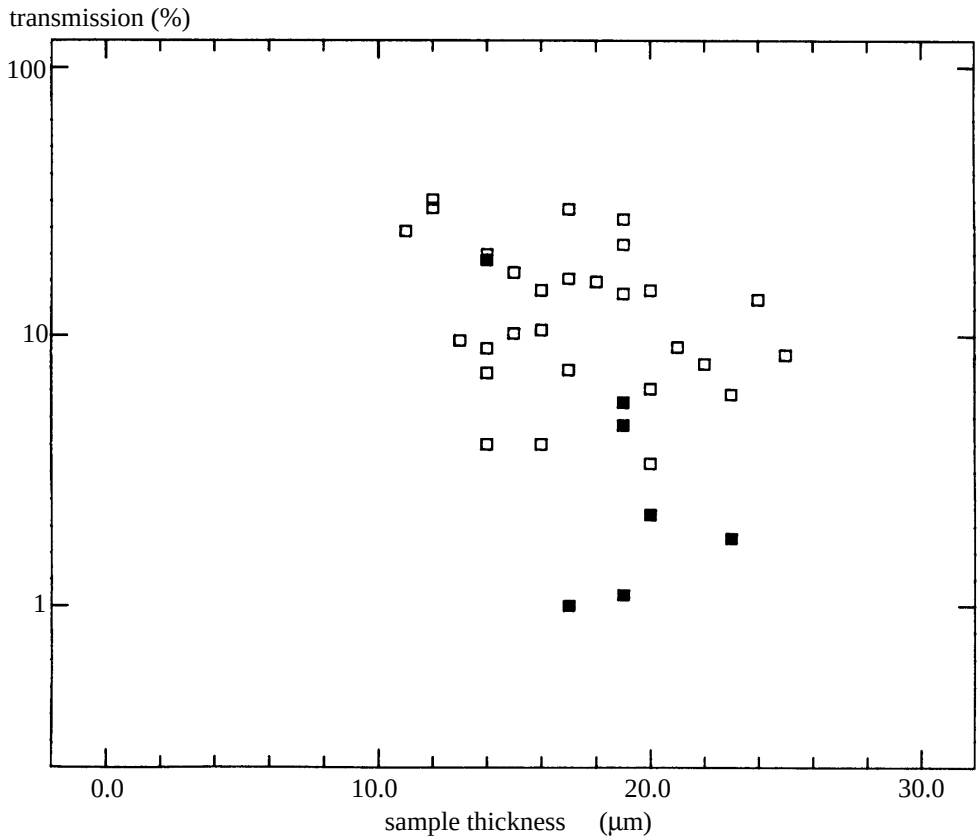

Figure 4.6 Transmission at q = 0° of the samples as a function of sample thickness. ■ Bovine dentine. □ Human dentine.

The measured collimated transmission of most sections at q = 0° is plotted as a function of the sample thickness in Figure 4.6.

4.6 DISCUSSION

4.6.1 The scattering coefficient

Comparison of the measured and the calculated scattering phase functions of the 2010 nm polysterene latex spheres shows agreement in form near 90°; the deviations at lower and higher scattering angles are probably caused by internal reflections and enlarging of the cross-section of the observation beam and the incident beam. This indicates that our equipment is sensitive enough to measure the phase functions of single light scatterers. The measured phase functions of 688 nm spheres showed similar deviations.

As our samples are made as thin as possible, the effect of multiple scattering will be small. The effective mean free path can be estimated by using $S = 8\ mm^{-1}$ at 633 nm (ten Bosch and Zijp, 1987), $S^{-1} = 1/8\ mm = 0.13\ mm$, which is long compared to the thickness of the samples. Taking a mean value for $g = 0.4$ (Table 4.2.), the real mean free path can be estimated at 0.011 mm, a value of the order of the sample thickness.

4.6.2 The phase functions

The phase functions as shown in Figures 4.4 and 4.5 have a minimum around 90°, possibly due to the shadow of the T-shaped sample holder, or to multiple scattering, because at this angle the light path through the material is much longer than the intertubular distance. In shape as well as in the location of minimum and ratio between maximum and minimum intensity, these curves resemble those of other tissues (Marchesini *et al.*, 1989).
The species of the sample cannot be deduced from the form of its phase function, because of the very large intra-species differences.
The curves in Figures 4.4(b) and 4.5(b) are higher than those in Figures 4.4(a) and 4.5(a) for angles in the region 3° - 90° and so the main part of the intensity is scattered perpendicular to the tubules. This is an other demonstration that the tubules are the main scatterers. The first-order maxima of the measured phase functions in the plane perpendicular to the tubules, can be explained in two ways. Firstly, maxima in the single scattering-phase functions of the tubules may cause similar maxima for thin sections (Zijp and ten Bosch, 1991). Secondly, they may be due to Fraunhofer diffraction. This would suggest an intertubular spacing of 6 μm for bovine dentine, and 5 μm for human dentine, both lower than the 10 μm and 6 μm intertubular distances measured on microphotographs of several other samples. The lack of second-order maxima may result from lack of constancy in the intertubular distance, the variations in plane of the tubules, and the variations from exact parallelism of the tubules. In view of these complications and possible coherence effects we did not investigate this further.

4.6.3 The *g* values

From Table 4.1 we see that the *g* values do not depend on the orientation of the polarization filter in front of the detector. We expected this because Figures 4.4 and 4.5 do not show any principal difference between these phase functions.
The *g* values we found are much lower than those found for human blood (0.974) and several soft tissues (chicken muscle 0.965 ± 0.004, bovine muscle 0.954 ± 0.016, and pig brain 0.940 ± 0.029) (Flock, Wilson and Patterson, 1987) and human dermis (0.82) (Jacques, Alter and Prahl, 1987). For good colour matching we recommend prosthetic dentine materials having a *g* value between 0.32 and 0.48.

Table 4.1 *g* Values and angles of first order maxima

g Values determined		
Polarization	Bovine $n = 10$	Human $n = 34$
Horizontal	0.32 ± 0.08	0.39 ± 0.07
Vertical	0.41 ± 0.09	0.48 ± 0.08
Angle of first-order maxima (°)		
	4.0 ± 0.8	5.0 ± 0.6

Mean values ± standard deviations

4.6.4 The transmission at q = 0°

Figure 4.6 demonstrates that there is no strong relation between the sample thickness and the transmission of the sections at q = 0°. No relation was expected because for thin sections the biological variations in tubule density and tubule cross-section affect the transmission more than the sample thickness. Nevertheless, an average linear scattering coefficient s can be estimated from these values using the Lambert-Beer law: $T = e^{-sd}$. For the bovine dentine samples the mean thickness is 18.7 µm and the mean value of ln(T) is -3.50. Thus s = 200 mm^{-1} and so $S = 3 \times s(1 - g) / 4$ = 89 mm^{-1}, which is much higher than our previous published values of 14 - 26 mm^{-1} (ten Bosch and Zijp, 1987). For human dentine the mean value of the sample thickness is 17.3 µm and the mean value of ln(T) is -2.14. Thus s = 120 mm^{-1} and so $S = 3 \times s\,(1 - g) / 4$ = 52 mm^{-1}, which is also much higher than our previous published values of 3 - 8 mm^{-1} (ten Bosch and Zijp, 1987). The s values compare favorable with values for soft tissue (e.g. Marchesini *et al.*, 1989, and Parsa, Jaques and Nishioka, 1989), which range 15 - 50 mm^{-1}. As dentine is a mineralised tissue with larger internal differences in refractive index, s values higher by a factor < 10 are not surprising.

Table 4.2 Optical properties of dental materials at 633 nm

Material	scattering s(mm^{-1})	absorption a(mm^{-1})	anisotropy g
bovine dentine	200[1]	0.35[2]	0.36[3]
human dentine	120[1]	0.60[2]	0.44[3]
bovine enamel	0.054[4]	0.097[4]	-
human enamel	0.11[4]	0.097[4]	-

[1]This work.
[2]From K value cited in ten Bosch and Zijp (1987) $a = K/2$.
[3]This work, average of values for perpendicular and horizontal polarization.
[4]From s_c and a_c cited in Spitzer and ten Bosch (1975).

The discrepancy in S values probably arises from our earlier assumption that the incoming light was diffuse (which it was not) or the scattering process was diffuse (g = 0), which now appears wrong (Table 4.1). Further work may be desirable to confirm these new values. We plan to make measurements on optically flat samples where roughness does not contribute to light scattering, in the hope of distinguishing between inhomogeneity scattering and scattering from tubules.

4.7 ACKNOWLEDGEMENT

The authors thank R. Graaff from the department of Obstetrics and Gynaecology for helpful discussions and critical reading of the manuscript.

4.8 REFERENCES

Arends J, Ruben J, Jongebloed WJ (1989) Dentine caries *in vivo*. *Caries Res* 23:36-41.

Flock ST, Wilson BC, Patterson MS (1987) Total attenuation coefficients and scattering phase functions of tissues and phantom materials at 633 nm. *Med Phys* 14:835-841.

Harris FS Jr, Sherman GC, Morse FL (1967) Experimental comparison of scattering of coherent and incoherent light. *IEEE Trans antennas propagation* AP-15:141-147.

Henyey LG, Greenstein JL (1941) Diffuse radiation in the galaxy. *Astrophys J* 93:70-83.

Jacques SL, Alter CA, Prahl SA (1987) Angular dependence of HeNe laser light scattering by human dermis. *Lasers Life Sci* 1:309-333.

Marchesini R, Bertoni A, Andreola S, Melloni E, Sichirollo AE (1989) Extinction and absorption coefficients and scattering phase functions of human tissues *in vitro*. *Appl Opt* 28:2318-2324.

Meador WE, Weaver WR (1979) Diffusion approximation for large absorption in radiative transfer. *Appl Opt* 18:1204-1208.

O'Brien WJ (1988) Fraunhofer diffraction of light by human enamel. *J Dent Res* 67:484-486.

Parsa P, Jacques SL, Nishioka NS (1989) Optical properties of rat liver between 350 and 2200 nm. *Appl Opt* 28:2325-2330.

Spitzer D, ten Bosch JJ (1975) The absorbtion and scattering of light in bovine and human dental enamel. *Calcif Tiss Res* 17:129-137.

ten Bosch JJ, van der Mei HC, Borsboom PCF (1984) Optical monitor of *in vitro* caries. *Caries Res* 18:540-547.

ten Bosch JJ, Zijp JR (1987) Optical properties of dentin. In: *Dentine and dentine reactions in the oral cavity*. A Thylstrup, SA Leach and V Qvist eds. (IRL Press, Oxford, England) pp. 59-65.

van de Hulst HC (1957) *Light scattering by small particles.* (Dover Publications, New York, 1981)

van der Burgt TP, ten Bosch JJ, Borsboom PCF, Plasschaert AJM (1985) A New method for matching tooth colors with color standards. *J Dent Res* 64:837-841.

Zijp JR, ten Bosch JJ (1993) Theoretical model for the scattering of light by dentin and comparison with measurements. *Appl Opt* 32:411-415. (Chapter 5)

Chapter 5 Theoretical model for the scattering of light by dentin and comparison with measurements

[Previously published as: Theoretical model for the scattering of light by dentin and comparison with measurements - J.R. Zijp and J.J. ten Bosch, Applied Optics, Vol. 32**,** 411-415, (1993), by permission of the Optical Society of America]

5.1 ABSTRACT

A theoretical model for the scattering of light by dentin is presented. The model that results is a superposition of several scattering contributions, *i.e.*, scattering by mineral crystals, collagen fibrils, and dentinal tubules. These tubules are oriented so that they cause an asymmetrical scattering process. The angular intensity functions are calculated for planes that are parallel or perpendicular to the plane of the tubules. The shape of the measured intensity function in the plane perpendicular to the tubules and the values of the scattering coefficient can be explained by the model that we present.

5.2 INTRODUCTION

5.2.1 Dentin

Dentin is the bone-like material in teeth (Figure 5.1). In the tooth crown the dentin is covered by enamel. Since both scattering and absorption of light are much stronger in dentin than in enamel, dentin plays the predominant role in the color of a tooth. Therefore we studied the behavior of light in dentin to achieve a better understanding of the causes of tooth color, which facilitate a better reproduction of this color by prosthetic teeth. In both enamel and dentin the light-scattering mean free path is much shorter than the absorption mean free path; thus scattering properties are quite important.

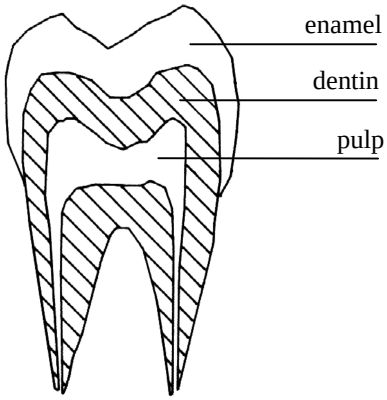

Figure 5.1 Schematic cross section of a tooth

The absorption and scattering coefficients of enamel have been measured; its hydroxyapatite crystals are mainly responsible for the scattering processes in this material (Spitzer and ten Bosch,1975). Quantifying incipient enamel caries, so-called white spots, by measuring light scattering is possible now (Brinkman *et al*., 1988).
We consider human dentin in this paper. Our aim is to explain the measured angular intensity functions and the value of the linear scattering coefficient has been as published (Zijp and ten Bosch, 1991).

5.2.2 Physical properties of dentin

Dentin can be described as a conglomerate of several compartments. Bulk dentin is the entire material except for the so-called tubules. In bulk dentin the peritubular dentin that circumferences the tubules and intertubular dentin can be distinguished (Figure 5.2). Intertubular dentin in turn is devided into collagen fibrils and interfibrillar compartments.

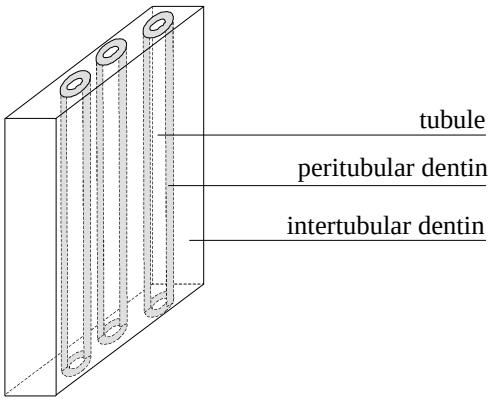

Figure 5.2 Schematic diagram of a thin slice of dentin, cut parallel to the dentinal tubules (not to scale).

Except for the tubules all compartments contain mineral crystals of hydroxyapatite, which are needle shaped with an ~5 nm thickness and an ~20 nm length (Mjör, 1984). The index of refraction of hydroxyapatite is 1.62. The distribution of components over the different compartments is shown in Table 5.1.
The density of tubules is 15 - 65 $\times$ 10^3 tubules / mm^2, the average being ~35 $\times$ 10^3 per mm^2 (Mjör, 1973). These tubules have an average diameter of 1.58 μm with a standard deviation (s.d.) of 0.28 μm (Fromme and Riedel, 1970). They are oriented from the pulp to the dentin-enamel-junction, and so in a small sample they lie more or less parallel (Figure 5.2). The tubules are surrounded by peritubular dentin with a diameter of 3.0 μm (s.d., 1.8 μm) and a mineral content of 90 vol. % (s.d., 6 vol. %). Between the tubules with their peritubular dentin lies intertubular dentin with a mineral content of 40 vol. % (s.d., 6 vol.%).
Intertubular dentin consists of 90 vol. % fibrils of collagen and incorporated mineral crystals and 10 vol.% interfibrillar dentin. The tropocollagen molecules in the fibrils are characterized as long thin rods of 280 $\times$ 1.5 nm with a molecular weight of ~360,000 (Mjör, 1973). The fibrils, with diameters of 50 - 150 nm (Tronstad, 1973), are more or less randomly oriented in this material.

5.3 THEORY

Some calculations in this paragraph give different angular intensity functions for light polarized perpendicular and parallel to the plane of scattering; they are denoted as $I_r(q)$ and $I_l(q)$, respectively (Figure 5.3).

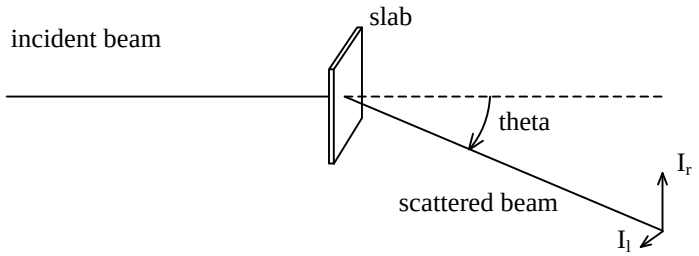

Figure 5.3 Definition of I_r and I_l with respect to the plane in which the scattering is measured.

The properties of biological tissues, like dentin, vary from sample to sample and within one sample. Therefore we use pseudorandom values as input values for the calculations, *e.g.*, fibril sizes, tubule sizes, and indices of refraction. These pseudorandom values are normally distributed around the input mean value with the input standard deviation. These mean values and standard deviations are extracted from literature or estimated. The input parameters for the calculations were restricted to exclude sets without a physical meaning. Refractive indices of the different structures were calculated from their composition; the values are included in Table 5.1.
The scattering processes in dentin are distinguished by two types: first, processes centered symmetrically round the incident beam, caused by randomly oriented mineral crystals and collagen fibrils; second, asymmetrical processes, caused by the oriented tubules. The resulting scattering coefficients, which are discussed below, are shown in Table 5.2

Table 5.1 Composition of dentin (vol. %) (whole dentin = 100 %) taken from Boonstra (1991), and resulting refractive indices.

compartment	mineral	collagen	non-collagenous proteins	water	refractive index
whole dentin:	48	25.5	2.5	24	1.49
tubules	0	0	0	16	1.33
bulk dentin:	48	25.5	2.5	8	1.52
peritubular dentin	25.7	0	0.6	2.3	1.59
intertubular dentin:	22.3	25.5	1.9	5.7	1.45
intrafibrillar compartment	21.2	25.5	0	3.2	1.49
interfibrillar compartment	1.1	0	1.9	2.6	1.41
refractive index	1.62	1.40	1.40 (assumed)	1.33	

Table 5.2 *s* Values from several scatterers in dentin

scatterer	s (mm^{-1})
mineral crystals	1.7×10^{-5}
collagen fibrils	19
tubules	140

5.3.1 Symmetrical Processes

Scattering by Mineral Crystals
The mineral crystals of dentin can be considered as Rayleigh scatterers because their sizes are considerably smaller than the wavelength of light. The mean free path caused by them can be estimated by considering their number and their scattering cross section. The number of crystals is estimated by the ratio of the average mineral content of dentin and the volume per crystal (*i.e.*, 1.3×10^{27} m^{-3}). The scattering cross section of each will be in the order of 5×10^{-23} m^2, (which are estimated from Mie-calculations of scattering spheres with a diameter of 9 nm and $n = 1.64$ in a medium with $n = 1.33$), resulting in a scattering coefficient of $s = 1.7 \times 10^{-5}$ mm^{-1}.

Scattering by Collagen Fibrils
From the elemental composition of the collagen molecules (Eastoe, 1963), their volume, and their mineral content, we estimated the refractive index of collagen fibrils to be $n = 1.49$. The refractive index of the surrounding interfibrillar dentin was estimated on the basis of the mineral content, the remaining proteins, and the water content to be $n = 1.41$. We can estimate the scattering cross section per fibril by using the formulas for the scattering cross section of an infinitely long cylinder as given by van de Hulst (1981), *i.e.*, to be of the order of 3.3×10^{-10} m^2 per meter length. The total length of fibrils per cubic meter dentin is estimated from the fibrillar content as 5.9×10^{13} m, resulting in a scattering coefficient $s = 19$ mm^{-1}.
We calculated the angular intensity function from a set of collagen fibrils by considering them as infinitely long randomly oriented cylinders. We used the formulations of Kerker (1969). The calculated intensity function is shown in Figure 5.4.

5.3.2 Asymmetrical Processes

The asymmetrical scattering process can be explained by Fraunhofer diffraction, by the interference of light scattered by a grid of single cylinders, and by the interference of light scattered by a grid of concentric double cylinders. For the latter two models we calculated the angular intensity functions resulting from a grid of 140 tubules by using 140 angular intensity functions as input to the calculations. Because in our measurements (Zijp and ten Bosch, 1991) the diameter of the incident beam is 0.83 mm, and the intertubular distance is ~ 6 μm, in the ideal case 140 tubules are illuminated by the incident beam.

Fraunhofer Diffraction
When a small sample is observed in a light microscope the tubules can be seen as nearly equally spaced dark rods with an axis-to-axis spacing of 6 μm (s.d. = 0.5 μm). The intertubular butt

straps of dentin between these tubules can act as Fraunhofer diffracting slits with an average width of 4.4 μm (s.d. = 1 μm). The calculated intensity function of a grid of 140 of these slits is shown in Figure 5.5.

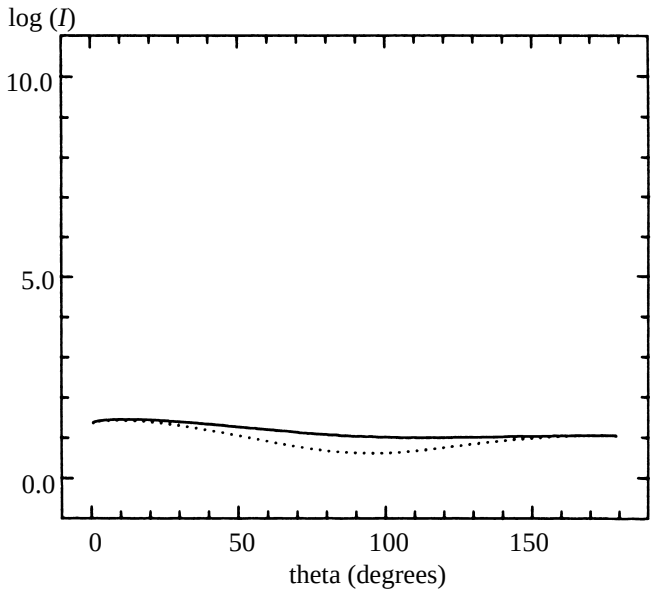

Figure 5.4 Angular intensity function calculated for randomly oriented collagen fibrils: solid curve, I_r; dotted curve, I_l (I is in arbitrary units).

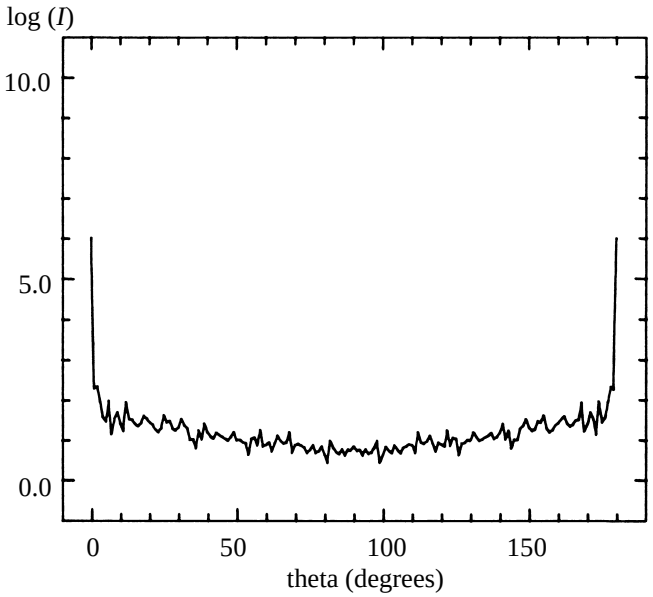

Figure 5.5 Fraunhofer diffraction pattern calculated for a set of slits between 140 dentinal tubules with varying slit widths. (I is in arbitrary units.)

Single-Cylinder Scattering

In this model we consider each dentinal tubule as an infinitely long straight circular cylinder filled with water (n = 1.33) in a medium of bulk dentin (n = 1.52, s.d. = 0.02). The tubules are oriented perpendicular to the plane in which the scattering is measured. The scattering intensity function of such cylinders is set out in detail by van de Hulst (1981). We calculated the interference pattern of 140 of these cylinders with an axis-to-axis spacing of 6 μm (s.d., 0.5 μm). The resulting angular intensity function is shown in Figure 5.6. From the number of tubules per square meter and their scattering cross section we calculated the scattering coefficient to be s = 140 mm^{-1}.

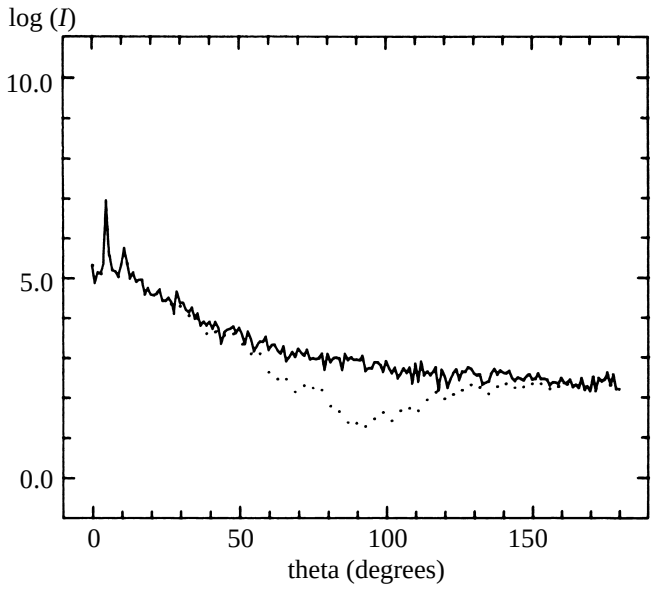

Figure 5.6 Angular intensity function calculated for the single cylinder model: solid curve, I_r; dotted curve I_l. (I is in arbitrary units.)

Concentric Double Cylinder

A more detailed model than the previous one is the concentric double-cylinder model. The same water-filled tubules are considered, but the peritubular cladding is also taken in account. Both the tubules and the cladding are considered to be infinitely long, circular and concentric straight cylinders. We estimated the refractive indices to be n = 1.59 (s.d., 0.02) for peritubular dentin and n = 1.45 (s.d., 0.02) intertubular dentin. The scattering intensity function of concentric cylinders is described by Kerker and Matijevic (1961). The calculated intensity function, *i.e.*, the interference pattern of a grid of 140 of such cylinders, is shown in Figure 5.7.

5.4 EXPERIMENTAL RESULTS

The measured scattering intensity functions for HeNe-laser light have been published (Zijp and ten Bosch, 1991). The samples we used were ~16 μm thick slabs, cut parallel to the tubules (Figure 5.2). The intensity functions measured in the plane perpendicular to the tubules showed first-order maxima at ~5° (s.d., 0.6°); those measured in the plane parallel to the tubules showed no other maxima than the forward one. The minima at 90° may be caused by the sample holder

or by multiple sattering at these angles. Typical examples of these intensity functions are shown in Figure 5.8. From Figure 4.6 we measured the thickness and the collimated transmittance of the slabs and calculated the mean scattering coefficient as s = 120 mm^{-1}; standard error of the mean (SEM), 9 mm^{-1}.

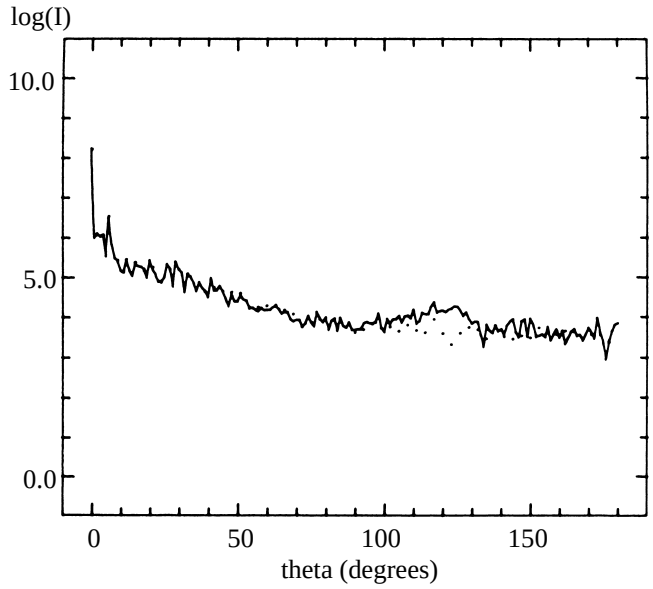

Figure 5.7 Angular intensity function for the double cylinder model: solid curve, I_r; dotted curve I_l (I is in arbitrary units.)

5.5 COMPARISON OF THEORY AND EXPERIMENTS

The low scattering coefficient of the mineral crystals ($s = 1.7 \times 10^{-5}$ mm^{-1}) does not lead to any significant Rayleigh scattering contribution to the whole scattering process.

The scattering coefficient calculated for the randomly oriented collagen fibrils in intertubular dentin is 19 mm^{-1}. This is small compared to the measured value s = 120 mm^{-1} and the other calculated contributions as shown below. The form of the calculated intensity function does not compare with the one measured in the plane parallel to the tubules.

The calculated Fraunhofer diffraction pattern of Figure 5.5 shows that this intensity function decreases much faster than the measured ones at small angles and is nearly flat at larger angles. It does not compare with the experimental one (Figure 5.8); we therefore conclude that the contribution of Fraunhofer diffraction is small.

Figures 5.6 and 5.7 show that the behaviour of $I_r(q)$ is about the same for the single- and double-cylinder model. The $I_l(q)$ functions show only a significant difference around 90°, but this difference could not be measured because of the shadow of the sample holder. Both calculated intensity functions show the experimentally measured maximum at ~5°. The calculated s = 140 mm^{-1} from the single-cylinder model compares well with the measured value s = 120 mm^{-1} (SEM, 9). This strongly supports our previously formulated suggestion (ten Bosch and Zijp, 1987), based on wavelength dependence, that the tubuli are the predominant cause of scattering. Since dental caries in dentine leads to an increase of the size of the dentinal tubules (Arends *et al*., 1989), a further study of scattering by sound and carious dentine seems to be indicated.

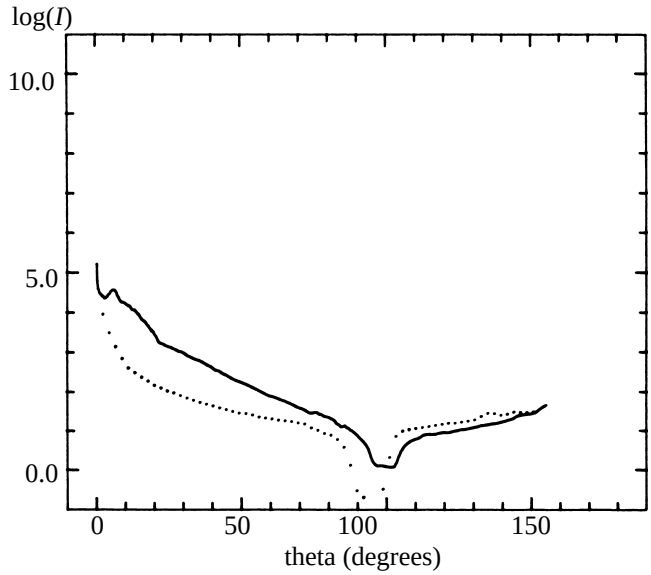

Figure 5.8 Typical example of a measured angular intensity function: solid curve, measured in a plane perpendicular to the tubules; dotted curve, measured on a plane parallel to the tubules. The difference between the two directions of polarization are not significant and therefore not shown. (*I* is in arbitrary units.)

Figure 5.8 shows that the scattering measured in the plane parallel to the tubules is much smaller than in the plane perpendicular to the tubules. However, the value measured in the parallel plane is not zero, and it is even much higher than the value calculated for the collagen fibrils. The reason for this is probably that in real dentin the tubules are not straight circular parallel cylinders.

5.6 CONCLUSION

The tubules are the most important scatterers in dentin. The collagen fibrils play only a minor role, and the mineral crystals do not contribute significantly. The role of peritubular dentin is not clear from the calculations.

5.7 REFERENCES

Arends J, Ruben J, Jongebloed WJ (1989) Dentine caries *in vivo. Caries Res* 23:36-41.

Boonstra WD (1991) *Protein-apatite interactions in dentine.* Ph.D. dissertation (State University of Groningen, Groningen, The Netherlands).

Brinkman J, ten Bosch JJ, Borsboom PCF (1988) Optical quantification of natural caries in smooth surfaces of extracted teeth. *Caries Res* 22: 257-262.

Eastoe JE (1963) The amino acid composition of proteins from the oral tissues-II. The matrix proteins in dentine and enamel from developing human deciduous tooth. *Arch Oral Biol* 8:633-652.

Fromme HG, Riedel H (1970) Messungen über die Weite der Dentinkanälchen an nichtentmineralisierten bleibenden Zähnen und Milchzähnen. *Dtsch Zahnärztl Z* 25:401-405.

Kerker M (1969) *The scattering of light and other electromagnetic radiation.* (Academic, San Diego, California) pp. 255-266.

Kerker M, Matijevic E (1961) Scattering of electromagnetic waves from concentric infinite cylinders. *J Opt Soc Am* 51:506-508.

Mjör IA (1973) Dentin and pulp. In: *Histology of the human tooth*. IA Mjör and JJ Pindborg eds. (Munksgaard, Copenhagen, Denmark) pp.45-76.

Mjör IA (1984) The morphology of dentin and dentinogenensis. In: *Dentin and dentino genesis.* A Linde ed. (CRC Press, Boca Raton, Florida) Vol. 1, pp. 2-18.

Spitzer D, ten Bosch JJ (1975) The absorption and scattering of light in bovine and human dental enamel. *Calcif Tiss Res* 17:129-137.

ten Bosch JJ, Zijp JR (1987), Optical properties of dentin. In: *Dentine and dentine reactions in the oral cavity*. A Thylstrup, SA Leach, and V Qvist eds. (IRL, Oxford, England) pp. 59-65. (Chapter 3)

Tronstad L (1973) Ultrastructural observations on human coronal dentin. *Scand J Dent Res* 81:101-111.

van de Hulst HC (1981) *Light scattering by small particles*. (Dover, New York) pp. 297-306.

Zijp JR, ten Bosch JJ (1991) Angular dependence of HeNe-Laser light scattering by bovine and human dentine. *Arch Oral Biol* 36:283-289. (Chapter 4)

Chapter 6 HeNe-laser light scattering by human dental enamel

[Previously published as: HeNe-laser light scattering by human dental enamel - J.R. Zijp, J.J. ten Bosch, and R.A.J. Groenhuis, Journal of Dental Research, Vol. 74, 1981-1898, (1995), by permission of the International Association for Dental Research]

6.1 ABSTRACT

Knowledge of the optical properties of tooth enamel and an understanding the origin of these properties is necessary for the development of new optical methods for caries diagnosis and the measurement of tooth color. We measured the scattering intensity functions for HeNe-laser light of 80 to 100 μm thick human dental enamel slabs. The asymmetry factors were calculated to be $g = 0.68$ at 633 nm. By measuring the collimated beam attenuation, we determined the scattering coefficient to be $s = 6.6$ mm^{-1}. From Fraunhofer diffraction patterns, obtained from transmission of the laser beam, we calculated the periodicity of the prismatic structure as 5.4 μm. We present a model containing scattering by crystals and by prisms. It shows that the prisms are the most important scatterers but that the crystals are responsible for the back scattering.

6.2 INTRODUCTION

Studying the optical properties of dental materials is necessary to extend the knowledge of the processes and structures that cause the color of teeth. The outer surface of a tooth crown consists of enamel. Sound enamel is nearly transparent. Its light scattering coefficient for fluxes, S, is decreasing from 9 to 1.5 mm^{-1} at increasing wavelengths from 400 to 700 nm. The absorption coefficient for fluxes, K, equals $K = 0.1$ mm^{-1} over this wavelength region (Spitzer and ten Bosch, 1975). Recently, the asymmetry factor for single scattering, $g = 0.68 \pm 0.09$, was obtained from experiments with a thick enamel sample, assuming a Henyey-Greenstein angular intensity function (Vaarkamp *et al.*, 1995).

By fitting linear combinations of isotropic and Henyey-Greenstein angular intensity functions, we can calculate much lower values of the asymmetry factors g (Fried *et al.*, 1995). The angular intensity function used in this method is given by:

$$E(q) = f_d + (1 - f_d)\left[\frac{(1 - g_{HG}^2)}{(1 + g_{HG}^2 - 2g_{HG}\cos q)^{3/2}}\right] \qquad (6.1)$$

with:

f_d as a fit parameter, expressing the isotropic contribution with respect to the Henyey-Greenstein part, and

g_{HG} as the asymmetry factor of the Henyey-Greenstein intensity function.

The reported values are $g_{HG} = 0.96$ (at all the three wavelengths used), $f_d = 0.35$ (at wavelengths of 1053 and 632 nm) and $f_d = 0.60$ (at 543 nm). This results in total asymmetry factors $g = 0.462$ (at 1053 and 632 nm) and $g = 0.240$ (at 543 nm).

Fraunhofer diffraction of light can be observed from thin enamel samples (O'Brien, 1988). Two-dimensional Fraunhofer patterns can be used to determine the distribution of the values

of the periodicity of the structure of prisms and the interfaces between them (Zijp and ten Bosch, 1995). The fluorescence properties of tooth enamel are well reviewed (Hefferren *et al.*, 1971; Scharf, 1971).
Better understanding the optical properties of dental enamel requires knowledge of its single scattering properties, *i.e.*, the scattering coefficients for collimated light, s, and single scattering intensity functions, $E(q)$. These should be measured from thin samples. We present such data in this paper and compare them with theoretical predictions. Preliminary results have been published before (Groenhuis, 1981).

6.3 MATERIALS AND METHODS, THEORETICAL CALCULATIONS

To understand the light scattering properties of biological tissues, we have to consider the structures within these materials. The main structures in human dental enamel are the mineral crystals and the key-hole shaped prisms in which they are organised. We shall consider these structures and their effects on the scattering properties separately.

6.3.1 Scattering by crystals

Human dental enamel consists 87 vol% of natural hydroxyapatite (HAP) crystals (Arends and ten Cate, 1981), with the balance water and organic material, mainly proteins. The HAP crystals are hexagonal cylinders with the following dimensions: thickness = 25 nm, width = 40 nm, and length = 160 nm (Scott and Symons, 1971). Other investigators have found that the lengths can vary over wide ranges (from 100 to 1000 nm, Jongebloed and Molenaar, 1975; from 21 to 10,000 nm, Rönnholm, 1962). Using the dimensions found by Scott and Symons the average crystal volume is 1.3×10^{-22} m^3, and we find the number of crystals to be $N_c \approx 6.7 \times 10^{21}$ m^{-3} in enamel. The refractive index for visible light of HAP crystals is 1.651 (McConnell, 1973), and that of whole enamel is 1.62 (Spitzer and ten Bosch, 1975). From the mineral content of whole enamel, we can calculate its refractive index (*cf.* Appendix 6.1).
To calculate the light scattering intensity function, we estimated the role of the crystals by assuming a circular cross-section and a random orientation overall (see Appendix 6.2).

6.3.2 Scattering by prisms

In enamel, the crystals are organised in keyhole-shaped prisms. These prisms are 4 to 6 μm wide and extend from the dentin-enamel-junction to the outer surface of the tooth. Schematic drawings of the prisms (*e.g.*, Griebstein, 1965), and photographs have been published (Zelander, 1973); similar figures can be found in many textbooks dealing with dental tissues. When the keyhole is divided into a head and a tail, the crystals within the head are oriented nearly parallel to the axis of the prism, and those within the tail are oriented nearly perpendicular to the prism axis (Griebstein, 1965). From a photograph (Zelander, 1973) we determined the geometric cross-sections (*i.e.*, perpendicular to their principal axes) of the prisms to be about 4.0×10^{-11} m^2.
Between the prisms there is an interprismatic area with an average thickness of about 0.1 μm (Arends and ten Cate, 1981). One can estimate the average geometric cross-section of interprismatic substance by measuring its average area per prism on the photograph (Zelander, 1973); this is about 1.5×10^{-12} m^2. Assuming that the volume fractions are equal to the cross-section fractions, the prism volume fraction can be estimated as $f_p = 0.96$. The number of prisms *per* unit volume was estimated as $N_p \approx 2.4 \times 10^{13}$ m^{-3}, based on a length of 1 mm.

In the interprismatic area, the crystal orientation is rather random, leading to a lower mineral content and a higher content of water and organic material. To estimate the mineral volume fraction in the interprismatic material, we filled a glass box with pencils which were also randomly distributed. The dimensions of the pencils were of the same proportion as those of the crystals. The dimensions of the box were much larger than the dimensions of the pencils. The volume fraction of the pencils appeared to be almost 0.70. We took this value as an estimation for the mineral volume fraction in the interprismatic area. Since the mineral volume fraction in whole enamel is about 0.87 (Arends and ten Cate, 1981), we estimate it as 0.88 in the prisms.
Calculation of the indices of refraction of the prisms and the interprismatic substance appears in Appendix 6.1.
In our measurement set-up, we observed the prisms at angles a = 20° - 90° and j = 60° - 90° (with a and j as defined by van de Hulst, 1981). Because the measured angular intensity functions did not show systematic differences on the site in the tooth where the slab was cut, we estimated a mean angular intensity function $E(q)$ of an ensemble of cylinders by averaging over these intervals of a and j. More details about the calculation of the angular intensity function are given in Appendix 6.3.

6.3.3 Diffraction by prisms

In enamel, the structure of prisms and interprismatic substance can be considered as a grating. The width of the prisms shows some variation, and the prisms are somewhat curved and not exactly aligned. We consider this as a grating with an irregular periodicity and curved slits. The irregular periodicity will cause an interference pattern with a sharp principal maximum, a wide first-order maximum and vanishing higher-order maxima. The curvature will cause spreading of the first-order maxima around the principal axis. Calculations on the diffraction pattern are explained in Appendix 6.4.

6.4 MATERIALS AND METHODS, EXPERIMENTS

6.4.1 Samples

We used 6 extracted human third molars. From each molar 5 slabs with a thickness of 80 to 100 μm were cut, parallel to the buccal surface. They were stored on wetted tissues in a refrigerator until measurements were performed.

6.4.2 Measurements

The angular intensity functions were measured with the equipment as described previously (Zijp and ten Bosch, 1991). In the present measurements, however, the scattering cells contained a solution which matched the refractive index of enamel. This solution was made of a saturated solution of potassium-iodine (KI) in water, to which mercury-iodine (HgI_2) was added until the refractive index of the solution was 1.62, and so matched the refractive index of enamel. We used a tunable HeNe-laser (LSTPC-1010, PMS Electro Optics, Boulder, Colorado) at wavelengths (and powers) of 632.8 nm (4 mW), 594.1 nm (0.6 mW) and 543.5 nm (0.3 mW). We measured the angular intensity functions in the planes parallel and perpendicular to the tooth axis. From the measured angular intensity functions parallel to the tooth axes the asymmetry factors for scattering, g, were calculated by:

$$g = \frac{\int_{0°}^{180°} dq\ E(q)\cos q\ \sin q}{\int_{0°}^{180°} dq\ E(q)\sin q} \tag{6.2}$$

We consider the Fraunhofer diffracted light as unscattered light, and so the undiffracted angular intensity functions, *i.e.*, those measured parallel to the prisms, should be used for calculating g.
In practice, it is impossible to calibrate the measurement of $E(q)$ with respect to the incident beam power E_0. Therefore, the scattering coefficient s was determined from the attenuation (by scattering) of the incident beam. Thus, we measured the transmission T at $q = 0°$ at the laser wavelength of 632.8 nm. The mean thickness t of each slab was calculated from 5 measurements with a micrometer. The measured scattering coefficient is calculated by: $s_m = -\ln(T)/t$. The absorption coefficient was assumed to be much smaller than the scattering coefficient (Spitzer and ten Bosch, 1975).

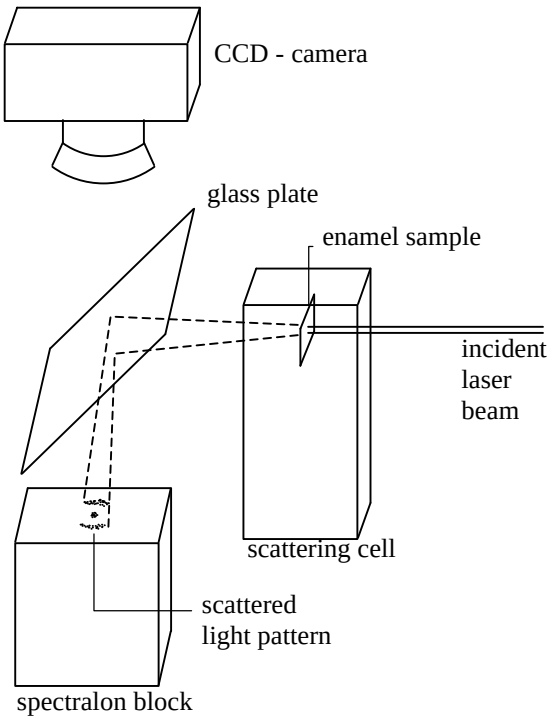

Figure 6.1 Set-up for measurement of the Fraunhofer diffraction pattern.

The Fraunhofer diffraction patterns were measured with 6 other slabs from 6 teeth prepared and stored as described. The measuring set-up is schematically shown in Figure 6.1. We used a HeNe-laser at 632.8 nm. The diffracted radiation was mirrored by a glass plate on a spectralon block (Labsphere, North Sutton, New Hampshire). This pattern was imaged by means of a M 1430-P CCD camera (EG&G-Par, Princeton, New Jersey), coupled to a computer by a 14-bits analog-to-digital converter. The images measured 300 × 300 pixels, and

were taken without and with neutral density filters of 10 %, 1 %, 0.1 % and 0.01 % transmission in the incident beam. These pictures showed different degrees of saturation of CCD-camera pixels, and were combined to get an intensity profile with a dynamic range of 6 orders of magnitude, without saturation. The form of such an intensity profile is shown schematically in Figure 6.2, in which the density of the dark spots represents the light intensity.

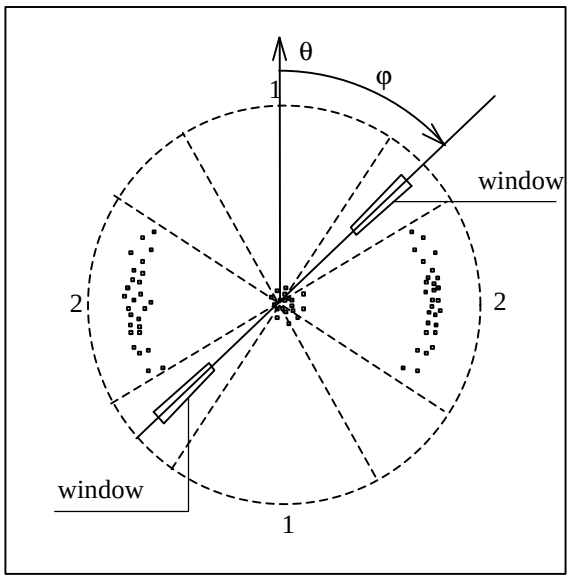

Figure 6.2 Schematic example of a measured Fraunhofer diffraction pattern, the black dot density represents the light intensity. The incident beam is a thin pencil beam in the centre of the picture. The sectors numbered 1 and 2 are used to calculate the functions $P_1(q)$ and $P_2(q)$, respectively. The windows at angle f are used to calculate $P_w(j)$.

From these images we calculated the light power P, transmitted in the sectors 1 and 2 (*cf.* Figure 6.2), as function of the angular deviation from the central spot, q = 0°. This resulted in $P_1(q)$ and $P_2(q)$. By performing the calculations as set out in Appendix 6.4, we could predict $P_2(q)$ curves for appropriate values of the mean periodicity of the prism structure, d_{mean}, and its standard deviation, s_d. The curve $P_3(q)$ that best fit to the experimental result, $P_2(q)$, was used to determine d_{mean} and s_d.
The measured diffraction patterns were further used to determine the angular distribution of the prisms. We calculated the total amount of transmitted light, $P_w(j)$, in the windows covering the first-order maxima (Figure 6.2.) as function of the angle j.

6.5 RESULTS

6.5.1 Calculations

Figure 6.3 shows the light scattering intensity function for a single crystal, multiplied by N_c (dashed line). Calculation of the scattering cross-section of each crystal (at a wavelength of 633 nm, Appendix 6.2) gives $C_{sca} \approx 1.4 \times 10^{-19}$ m^2. The number of crystals and their scattering cross-section determine the linear scattering coefficient $s_c = N_c \times C_{sca} \approx 0.94$ mm^{-1}. This coefficient is proportional to the estimated lengths of the model crystals (so far assumed as 160 nm), because N_c is proportional to the inverse of their lengths and C_{sca} is proportional to the square of their lengths.

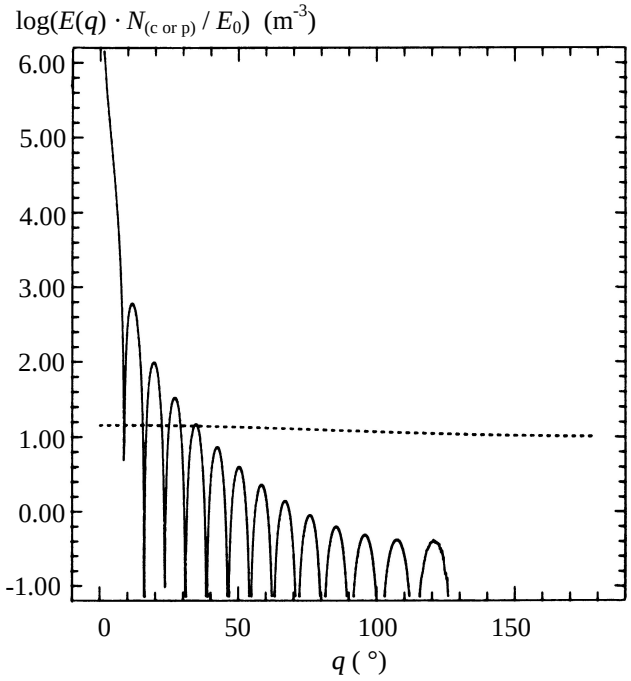

Figure 6.3 Calculated angular intensity functions. Dashed line for randomly oriented cylinders as a model for the mineral crystals. Solid line for oriented cylinders as a model for the prisms. The ordinate value expresses the irradiance at the detector per unit irradiance of the incident beam per volume irradiated enamel (in m^3), where the detector is positioned in a direction q with respect to the incident direction.

The angular intensity function for a single prism, multiplied by N_p, is shown in Figure 6.3 as the solid line. The scattering cross-section for each prism is estimated as $C_{sca} \approx 2.4 \times 10^{-10}$ m^2 (at a wavelength of 633 nm, Appendix 6.3). Calculations with different prism lengths showed that C_{sca} is almost proportional with the length of the model prism.

The number of prisms and their scattering cross-section determine the corresponding scattering coefficient, which can be estimated as $s_p = N_p \times C_{csa} \approx 5.8$ mm^{-1}. This scattering coefficient is independent of the lengths of the model crystals.

6.5.2 Experiments

When the thin enamel slabs are observed in daylight, they appear to be pale blue in reflection and pale yellow in transmission.

Typical examples of measured angular intensity functions are shown in Figure 6.4. The calculated asymmetry factors, *g*, from these functions are shown in Table 6.1.

From 55 measurements (of 11 samples) of the transmission at $q = 0°$ we found $s_m = 6.6 \pm 2.7\ mm^{-1}$.

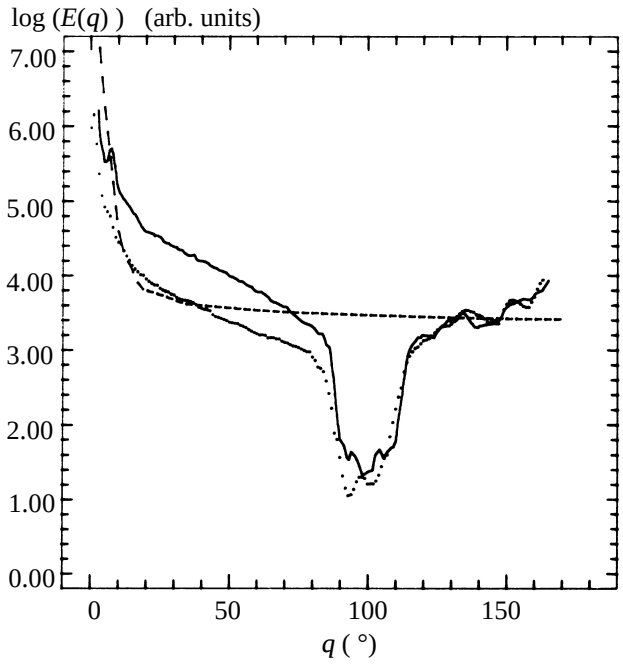

Figure 6.4 Typical examples angular intensity functions of enamel at 633 nm. Full and dotted line: measured, with the scattering plane perpendicular and parallel to the tooth axis, respectively. Dashed line: calculated, perpendicular to the tooth axis.

Table 6.1 Asymmetry factors, *g*, of enamel

Wavelength (nm)	n*	Mean ± s.d.**
633	9	0.68 ± 0.10
594	4	0.68 ± 0.20
543	4	0.74 ± 0.23

*Some samples were broken after measurement at 633 nm
**Standard deviation includes variation among the samples

Typical examples of the diffraction patterns as a function of the diffraction angle q are given as $P_1(q)$ and $P_2(q)$ in Figure 6.5. Predicted curves $P_3(q)$ were fitted to the $P_2(q)$ curves. By doing so, from 6 measurements on 6 samples, we found overall mean values of $d_{mean} = 5.4$ μm and $s_d = 1.0$ μm. The fit corresponding to $P_2(q)$ is also shown in Figure 6.5.
Figure 6.6 shows $P_w(j)$ for one of the samples. It illustrates the distribution of the curvature or misalignment of the prisms. We found the full width at half-maximum (FWHM) of all the 6 measured distributions to be $\Delta j = 74° \pm 11°$.

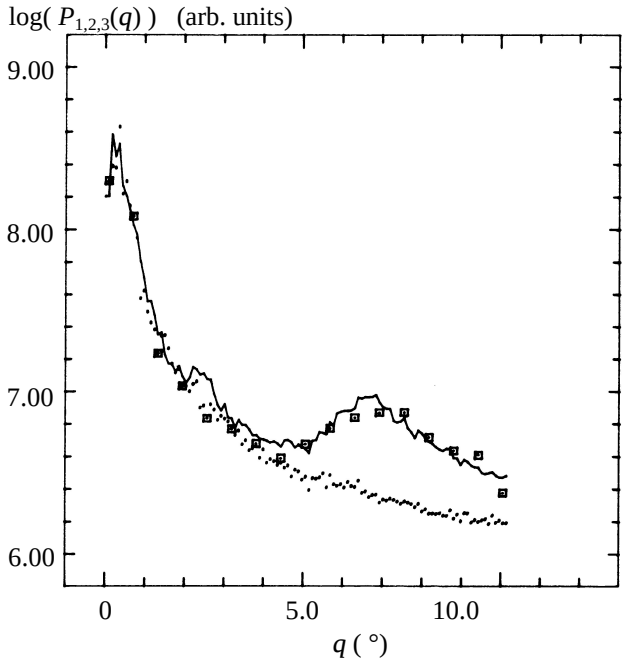

Figure 6.5 Typical example of the measured reflected power $P_1(q)$ (solid line) in sector 1, $P_2(q)$ (dotted line) in sector 2, and $P_3(q)$ (squares) fitted curve, as function of the angle q.

6.6 DISCUSSION

The observation that the slabs look blueish in reflection and yellowish in transmission leads to the conclusion that structures smaller than the wavelength of light play a considerable role in the light scattering process. This is supported by the measured asymmetry factors g (Table 6.1), because structures as small as the mineral crystals would cause low asymmetry factors, $g \approx 0$, and those as large as the prisms would cause high asymmetry factors $g \approx 1$ (Figure 6.3). The measured g values are inbetween these values. The g value we measured at 633 nm is equal to that found peviously by a different method (Vaarkamp *et al.*, 1995). Our measured g values deviate significantly from those found by the fitting procedure (Fried *et al.*, 1995) . This procedure has the disadvantage that addition of a small isotropic fraction to the resulting intensity function will result in a large reduction of the calculated g value. This is a consequence of the fact that the Henyey-Greenstein intensity functions are very sharply forward. We observed an increase of the standard deviation of the measured g values with decreasing wavelength, which is due to decreasing laser power. Therefore, we

were unable to determine the increase of g with decreasing wavelength that is theoretically expected.
The measured angular intensity function (Figure 6.4) shows a minimum around 90°, this is caused by the shade cast by the sample holder. We expected the true angular intensity function to have a smooth form, and minimum, but not one so deep between 80° and 120°. By adding and smoothing both theoretical functions of Figure 6.3, we will get an intensity function peaked sharply forward. We expect that the resonances will vanish in practice, because the prisms are not uniform, since the crystals within them are somewhat oriented. Also, the prisms do not have a circular cross-section, as do the cylinders in the model.

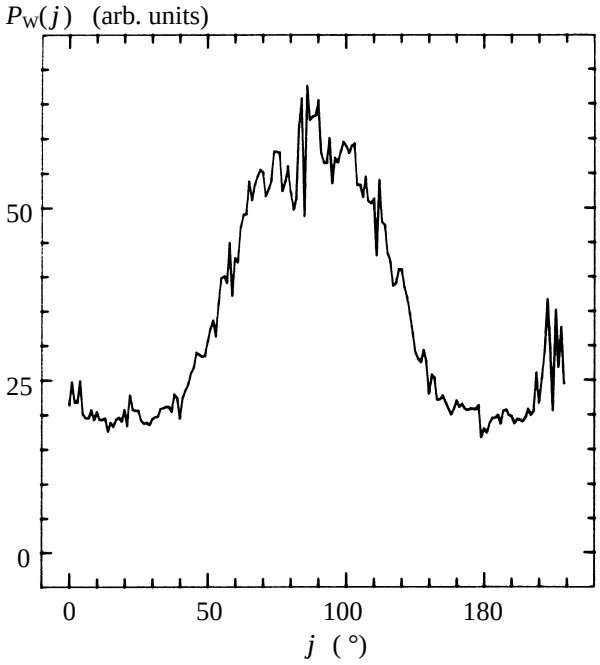

Figure 6.6 Typical example of the measured reflected power in the windows $P_w(j)$ as function of the angle j.

The calculated linear scattering coefficient, s, can be found by adding those found from the calculations for scattering by mineral crystals and prisms. We found $s = 6.7$ mm^{-1}. It should be noted that this result is not dependent upon the length of the modeled prisms. This value matches the measured value, $s_m = 6.6 \pm 2.4$ mm^{-1}.
Adding the functions shown in Figure 6.3 results in an angular scattering intensity function which shows too little back scattering. This back scattering can be introduced by assuming stronger scattering from the crystals, which can be obtained by assuming longer crystals than in the model presented in Appendix 6.2. This assumption would be in agreement with reports on very long crystals (Orams *et al.*, 1974; Daculsi *et al.*, 1984), which are fractured in the preparation of the samples. If we thus assume the scattering from the crystals to be stronger by a factor 10, the theoretical curve obtained will better match the measured one (*cf.* Figure 6.4, dashed line). This procedure, however, leads to a scattering coefficient which would be too high. This theoretical curve does not show back scattering as strong as those measured,

probably caused by reflectance of the forward scattered radiation at the solution-glass and glass-air surfaces of the scattering cell.
The values of d_{mean} (5.4 μm) and s_d (1.0 μm) compare well with other measurements of the diameter of enamel prisms (Zelander, 1973).
The data presented are all from third molars. Since it has been shown that the scattering coefficient of enamel is weakly correlated to tooth color (ten Bosch and Coops, 1995), it may be expected that the scattering in enamel of teeth with usually darker color, *e.g.*, cuspids, is different.
If the enamel samples were cut in other orientations, *e.g.*, perpendicular to the surface, this would affect the measured and calculated optical parameters. In that case, we would expect lower scattering coefficients, because waveguide effects will play a considerable role (Altshuler and Grisimov, 1989).

6.7 ACKNOWLEDGEMENTS

This work was supported by the University of Groningen. The authors wish to thank Mrs. H. Middel and Dr. F.K.L. Spijkervet of the Department of Oral and Maxillofacial Surgery of the Academic Hospital Groningen for providing the extracted molars.

6.8 REFERENCES

Altshuler GB, Grisimov VN (1989) New optical effects in the human hard tissues. *SPIE* 1353:97-101.

Arends J, ten Cate JM (1981) Tooth enamel remineralization. *J Crystal Growth* 53:135-147.

Born MA, Wolf E (1980) *Principles of optics*. 6th ed. (Pergamon Press, Oxford) p. 404.

Daculsi G, Menanteau J, Kerebel LM, Mitre D (1984) Length and shape of enamel crystals. *Calcif Tissue Int* 36:550-555.

Emslie AG, Aronson JR (1973) Spectral reflectance and emittance of particulate materials. 1: theory. *Appl Opt* 12:2563-2572.

Fried D, Glena RE, Featherstone JDB, Seka W (1995) Nature of light scattering in dental enamel and dentin at visible and near-infrared wavelengths. *Appl Opt* 34:1278-1285.

Griebstein WJ (1965) Discussion of fourth session. In: *Tooth enamel*. Stack MV, Fearnhead RW, eds. (John Wright & Sons Ltd, Bristol) p. 191.

Groenhuis RAJ (1981) *Scattering and absorption of light by turbid materials, especially dental enamel* (dissertation). (State University of Groningen, The Netherlands).

Hefferren JJ, Hall JB, Bennet E (1971) Luminescence as a tool to study enamel interactions. In: *Tooth enamel II*. Fearnhead RW, Stack MV, eds. (John Wright & Sons Ltd., Bristol) pp.161-165.

Jongebloed WL, Molenaar I (1975) Morphology and size-distribution of sound and acid-treated enamel crystallites. *Calcif Tissue Res* 19:109-123.

McConnell D (1973) *Apatite. Its crystal chemistry, mineralogy, utilization, and geologic and biologic occurrences*. (Springer-Verlag, New York).

O'Brien WJ (1988) Fraunhofer diffraction of light by human enamel. *J Dent Res* 67:484-486.

Orams HJ, Phakey PP, Rachinger WA, Zybert JJ (1974) Visualisation of micropore structure in human dental enamel. *Nature* 252:584-585.

Rönnholm E (1962) The ameleogenesis of human teeth. *J Ultrastruct Res* 6:249-303.

Scharf F (1971) Über die natürliche Lumineszenz der Zahngewebe Schmelz und Dentin. *Stoma* (Heidelb) 24:10-25.

Scott FR, Symons NBB (1971) *Introduction to dental anatomy*. 6th ed. (Livingstone, Edinburg and London).

Spitzer D, ten Bosch JJ (1975) The absorption and scattering of light in bovine and human dental enamel. *Calcif Tissue Res* 17:129-137.

ten Bosch JJ, Coops JC (1995) Tooth color and reflectance as related to light scattering and enamel hardness. *J Dent Res* 74:374-380.

Vaarkamp J, ten Bosch JJ, Verdonschot EH (1995) Propagation of light through human dental enamel and dentine. *Caries Res* 29:8-13.

van de Hulst HC (1981) *Light scattering by small particles*. (Dover Publications, New York)

Zelander T (1973) The enamel. In: *Histology of the human tooth*. Mjör IA, Pindborg JJ, eds. (Munksgaard, Copenhagen).

Zijp JR, ten Bosch JJ (1991) Angular dependence of HeNe-laser light scattering by bovine and human dentine. *Arch Oral Biol* 36:283-289.

Zijp JR, ten Bosch JJ (1995) Two dimensional patterns of Fraunhofer diffraction by dental enamel. *SPIE* 2626:113-120.

Appendix 6.1 Calculation of the refractive indices of the prisms, the interprismatic area and whole enamel.

The refractive index of a whole substance composed of surrounding material and particles with a different refractive index can be calculated by (Emslie and Aronson, 1973):

$$\bar{n} = n_s \sqrt{1 + \frac{2 f_p \left(\left(\frac{n_p^2}{n_p^2 - n_s^2} \right) \ln\left(\frac{n_p}{n_s} \right)^2 - 1 \right)}{1 - f_p + \frac{2 f_p n_s^2}{n_p^2 - n_s^2} \left(\left(\frac{n_p^2}{n_p^2 - n_s^2} \right) \ln\left(\frac{n_p}{n_s} \right) - 1 \right)}} \qquad (6.3)$$

with:

$\bar{n}$ as the refractive index of the substance,
n_p as the refractive index of the particles, *i.e.*, the mineral crystals = 1.651 (McConnell, 1973),
n_s as the refractive index of the surrounding material, *i.e.*, proteins and water = 1.40 (estimated), and
f_p as the volume fraction of the particles in the substance.

We can use Equation 6.3 to calculate the refractive index of the prisms. With $f_p = 0.88$, being the volume fraction of mineral crystals in the prisms, we find $\bar{n}_{prism} = 1.619$.
The refractive index of the interprismatic substance can be found: With $f_p = 0.70$, being the volume fraction of mineral crystals in the interprismatic area, we find $\bar{n}_{int.pr.} = 1.573$.
Applying the same method for whole enamel with $f_p = 0.87$, being the volume fraction of mineral crystals in whole enamel, we find $\bar{n}_{enamel} = 1.616$. This value compares with the measured value of 1.62 (Spitzer and ten Bosch, 1975).

Appendix 6.2 Calculation of the single scattering properties of the mineral crystals.

In this calculation, we assume that, for this treatment, the mineral crystals can be considered as randomly oriented circular cylinders. Their scattering properties can be calculated by Rayleigh-Gans theory (van de Hulst, 1981, p. 98), because both its constraints are fulfilled:

$$\left| \frac{n_{particle}}{\bar{n}} - 1 \right| << 1 \quad \text{and} \quad ka\bar{n} \left| \frac{n_{particle}}{\bar{n}} - 1 \right| << 1 \qquad (6.4)$$

with:

$n_{particle}$ as the refractive index of the particles (mineral crystals) = 1.651,
$\bar{n}$ as the refractive index of the environment of the particles (whole enamel) = 1.616,
a as the "radius" of the mineral crystals = 17 nm, and
k as the wavenumber of the light = 9.93×10^7 m^{-1} (at a wavelength of 633 nm, in vacuum).

The angular intensity function for this approximation, with the extra constraint that $ka << 1$, is given by (van de Hulst, 1981, pp. 87, 98) :

$$E(q) = \frac{a^4 k^4 l^2 \bar{n}^{-4} \left(\frac{n_c}{\bar{n}} - 1 \right)^2 (1 + \cos^2 q)}{8r^2} \overline{R^2(q)} E_0$$

$$\text{with} \quad \overline{R^2(q)} = \frac{1}{z} \sum_{n=0}^{\infty} \frac{(-1)^n (2z)^{2n+1}}{(2n+1)(2n+1)!} - \left(\frac{\sin z}{z} \right)^2 \tag{6.5}$$

$$\text{and} \quad z = kl \sin \frac{q}{2}$$

with the values a, k, $\bar{n}$ and n_p as used in Equation (6.4) and:
E_0 as the irradiance of the incident radiation (W/m^2),
$E(q)$ as the irradiance of the scattered radiation at the detector(W/m^2),
l as the length of the cylinder (crystal) = 160 nm,
n_c as the refractive index of the crystals = 1.651,
q as the scattering angle, and
r as the distance from the scatterer to the detector (we used r = 1 m in this calculation).

In Figure 6.3 (dashed line) the function $E(q) \cdot N_c / E_0$ (in m^{-3}) is shown.
The scattering cross-section of such a model crystal is given by the Rayleigh cross-section (van de Hulst, 1981, p. 68):

$$C_{sca} = \frac{a^4 k^4 l^2 \bar{n}^{-4} p}{6} \left| \left(\frac{n_p}{\bar{n}} \right)^2 - 1 \right|^2 \tag{6.6}$$

Using the data previously given, we find $C_{sca} \approx 1.4 \times 10^{-19}$ m^2. Note that C_{sca} is proportional to the square of the length of the model crystal.

Appendix 6.3 Calculation of the single scattering properties of the prisms.

In the case of scattering by prisms, the conditions like those in Equation (6.4) are not quite fulfilled here, but as an estimation of the forward scattered radiation we applied Rayleigh-Gans theory. We must be aware that the prisms are not randomly oriented. As a model for the prisms we used a circular cylinder, with radiation obliquely incident on it. The scattering intensity functions of such cylinders are given by (van de Hulst, 1981, pp. 87, 94):

$$E(a, j, q) = \frac{a^4 k^4 l^2 \bar{n}^{-4} \left(\frac{n_p}{\bar{n}} - 1 \right)^2 (1 + \cos^2 q)}{8r^2} \left| R(a, j, q) \right|^2 E_0$$

$$\text{with} \qquad R(\alpha, j, q) = \frac{2}{u} J_1(u)\left(\frac{\sin v}{v}\right),$$

$$u = 2ka \sin\frac{q}{2} \sin b, \qquad v = kl \sin\frac{q}{2} \cos b \tag{6.7}$$

$$\sin b = \left(\sin^2 \alpha \sin^2 j - (\sin\alpha \cos j \sin\frac{q}{2} + \cos\alpha \cos\frac{q}{2})^2 \right)^{\frac{1}{2}}$$

$$\text{and} \qquad \cos b = \sin\alpha \cos j \cos\frac{q}{2} - \cos\alpha \sin\frac{q}{2}.$$

with:

a as the radius of the prism model = 2.5 µm,
l as the length of the prism model = 1 mm,
n_p as the refractive index of the prism = 1.619,
$\bar{n}$ as the refractive index of whole enamel = 1.616,
α as the angle between the cylinder axis and the incident direction,
q as the scattering angle, and
j as the angle between a plane through the cylinder axis and the incident direction (*i.e.* the incident plane) and the scattering plane.

In Figure 6.3 (solid line) the function $E(q) \cdot N_p / E_0$ (in m^{-3}) is shown, in which $E(q)$ is the average value for an ensemble of prisms oriented at angles α = 20° - 90° and j = 60° - 90°.
To estimate the scattering cross-section, C_{sca}, of a single prism we, have to integrate the scattered radiation over all directions (van de Hulst, 1981, p 95):

$$C_{sca} = \frac{2\int_{20°}^{90°} d\alpha \int_{0°}^{180°} dj \int_{0°}^{180°} dq \ \sin q \ E(q, \alpha, j)}{E_0 \int_{20°}^{90°} d\alpha} \tag{6.8}$$

This results in $C_{sca} = 2.4 \times 10^{-10}$ m^2.

Appendix 6.4 Calculation of the Fraunhofer diffraction of prisms

Radiation perpendicularly incident on a regular grating of slits is Fraunhofer diffracted. This radiation can be observed by placing a screen behind the grating. The normalized intensity function of the diffracted radiation is given by (Born and Wolf, 1980):

$$I(q) = N^2 \left(\frac{\sin(\frac{Nkd}{2}\sin q)}{N\sin(\frac{kd}{2}\sin q)} \right)^2 \tag{6.9}$$

with:
d as the distance between the slits,
N as the number of the slits, and
q as the angle with the incident direction.

If the periodicity of the grating is a value with some variation, a wide first-order maximum and vanishing higher-order maxima will occur. For simplicity, we calculated as a model the sum of diffraction patterns as given by Equation (6.9), while using the values of d that vary according to a normal distribution with mean value d_{mean} and standard deviation s_{d}. Adding such a sum of diffraction patterns to the angular intensity function arising from scattering without diffraction, is represented by:*

$$P_3(q) = P_1(q) + C\sum_{n=0}^{5000}\left(\frac{\sin\left(\frac{Nkd_n}{2}\sin q \right)}{N\sin\left(\frac{kd_n}{2}\sin q \right)} \right)^2 \tag{6.10}$$

with the previously used data and:
$P_3(q)$ as the total amount of transmitted light as function of the scattering angle q calculated in sector 2 (Figure 6.2),
$P_1(q)$ as the total amount of transmitted light as function of the scattering angle q measured in sector 1 (Figure 6.2),
C as an arbitrary constant,
d_{n} as the periodicity of the grating, drawn, for every value of n, pseudo-randomly from a normal distribution, with a mean value d_{mean} and a standard deviation s_{d}, and
N as the number of slits. (We took N = 200, being the ratio of the diameter of the laser beam ≈ 1 mm and the expected periodicity ≈ 5 μm.)

$P_3(q)$ was fit to $P_2(q)$, which was measured, the fit parameters being d_{mean} and s_{d}.
If the slits are somewhat curved, the diffraction pattern will spread around the major direction of diffraction, as shown in Figure 6.2. So, by measuring $P_{\text{w}}(j)$ in a window covering the first order maximum, we can estimate the curvature of the prisms.

*This paragraph has been changed after publication to give a better descrition of the method used.

Chapter 7 Optical properties of carious bovine dental enamel

[To be published]

7.1 ABSTRACT

The increased whiteness of white spot lesions is caused by the increased scattering of light incident on these lesions. We determined the increase of the scattering coefficient of bovine dental enamel quantitatively. We measured the spectral reflectance of enamel slabs during demineralization, against a black and a white background, to calculate the Kubelka-Munk absorption and scattering coefficients, *K* and *S*, respectively. For sound enamel we found *K* decreasing from 0.9 (at 380 nm) to 0.02 per mm (at 680 nm), *S* decreased from 15 to 0.06. We demineralized in gel at pH 5.0, and calculated the demineralization progress constant as 5 ± 2 μm / ($h^{½}$). For demineralized enamel *K* decreased from 1.2 to 0.5 per mm, and *S* decreased from 36 to 3 per mm over this wavelength range. By calculations from theory, and analysis of the measurements, we show that the crystallites are the dominant scatterers when lesions are observed.

7.2 INTRODUCTION

7.2.1 Background

Carious lesions in their earliest stage can be observed as white spots. The increased whiteness of these spots is caused by increased scattering of the incident light. The incident light covers shorter paths within the material before it is backscattered and so its absorption is smaller. Measurement of the severity of caries can be done by measuring the scattering at the enamel surface of teeth (Brinkman *et al.*, 1988). Also quantitative laser fluorescence methods used to measure caries severity are based upon differences between scattering in sound and carious enamel (ten Bosch, 1996). The aim of this paper is to present measurements and to describe the origins of the increased light scattering.

7.2.2 Properties of sound enamel

The Kubelka-Munk light scattering and absorption coefficients, *S* and *K* respectively, of sound bovine and human enamel have been measured before (Spitzer and ten Bosch, 1975). Their values can be calculated from the graphs of Spitzer with $K = a_c/0.515$ and $S = s_c/1.385$. We explained the linear light scattering coefficient *s* of sound human dental enamel by the structures present (Zijp *et al.*, 1995), like the enamel prisms and the mineral crystals. Intact crystallites of bovine enamel have widths of 57 ± 7 nm (Arends and Jongebloed, 1978) and lengths which are large with respect to their diameters. The mineral content of sound bovine enamel is 80 vol% (Robinson *et al.*, 1988).

Bovine enamel is organised in two main structures, prisms in longitudinal rows separated by interrow sheets (Sato *et al.*,1999). On microphotographs (Figure 7.1) of samples similar to those we used in our experiments we measured these structures. Firstly the prisms (67 vol %) having an elliptic cross section, with a mean dimensions of 6.3×2.2 μm. Secondly the

interrow sheets (14 vol %) with a mean thickness of 0.4 μm. The prisms and the sheets are more dense than the interstructural material present between these main structures.

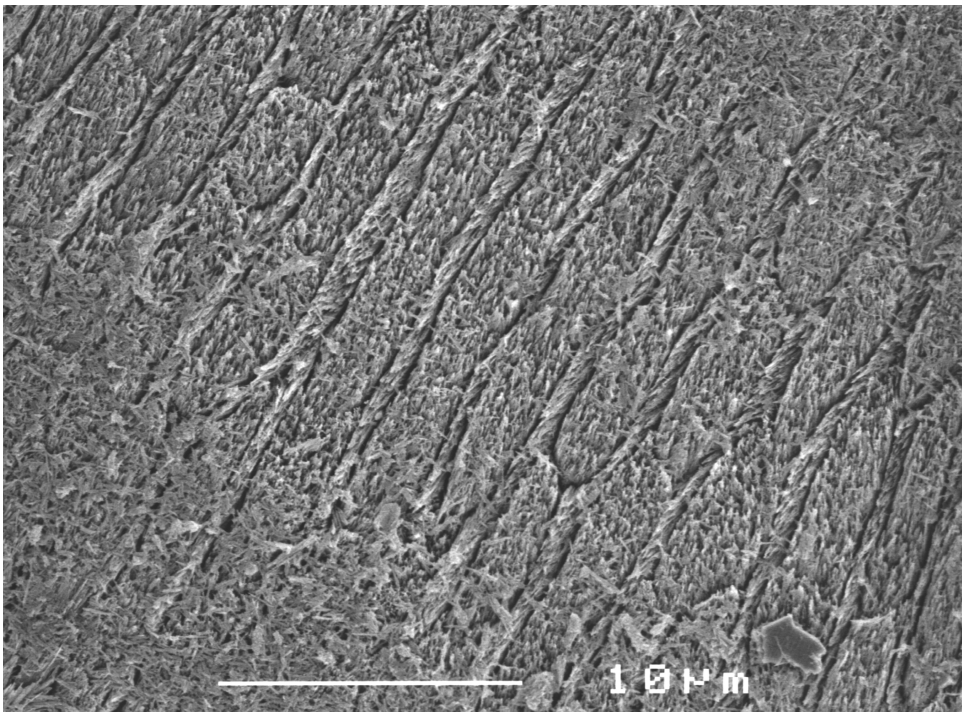

Figure 7.1 Scanning electron microphotograph of bovine enamel as we prepared it. The elliptical shaped prisms are arranged in longitudinal rows, separated by interrow sheets. The sample was polished and etched for 15 s in 0.1 N hydrochlorous acid.
Photograph by courtesy of I. Stokroos, Centre for Electronmicroscopy.

7.2.3 Carious enamel

The body of the lesion is the largest zone (Nikiforuk, 1985) within a carious lesion, and so the most important zone for light scattering considerations. Its mineral content has decreased from 80 vol% down to values of about 60 vol% (Arends et al., 1992) to 55 vol% (ten Cate and Arends, 1980). This volume is partly taken up by water and organic material.
In laboratory experiments caries is mostly simulated by demineralization of dental material with acid solutions, acidified gels, or chelating agents. The shape of the demineralized crystallites depends on the type of solvent chosen, and of the pH values of these solvents. However, demineralization with lactic acid approximates the natural lesion (Johnson , 1966). Some investigators (Featherstone and Mellberg, 1981; Featherstone and Rogers, 1981; Poole *et al*., 1981) showed that the *in vitro* lesion depth is proportional to the square-root of the time. From these papers we estimate the demineralization progress constant for our situation as b = 7.1 μm/($h^{½}$) (Appendix 7.1).

7.2.4 Scattering by crystallites

The caries process decreases the diameter of the mineral crystals in the lesion body (Silverstone, 1983). Now two opposite effects occur at the same time. Firstly, reduction of the size of the crystallites increases the space between the crystallites. This causes a decrease of the refractive index of the environment of the crystallites, which contains all other crystallites and intercrystalline space. This results in an increase of the scattering cross section of the crystallites. Secondly, the decrease of the size of the crystals causes a decrease of the scattering cross section, and so a decrease of the scattering coefficient. We used Rayleigh-Gans theory to calculate the contribution of the mineral crystals to scattering in the case of sound *bovine* enamel (Appendix 7.2 and Appendix 7.3). We calculated S as decreasing from 21 mm^{-1} (at 380 nm) to 2.4 mm^{-1} (at 680 nm). The constraints of the Rayleigh-Gans theory are not fulfilled in the case of demineralized enamel, so we are not allowed to use this theory for demineralized enamel. To estimate the effect of the increase of the refractive indices we calculated the scattering coefficient of a suspension of spheres with a volume equal to the volume of the crystallites, and refractive indices equal to those present in sound and carious enamel. The calculated scattering coefficient S in the carious case was three times higher than in the sound case.

7.2.5 Scattering by prisms

In the very early stage of the caries process only the interprismatic crystals are dissolved. Also the interprismatic space, which contains water and proteins, within the body of the lesion increases. The size of the prisms is only slightly reduced. In a second stage of the demineralization process also the mineral crystals within the prisms are attacked and dissolved to a remaining degree of mineralization of 55 - 60 vol%. In a third stage the demineralization will further decrease so that cavitation will occur. We will not consider this process in this work.

We estimated the scattering coefficient S caused by prism scattering as 1.2×10^{-4} mm^{-1} (at 380 nm) decreasing to 8.7×10^{-5} (at 680 nm) for sound bovine enamel (Appendix 7.2 and Appendix 7.4)

7.3 MATERIALS AND METHODS

The large pores in carious enamel prohibited measurements as we did for sound enamel (Appendix 7.5). The measurement equipment now used determines the spectral reflectance of slabs under diffuse illumination (Molenaar *et al.*, 1999). From the labial face of 10 bovine incisors we prepared 10 plano-parallel slabs of sound enamel, each with a thickness $d_{initial}$ of about 300 μm. One side of each slab was varnished with colourless clear nail varnish. We measured their spectral reflectance against a black background R'_{black} and the spectral reflectance against a white background R'_{white}. These reflectances were used to calculate the Kubelka-Munk absorption and scattering coefficients of each slab (Kortüm, 1969; Molenaar *et al.*, 1999), K_{sound} and S_{sound} respectively.

From their unvarnished sides the slabs were demineralized in a 6 % carboxymethylcellulose (CMC) gel, containing 0.1 mol/l lactic acid, titrated to pH 5 with a 10 mol/l potassium hydroxide (KOH) solution, at a temperature of 37 °C.

At several times, that was after 24, 43, 137, 159, 181, 204, 495, 540, and 564 hours, during the demineralization process the slabs were removed from the gel, rinsed, and superficially dried. Their reflectances, $R'_{12,black}$ and $R'_{12,white}$, were measured with the same method as applied at the sound slabs. The indices 12 indicate that we are measuring at the carious face of

the two layered system, with 1 as the carious layer, and 2 as the sound layer. Each layer was considered to be homogeneous. From these reflectances we calculated the reflectances R_{12} and the transmissions T_{12}, valid for refractive index matched double layered samples.
At the end of our experiments, after 564 hours of demineralization, we determined the lesion depth $d_{lesion}(564)$ of each sample. This was done by breaking the samples, polishing the fractured surfaces and observing them in a confocal microscope. The lesion appeared whiter than the sound tissue, and the sound tissue showed more structure at low resolution than the lesion. For each sample the demineralization progress constant b was calculated from $d_{lesion}(564)$. The values b were used to calculate the lesion depth d_{lesion} as a function of time for each sample. Assuming that the optical properties of sound tissue did not change over time, using $d_{sound} = (d_{initial} - d_{lesion})$, S_{sound} and K_{sound}, we calculated the reflectance and transmission of the sound layer, R_2 and T_2 respectively. R_{12} and T_{12}, together with R_2 and T_2, led to R_1 and T_1 of the demineralized layer (Kortüm, 1969). The latter values were used to calculate the Kubelka-Munk coefficients, $K_{carious}$ and $S_{carious}$, of the carious enamel.

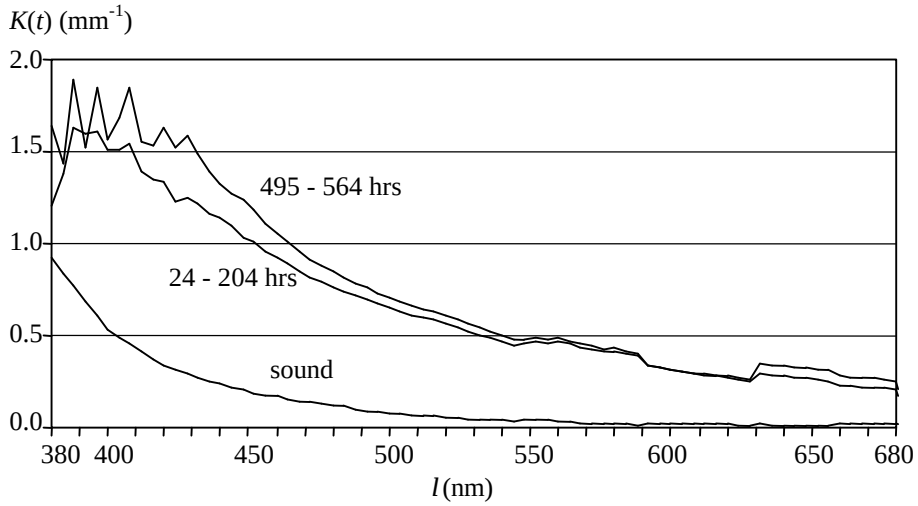

Figure 7.2 Mean values of the measured Kubelka-Munk absorption coefficients K of lesion material as a function of the wavelength. The curves for demineralization time ranges 24 - 204 hours differ not significantly. The same is true for the curves for 495 - 564 hours.

7.4 RESULTS

The mean demineralization progress constant was determined as $b_{measured}$ = 5 μm / ($h^{½}$), SD = 2.
Figure 7.2 shows the mean values of the measured Kubelka-Munk absorption coefficients K as a function of the wavelength. Figure 7.3 shows the mean values of the measured Kubelka-Munk scattering coefficients S of the same samples. We averaged over all samples and several demineralization periods because the separate curves did not differ significantly. The curves for sound enamel show the mean value of the 10 slabs used at the beginning of the experiment. The other curves originate from 10 or less samples, firstly because some samples were broken during the experiment, secondly because for some samples the calculations did

not produce physically meaningful results. The standard deviations of the mean values of *K* and *S* is about 10% for wavelengths below 550 nm, and 20% for longer wavelengths.

7.5 DISCUSSION

The value of *b* that we determined from the measurements as b_m = 5 μm / ($h^{½}$), compares with the estimated value b_{calc} = 7.1 μm/($h^{½}$) (Appendix 7.1).
In Appendix 7.3 and 7.4 we explain the calculations we performed to estimate the scattering coefficients due to scattering by the crystals and prims in sound bovine enamel. Previously (Zijp *et al.*, 1995) we showed that in human enamel the linear coefficient is mainly determined by scattering by prisms. In the present appendices we show that the Kubelka-Munk coefficients, *S* and *K*, are mainly determined by scattering by the crystals. Their contribution to multiple scattering is higher than that of prisms because for small particles the asymmetry parameter for scattering *g* is close to 0.

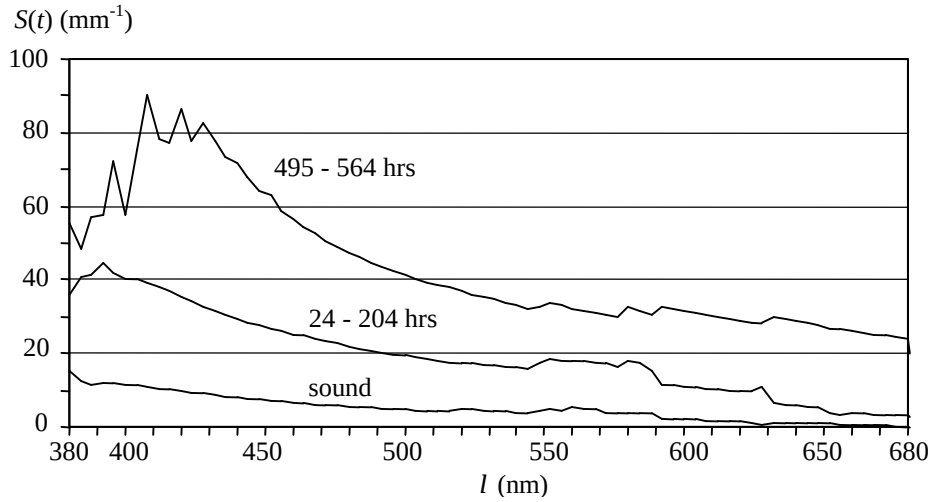

Figure 7.3 Mean values of the measured Kubelka-Munk scattering coefficients *S* of lesion material as a function of the wavelength. The curves for demineralization time ranges 24 - 204 hours differ not significantly. The same is true for the curves for 495 - 564 hours.

The values of *K* for sound enamel, as shown in Figure 7.2, at 380 nm are about a factor 2 higher than those previously found (Spitzer and ten Bosch, 1975). At 680 nm the value we found is about a factor 4 lower than the previously found values. The values of *S*, as shown in Figure 7.3 for sound enamel, differ up to a factor of 1.5 with these earlier results at wavelengths lower than 500 nm, while at higher wavelength there is agreement between these measurements. The differences may be explained by different illumination geometries. The applied Kubelka-Munk theory demands that the radiation distribution within the sample is diffuse. To achieve this we applied diffuse illumination. Spitzer and ten Bosch used collimated illumination in combination with roughened sample surfaces to approximate diffuse illumination inside the sample. This most probably leads to a less diffuse light distribution inside the sample than the method we used here. We applied diffuse illumination, but refraction at the top face of the samples causes some collimation. The light needs to be

scattered several times to become ideally diffuse again. This will happen in thin layers if the scattering coefficient is high enough, that is especially at the shorter wavelengths. At wavelengths longer than about 650 nm the scattering may be too low to cause this redistribution, and so Kubelka-Munk theory fails to give appropriate results.
The calculated values of S_{sound} are about 1.5 times higher than the measured values, except for the one measured at 680 nm. We have to be aware of the fact that the models used for the calculations are much simpler than the structures present in reality.
The measured values of *S* are highly dependent on the wavelength. Analysis of this dependence (Appendix 7.6) shows that the crystallites are the most important scatterers at wavelengths ranging from 400 - 510 nm, for both sound and carious enamel. This observation is different from our conclusion for human enamel (Zijp *et al.*, 1995), for which we showed that the prisms are the most important scatterers. Firstly this is due to the large difference in enamel structure between these two species. Secondly, human enamel was measured at somewhat higher wavelengths (543 - 633 nm). Other investigations (Fried *et al.*, 1995) using multiple scattering also showed that a relatively high fraction of small particles is reponsible for the total scattering process.
The values of *S* and *K* after demineralization can be separated into two groups. Those after 24 - 204 hours of demineralization are considerably lower than those obtained after 495 - 564 hours. Probably the demineralization, as we performed it, is a three step process. Firstly an almost immediate disappearance of the interprismatic crystals. Secondly increasing the lesion depth without much change of the properties of the lesion material. Thirdly, demineralization of the lesion material to a lower mineral content.
We did not expect an increase of *K* during this experiment. We do not have an explanation for this increase. The increase of *K* is relatively smaller than the increase of *S*; it is probably caused by cross talk between *K* and *S* in the calculations.

7.6 ACKNOWLEDGMENTS

This work was supported by the University of Groningen. The authors are greatly indebted to J.L. Ruben for his help with preparation of samples and demineralizing gels and to I. Stokroos for scanning electron miscroscopy support. We also wish to thank Drs. S.J. Brookes (Leeds), R. Graaff, M.C.D.N.J.M. Huysmans, and R.P. Shellis (Bristol) for helpful discussions.

7.7 REFERENCES

Arends J, Christoffersen J, Christoffersen MR, Øgaard B, Dijkman AG, Jongebloed WL (1992) Rate and Mechanism of enamel demineralization in situ. *Caries Res* 26:18-21.

Arends J, Jongebloed WL (1978) Crystallites dimensions of enamel. *J Biol Buccale* 6:161-171.

Brinkman J, ten Bosch JJ, Borsboom PCF (1988) Optical quantitation of natural caries in smooth surfaces of extracted teeth. *Caries Res* 22:257-262.

Emslie AG, Aronson JR (1973) Spectral reflectance and emittance of particulate materials 1: theory. *Appl Opt* 12:2563-2572.

Featherstone JDB, Mellberg JR (1981) Relative rates of progress of artificial carious lesions in bovine, ovine and human enamel. *Caries Res* 15:109-114.

Featherstone JDB, Rogers BE (1981) Effect of acetic, lactic and other organic acids on the formation of artificial carious lesions. *Caries Res* 15:377-385.

Fried D, Glena RE, Featherstone JDB, Seka W (1995) Nature of light scattering in dental enamel and dentin at visible and near-infrared wavelengths. *Appl Opt* 34:1278-1285.

Graaff R, Aarnoudse JG, Zijp JR, Sloot PMA, de Mul FFM, Greve J, Koelink MH (1992) Reduced light-scattering properties for mixtures of sperical particles: a simple approximation derived from Mie calculations. *Appl Opt* 31:1370-1376.

Johnson NW (1966) Differences in the shape of *human* enamel crystallites after partial destruction by caries, EDTA and various acids. *Archs Oral Biol* 11:1421-1424.

Kortüm G (1969) Reflextionsspektroskopie. Heidelberg: Springer-Verlag.

McConnel D (1973) Apatite. Its crystal chemistry, mineralogy, utilization, and geologic and biologic occurrences. New York: Springer-Verlag.

Meador WE, Weaver WR (1979) Diffusion approximation for large absorption in radiative transfer. *Appl Opt* 18:1204-1208.

Molenaar R, ten Bosch JJ, Zijp JR (1999) Determination of the Kubelka-Munk scattering and absorption coefficients by diffuse illumination. *Appl Opt* 38:2068-2077.

Nikiforuk G (1985) *Understanding dental caries 1. Etiology and mechanisms*. Basel: Karger

Poole DFG, Shellis RP, Tyler JE (1981) Rates of formation in vitro of dental caries-like enamel lesions in man and some non-human primates. *Archs Oral Biol* 26:413-417.

Robinson C, Kirkham J, Hallsworth AS (1988) Volume distribution and concentration of protein, mineral and water in developing bovine enamel. *Archs Oral Biol* 33:159-162.

Sato I, Sunohara M, Mikami A, Yoshida S, Sato T (1999) Comparison between deciduous and permanent incisor teeth in morphology of bovine enamel. *Okajimas Folia Anat Jpn* 76:131-136.

Silverstone LM (1983) Remineralization and enamel caries: significance of fluoride and effect on crystal diameters. In: *Demineralization and remineralization of teeth*. Leach SA, Edgar WM, eds. (IRL Press, Oxford) pp. 185-205.

Spitzer D, ten Bosch JJ (1975) The absorption and scattering of light in bovine and human dental enamel. *Calcif Tissue Res* 17:129-137.

ten Bosch JJ (1996). Light scattering and related methods in caries diagnosis. In: *Early detection of dental caries*. Stookey GK, editor. (Indiana University, Indianapolis) pp. 81-90.

ten Cate JM, Arends J (1980) Remineralization of artificial enamel lesions in vitro III. A study of the deposition mechanism. *Caries Res* 14:351-358.

van de Hulst HC (1981) *Light scattering by small particles*.(Dover Publications, New York)

Zijp JR, ten Bosch JJ, Groenhuis RAJ (1995). HeNe-laser light scattering by human dental enamel. *J Dent Res* 74:1891-1898.

Appendix 7.1 Estimation of the value of the demineralization progress constant *b*.

Some investigators (Featherstone and Mellberg, 1981; Featherstone and Rogers, 1981; Poole *et al*., 1981) showed that in conditions similar to ours the carious lesion depth d_{lesion} is proportional to the square-root of the time *t*:

$$d_{\text{lesion}}(t) = b \times \sqrt{t}\,. \tag{7.1}$$

The value of *b* depends on the species from which the enamel is originating, on the pH, on the demineralizing agent and on the medium (solvent or gel) containing this agent.
For human enamel b = 4.63 μm/(h^{½}) in gel at pH = 5.0 (Poole *et al*., 1981). At pH = 4.0 values of b = 22.4 μm/(h^{½}) for bovine and b = 14.5 μm/(h^{½}) for human enamel were found (Featherstone and Mellberg, 1981). Assuming that the ratio of the values of *b* are not dependent on pH, we can estimate b_{calc} for bovine enamel at pH = 5.0 from these as:

$$b_{\text{calc}} = \frac{22.4 \times 4.63}{14.5} = 7.1 \text{ μm/(h}^{½}\text{)}.$$

Appendix 7.2 Calculation of the refractive indices of sound and carious bovine enamel and its structures.

The mean refractive index of an inhomogeneous substance composed of particles in a surrounding medium with a different refractive index can be calculated by (Emslie and Aronson, 1973):

$$\bar{n} = n_s \sqrt{1 + \frac{2 f_p \left[\left(\frac{n_p^2}{n_p^2 - n_s^2} \right) \ln \left(\frac{n_p}{n_s} \right)^2 - 1 \right]}{1 - f_p + \frac{2 f_p n_s^2}{n_p^2 - n_s^2} \left[\left(\frac{n_p^2}{n_p^2 - n_s^2} \right) \ln \left(\frac{n_p}{n_s} \right)^2 - 1 \right]}} \tag{7.2}$$

with:
$\bar{n}$ as the refractive index of the substance
n_p as the refractive index of the particles, *i.e.* the mineral crystals = 1.651 (McConnell, 1973),
n_s as the refractive index of the surrounding material, *i.e.* proteins and water = 1.400 (estimated), and
f_p as the volume fraction of the particles in the substance.

Refractive indices within sound enamel
We can use Equation 7.2 to calculate the refractive index of the prisms. With $f_p = 0.83$, being the volume fraction of mineral crystals in the prisms, we find $\bar{n}_{prism} = 1.601$.
The refractive index of the interprismatic substance can be found with $f_p = 0.73$, being the volume averaged mineral content (calculated from sheets and interstructural material) of the interprismatic substance, we find $\bar{n}_{int.pr.} = 1.582$.
The refractive index for whole enamel can be calculated by using $f_p = 0.80$, being the volume fraction of the mineral crystals in this material. We find $\bar{n}_{enamel} = 1.599$.

Refractive indices within demineralized enamel (mineral content 57.5 vol%)
The same method can be applied for carious prisms, which contain a mineral volume fraction of $f_p = 0.71$, we find $\bar{n}_{demin.prism} = 1.576$.
We consider the interprismatic substance as the sheets together with the interstructural material. The total mineral content of this interprismatic substance $f_p = 0.30$, and so we find $\bar{n}_{int.pr.} = 1.474$.
The refractive index for whole demineralized enamel can be calculated using $f_p = 0.575$, being the volume fraction of the mineral crystals in this material. We find $\bar{n}_{demin.\ enamel} = 1.542$.

Appendix 7.3 Calculation of the scattering properties of the mineral crystals within sound bovine enamel.

In this calculation, we assume that, for this treatment, the mineral crystals can be considered as circular cylinders that are randomly oriented with respect to the incident radiation, because this radiation is diffuse. Furthermore, we assume their length being equal to those of human enamel. Their scattering properties can be calculated by Rayleigh-Gans theory (van de Hulst, 1981, p. 98), because both its constraints are fulfilled:

$$\left|\frac{n_p}{\bar{n}} - 1\right| << 1 \quad \text{and} \quad ka\bar{n}\left|\frac{n_p}{\bar{n}} - 1\right| << 1 \tag{7.3}$$

with:
n_p as the refractive index of the particles (mineral crystals) = 1.651,
$\bar{n}$ as the refractive index of the environment of the particles (whole enamel) = 1.599,
a as "radius" of the mineral crystals = 29 nm, and
k as the wavenumber in vacuum of the light used, *i.e.* $2\pi/l$, with l as the wavelength (380 - 680 nm in vacuum).

The angular intensity function for this approximation, with the extra constraint that $ka\bar{n} << 1$ (van de Hulst, 1981, p. 87 and p. 98) can be calculated (Zijp *et al.*, 1995). Using this intensity function the asymmetry parameter for scattering g can be calculated by:

$$g = \frac{\int_{0°}^{180°} dq \cos q \sin q \; E(q)}{\int_{0°}^{180°} dq \sin q \; E(q)} \tag{7.4}$$

The scattering cross section of such a model crystal is given by the Rayleigh cross section (van de Hulst, 1981, p. 68):

$$C_{sca} = \frac{a^4 k^4 l^2 (\bar{n})^4}{6} \left| \left(\frac{n_c}{\bar{n}} \right)^2 - 1 \right|^2 \tag{7.5}$$

with the values a, k, $\bar{n}$ and n_p as used in equation (2) and:
l as the length of the cylinder (crystal) = 160 nm, and
n_c as the refractive index of the crystals = 1.651.
Note that C_{sca} is proportional to the square of the length of the model crystal.
Using these data the cross section C_{sca} at various wavelengths are given in the table below. To calculate the linear scattering coefficient s we have to multiply the values C_{sca} with the number of crystals per unit enamel volume, which we estimated as $N_c = 2.0 \times 10^{21}$ m$^{-3.}$
The Kubelka-Munk absorption and scattering coefficients, S and K, respectively can be calculated from the linear scattering coefficient by (Meador and Weaver,1979):

$$S = \frac{3s(1-g) - a}{4} \qquad K = 2a \tag{7.6}$$

with a as the absorption coefficient. Because $a << s(1\text{-}g)$ we calculate $S \approx \frac{3s}{4}(1\text{-}g)$. The values are given in Table 7.1.

Table 7.1 Calculated scattering cross section C_{sca}, linear scattering coefficient s, asymmetry parameter g, Kubelka-Munk scattering coefficient S_{calc} due to scattering by mineral crystals in sound enamel, and measured values S_{sound}.

λ (nm)	C_{sca} (m^2)	s (mm^{-1})	g	S_{calc} (mm^{-1})	S_{sound} (mm^{-1})
380	1.9×10^{-17}	36	0.22	21	15
400	1.5×10^{-17}	30	0.21	18	12
500	6.2×10^{-18}	12	0.16	7.6	4.7
600	3.0×10^{-18}	5.9	0.13	3.8	2.1
680	1.8×10^{-18}	3.6	0.11	2.4	0.063

Appendix 7.4 Calculation of the scattering properties of the prisms within sound bovine enamel.

We used Rayleigh-Gans theory for the estimation of the scattering coefficients for scattering by prisms only in the sound case. The conditions like those in formulae (7.4), now with a as the radius of the prisms, are fulfilled. In the case of carious enamel these conditions are not fullfilled. The prisms are considered to be randomly oriented with respect to the incident radiation because this radiation is diffuse. As a model for the prisms we used a circular cylinder, with radiation obliquely incident on it. The scattering cross section of such cylinders is given by (van de Hulst, 1981, p. 95):

$$C_{sca} = \frac{2\int_{0°}^{90°} da\,\sin a \int_{0°}^{180°} dq\,\sin q \int_{0°}^{180°} dj\;E(a,q,j)}{E_0 \int_{0°}^{90°} da\,\sin a}$$

with :

$$E(a,j,q) = \frac{a^4 k^4 l^2 \bar{n}^{-4}\left(\frac{n_p}{\bar{n}} - 1\right)^2 (1+\cos^2 q)}{8r^2} \left|R(a,j,q)\right|^2 E_0,$$

$$R(a,j,q) = \frac{2}{u} J_1(u)\left(\frac{\sin v}{v}\right), \qquad (7.7)$$

$$u = 2ka\sin\frac{q}{2}\sin b, \quad v = kl\sin\frac{q}{2}\cos b,$$

$$\sin b = \left(\sin^2 a\,\sin^2 j - (\sin a\,\cos j\,\sin\frac{q}{2} + \cos a\,\cos\frac{q}{2})^2\right)^{\frac{1}{2}},$$

$$\text{and} \quad \cos b = \sin a\,\cos j\,\cos\frac{q}{2} - \cos a\,\sin\frac{q}{2}.$$

with:

a as the radius of the prism model = 1.85 µm,
l as the length of the prism model = 1 mm,
n_p as the refractive index of the prism = 1.601,
$\bar{n}$ as the refractive index of whole enamel = 1.599,
a as the angle between the cylinder axis and the incident direction,
q as the scattering angle, and
j as the angle between a plane through the cylinder axis and the incident direction (*i.e.* the incident plane) and the scattering plane.

To calculate the linear scattering coefficient s we have to multiply the scattering cross sections C_{sca} with the number of prisms per unit volume, which we estimated

as $N_p = 6.2 \times 10^{13}$ m^{-3}. These values and the Kubelka-Munk scattering coefficients $S = 3\,s(1 - g)\,/4$ are given in Table 7.2

Table 7.2 Scattering cross section, C_{sca}, linear scattering coefficient, *s*, asymmetry parameter, *g*, and Kubelka-Munk scattering coefficient, *S*, due to scattering by prisms in sound bovine enamel

λ (nm)	C_{sca} (m^2)	*s* (mm^{-1})	*g*	*S* (mm^{-1})
380	2.4×10^{-12}	0.15	0.999	1.2×10^{-4}
400	2.2×10^{-12}	0.13	0.999	1.2×10^{-4}
500	1.3×10^{-12}	0.080	0.998	1.1×10^{-4}
600	8.5×10^{-13}	0.053	0.998	9.4×10^{-5}
680	6.5×10^{-13}	0.040	0.997	8.7×10^{-5}

Appendix 7.5 Differences between scattering measurements on sound and carious enamel.

In case of sound enamel we measured the single scattering angular intensity function (Zijp and ten Bosch, 1995) while the samples were immersed in a refractive index matching liquid to reduce the influence of surface roughness. We tried to do the same with the demineralized samples, but the pores within this material were so large that the matching liquid diffused into the samples. This caused refractive index matching between the remaining crystallites and their environment, and so, decrease of scattering. We observed that the carious slabs became more clear than sound slabs within 10 minutes after immersion in the refractive index matching liquid.

We are not able to prepare large slabs of carious enamel that are thin enough to show single scattering. That is why we prepared large sound enamel slabs. These slabs were demineralized from one side, and we measured the reflectance of these slabs. The slabs were considered as consisting of two layers: a sound layer and a demineralized layer, each layer was considered to be homogeneous.

Appendix 7.6 Determination of the wavelength dependence of the values of *S*.

The Kubelka-Munk scattering coefficient *S*, which is proportional to the reduced scattering coefficient $s' = s\,(1 - g)$ can be calculated exactly for spherical scatterers. For small spheres with radius $a << l$, *S* is proportional to l^{-4}. For spheres with radius $a >> l$, *S* is proportional to $l^{-0.37}$ (Graaff *et al.*, 1992).

We divided the measured *S* values into three groups: the sound values, those found after 24 - 204 hours of demineralization, and those found after 495 - 564 hours of demineralization. For each of these groups we averaged the values of log(*S*), and plotted these

as a function of log(l). From these curves, shown in Figure 7.4, we determined the slope at the wavelength range 400 - 510 nm. In case of the sound enamel we found a slope of -4.0. For the 24 - 204 hours demineralization group we found a slope of -3.5. Both these values demonstrate that we are dealing with scattering by structures much smaller than the wavelength. So we may conclude that small structures, as the mineral crystals, are the most important scatterers when multiple scattering is considered.

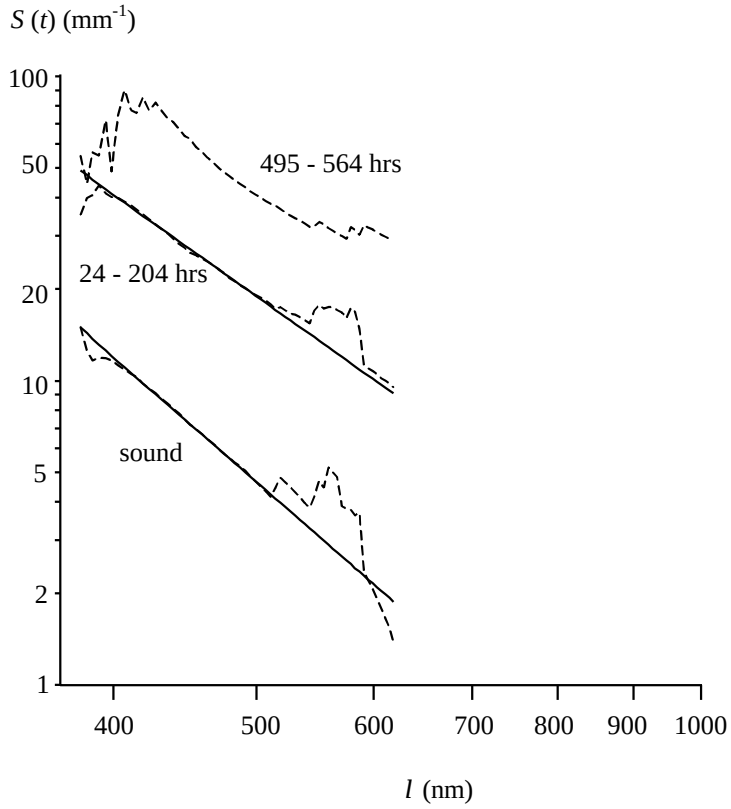

Figure 7.4 Averaged S values (dashed lines) of the three groups of lesion material as a function of the wavelength, on a log-log scale. The full lines show the slope found for the 400 - 510 nm wavelength range.

Chapter 8 **General discussion**

8.1 RETROSPECT

The aim of our research was to determine the optical properties of dental tissues, and to explain the relations between the optical properties of dental tissues and the structures present, especially those of human origin. At the time we started our research more work had been done on fluorescence and phosphorescence properties of dental tissues than on their light absorption and scattering properties. We concentrated on the scattering properties for visible light, because the scattering coefficients are much larger than the absorption coefficients in dental tissues. We developed models, which helped us to explain the scattering properties.

8.2 DENTINE

We showed that in dentine the tubules are the most important scatterers. The collagen fibrils play only a minor role, and the mineral crystals do not contribute significantly to the scattering process. The number of tubules along a straight line perpendicular to these tubules is of the same order of magnitude as the linear scattering coefficient. This supports our conclusion that the tubules are the most important scatterers.

In the discussion section of Chapter 4 we calculated values of the Kubelka-Munk scattering coefficient *S*, that were much higher than those measured earlier in Chapter 3. We calculated the *S* values using a measured *s* and an asymmetry parameter *g* from Table 4.1. These asymmetry parameters were calculated from measurements. The latter were performed in the plane parallel to the tubules. The tubules therefore did not contribute to scattering. Thus the reported *g*-value was due only to randomly oriented structures, such as the collagen fibrils and the mineral crystals. Its value is much lower than the *g*-value for the whole scattering process, in which the tubules, having a higher *g* value, play a large role. As the Kubelka-Munk scattering coefficient *S* represents the whole scattering process, we should incorporate also the scattering by tubules. It is hard to give an overall value for *g* to be used, because scattering by the tubules is mainly, but not solely, in the plane perpendicular to the tubules. It is obvious that this *g* value is higher, and so, incorporating this value in the calculations leads to lower value of *S*. This may explain the large difference between the calculated values (52 mm^{-1}) and the measured values (3 - 8 mm^{-1}). As a consequence we also have to reconsider our recommendation (Chapter 4) that material mimicking dentine should have a low asymmetry parameter.

We wanted to measure scattering of light independently for two linear polarisation directions with respect to the tubular direction, *i.e.* in planes parallel and perpendicular to the tubules. We performed these measurements with an incident beam that was linearly polarised in a direction that made an angle of 45° with respect to the scattering plane. In this case incident radiation can be dissected in parallel and perpendicular components. We aimed to measure the scattered radiation from these components separately. Progressing insight learned us that cross polarisation takes place, and so, we were not able to measure these scattered components independently. Cross polarisation is the effect that some parallel polarised incident light is scattered as perpendicularly polarised light, and some perpendicularly polarised light is scattered as parallel polarised. This effect occurs when the scatterer is not symmetrical with respect to the scattering plane, like in our case randomly oriented crystals and collagen fibres.

The Kubelka-Munk absorption coefficient K of human dentine is about 1.2 mm^{-1} at 400 nm (Figure 4.1). This value is about four times higher than the value measured from bovine enamel by Spitzer and ten Bosch (1975). The protein content of bovine enamel is about 0.06 % (Glimcher *et al*., 1965) and the noncollagenous protein content in human dentin is about 2.5 %.

8.3 ENAMEL

8.3.1 Sound enamel

We observed that sound dental enamel slabs are blueish when observed in reflection and yellowish when observed in transmission (Chapter 6). From this we concluded that the scattering by mineral crystals plays a considerable role in the light scattering processes. From our observation (Chapter 7) that the Kubelka-Munk scattering coefficient *S* showed strong wavelength dependence, we concluded that the mineral crystals are the most important scatterers when multiple scattering is observed.

This seems to be in contradiction with the calculated linear scattering coefficients (Chapter 6), because the coefficient for scattering by prisms ($s_p = 5.8\ mm^{-1}$) is much larger than the coefficient for scattering by crystals ($s_c = 0.94\ mm^{-1}$). The fundamental difference is that scattering by prisms is on average a scattering at small angles ($g \approx 1$), while scattering on crystals is mostly at much larger angles ($g \approx 0$). This causes that light scattered by crystals contributes more to reflection than light scattered by prisms.

The models presented in Chapter 6 and 7 contain refractive indices which are calculated with an apparently accuracy of three decimals. However, these values are not very accurate. In these model calculations for scattering the differences between refractive index values are much more important than the values themselves. Moreover, it is not suitable to speak about *the* refractive index of dental enamel. The density of human enamel decreases from the surface of the tooth ($r \approx 3.01 - 2.98 \times 10^3\ kg/m^3$) inward ($r \approx 2.88 - 2.85 \times 10^3\ kg/m^3$) (Weatherell and Robinson, 1973). These density variations will cause a variation in the refractive index of about 0.02 with respect to its value of about 1.62. This variation is much larger than some differences in refractive indices of the structures present (*e.g.* Appendix 6.1, $\bar{n}_{prism} = 1.619$, $\bar{n}_{enamel} = 1.616$). Small variations in the differences of the refractive indices, result in large variations in calculated scattering coefficients. Using varying refractive indices in the models taught us that scattering coefficient variations of a factor 3 are reasonable.

8.3.2 Carious enamel

In carious enamel the differences in refractive indices of the structures present are increased, resulting in much higher scattering coefficients than in sound enamel. Our model (Chapter 7) for sound bovine enamel shows that both the linear and the Kubelka-Munk scattering coefficients for scattering by crystals are orders of magnitudes larger than those for scattering by prisms. Increase of the refractive index differences as caused by caries will raise the coefficient for scattering by crystals with a factor of about 3. For prisms in carious enamel, the conditions for application of Rayleigh-Gans theory are not fulfilled. That is why we were not able to estimate the coefficient for scattering by prisms in carious enamel. The observation that the Kubelka-Munk scattering coefficient is strongly dependent on the

wavelength indicates that the crystals are the most important scatterers in carious bovine enamel.
But we can also hang on to quite another explanation. Firstly, we observed a very fast (during the first 24 hours) increase of the scattering coefficient. The only very fast process occurring is demineralisation of the interprismatic area. Secondly, this increased scattering coefficient is highly dependent on the wavelength ($\sim l^{-4}$) and so due to small structures. Combination of these two observations may indicate that small structures are becoming important scatterers in the interprismatic area. Probably small pores are formed in this area and act as these small scatterers. As light scattering is caused by differences in refractive index, it does not matter whether the scatterers have a higher or a lower refractive index than their environment. One could compare this with scattering clouds (the water drops having a higher refractive index than their environment of air) and lather (air bubbles having a lower refractive index than the surrounding water). So, by observing the wavelength dependence of scattering we can not distinguish between mineral crystals (having a higher refractive index) or pores (having a lower refractive index). This theory, of a fast pore forming process, is supported by the fact that the electrical impedance measured with an electrical caries meter drops dramatically once the enamel is getting a little carious.
The increase of the absorption as observed in carious enamel may be due to cross talk within the calculations, but may also be caused by the change of the chemical environment of the proteins. Because the demineralisation was performed in a colourless gel and no other dye could penetrate into the demineralised enamel the proteins are the most likely absorbers. The environment of the protein molecules determines their conformation, and so may change the excitation levels of the chromophores and thus their absorption behaviour.

8.4 LOOKING AHEAD

After our research some aspects of the optical properties of enamel and dentine are more or less known. We particularly looked for the origin of the scattering properties. We have presented data for sound dentine and enamel, and carious enamel. However, the data for carious enamel is based on bovine enamel only. Since the structure of bovine enamel is not exactly the same as the structure of human enamel, and structures have shown to be important in scattering, further investigations using human enamel are indicated.
For explanation of the absorption we need to know the chromophores at visible wavelengths present in these materials. These chromophores are not yet known. The proteins present in enamel and dentine are colourless, so they are not considered as the most likely absorbers of visible light. Sometimes it is suggested that remains of cells that were active during the formation of dental hard materials are present in the mature material, and cause some absorption. Sometimes it is suggested that remains of blood, *e.g.* iron ions, are the cause of the colour of teeth. Bleaching of discoloured teeth is done by application of peroxides, this indicates that the chromophores are organic substances. Investigation of these substances and their relation with the optical properties may be a challenge for the future.
When teeth become older their colour will change, teeth from elder people are on average more yellow than teeth from younger ones. Firstly, it is believed that dyes from food, drinks, and the use of tobacco diffuse into enamel causing some discolouration. Secondly, during its maturation enamel may become more homogeneous. Less inhomogeneities causes less light scattering and an increased translucency of the enamel. This is observed as a relative higher absorption, and so a more saturated colour of the enamel. The increased transparency of enamel also may cause that a larger part of the observed light is reflected by the more

coloured dentine. The relationship between the scattering and absorption coefficients and age are therefore interesting subjects to further investigations.
The interest in the causes of fluorescence is growing. It is not exactly known which fluorescing molecules are present in dental tissues. Research on this subject is needed to explore the sources of fluorescence.

8.5 CONCLUSION

An overview of the optical properties of dental hard tissues as published by several authors is given in Table 8.1. It is not appropriate to talk about the true values, because biological variation between the values is present and it is hard to estimate systematic errors made during the measurements. The table can be used as a source for mean values to be used.
We prefer to summarise the values from Table 8.1 in a condensed way as *a*, *s*, and *g*, for a wavelength of 550 nm, which is about the middle of the visible wavelength range. One of the problems is that the relations between the Kubelka-Munk coefficients and the linear coefficients are not known exactly. For bovine dentine we estimate *a* to be 0.20 ± 0.10 mm^{-1} and *s* to be 200 ± 50 mm^{-1}. The large variation of *s* reflects an actual variation with the place in the tooth.
For bovine enamel we estimate *a* as 0.05 ± 0.03 mm^{-1} and *s* as 17 ± 12 mm^{-1}. Here the *s* value is very uncertain because *g* is unknown, we expect *g* to lie somewhere between 0.8 and 0.0. For carious bovine enamel we estimate *a* to be 0.25 ± 0.05 mm^{-1} and *s* as 30 ± 7 mm^{-1}.
For the human dentine we estimate the values *a* as 0.3 ± 0.3 mm^{-1} and *s* as 120 ± 60 mm^{-1}, *s* depends on the place in the tooth. For human enamel *a* is smaller than 1 mm^{-1} and *s* is about 10 ± 3 mm^{-1}. For carious human enamel we only know the calculated value of *s* to be about 55 mm^{-1}.

8.6 REFERENCES

Fried D, Glena RE, Featherstone JDB, Seka W (1995). Nature of light scattering in dental enamel and dentin at visible and near-infrared wavelengths. *Appl Opt* 34:1278-1285.

Glimcher MJ, Friberg UA, Levine PT (1965) The isolation and amino-acid composition of the enamel proteins of erupted bovine teeth. In: *Tooth enamel* (MV Stack, RW Fearnhead, eds, John Wright, Bristol), pp. 63-73.

Groenhuis RAJ, ten Bosch JJ, Ferwerda HA (1981) Scattering of light by dental enamel: theoretical model compared with experimens. In: *Scattering and absorption of turbid materials, especially dental enamel* (Groenhuis RAJ, dissertation, University of Groningen, Groningen, The Netherlands)

Spitzer D, ten Bosch JJ (1975). The absorption and scattering of light in bovine and human dental enamel. *Calcif Tissue Res* 17:129-137.

Vaarkamp J, ten Bosch JJ, Verdonschot EH (1995). Propagation of light through human dental enamel and dentine. *Caries Res* 29:8-13.

Weatherell JA, Robinson C (1973) The inorganic composition of teeth. In: *Biological Mineralization* (I. Zipkin ed., John Wiley & Sons, New York), pp. 43-74.

Table 8.1 Values of the optical properties of dental hard tissues

Quantity	λ (nm)	a (mm^{-1})	s (mm^{-1})	g	m_t (mm^{-1})	K (mm^{-1})	S (mm^{-1})
Bovine dentine	500		200[4]			0.32[3]	6[3]
Bovine enamel	400					0.23[1]	8[1]
	550					0.15[1]	3[1]
	700					0.17[1]	0.5[1]
	400					0.53[7]	12[7]
	550					0.042[7]	4.4[7]
	680					0.019[7]	0.063[7]
	500		10[2]				
	600		7.0[2]				
	700		5.5[2]				
Carious bovine enamel	400					1.5[7]	40[7]
	550					0.47	18[7]
	680					0.25[7]	3.2[7]
Human dentine	500		120[4]			0.6[3]	15[3]
Human enamel	400					0.32[1]	6.8[1]
	550					0.17[1]	2.8[1]
	700					0.17[1]	1[1]
	633			0.68[5]			
	633		6.6[6]	0.68[6]			
	594			0.68[6]			
	543			0.74[6]			
	534	<1[8]	10.5[8]	0.24[8]	10.5[8]		
	632	<1[8]	6.0[8]	0.46[8]	6.0[8]		
	1053	<1[8]	1.5[8]	0.46[8]	1.8[8]		
	500		4.5[2]				
	600		3.3[2]				
	700		2.7[2]				
Carious human enamel	600		55[2*]				

[1] Spitzer and ten Bosch, 1975
[2] Groenhuis *et al.*, 1981, [2*] only calculated
[3] Chapter 3
[4] Chapter 4
[5] Vaarkamp *et al.*, 1995
[6] Chapter 6
[7] Chapter 7
[8] Fried *et al.*, 1995

Chapter 9 **Summary**

9.1 Summary

Chapter 1 gives an introduction on the importance of the optical properties of dental tissues for the phenomena we see in our daily life, and optical phenomena that can be measured for dental care. It contains a review of previous and contemporal research on optical properties of dental tissues. Mutual relations between data found by other investigators are discussed.

The first part of Chapter 2 describes the instrumentation used for measurement of the optical properties of dental materials. It gives considerations for using or not using certain techniques for specific measurements. The second part of this chapter describes the calculation of angular intensity functions for scattering of light by spheres and cylinders at perpendicular incidence. This part is meant for those who want to understand exactly which functions are used for calculations in the following chapters.

Chapter 3 describes measurements on the optical properties of crown dentine. The luminescence spectra were taken from the literature. The Kubelka-Munk absorption coefficient (here designated as A, but K is more common) and the Kubelka-Munk scattering coefficient S are determined from 170 μm thick wet sections. Bovine incisors and human premolars were used. Several sections were cut parallel to the labial plane from the same tooth. Diffuse reflection and transmission of these sections were measured at visible wavelengths. Kubelka-Munk theory was used. Transversal microradiography was used to determine the mineral content of each section. For human premolars the absorption coefficient for fluxes A appeared to be wavelength-dependent with a minimum around 550 nm, A increases with the depth in the tooth crown from buccal to lingual. The scattering coefficient for fluxes S only slightly decreases with increasing wavelength. S has a maximum above the pulp, probably due to the higher number of tubules present at this site. It is shown that there exists no relation between the scattering coefficient and the mineral content.

In Chapter 4 the measurements of the angular intensity functions (called phase functions here) of 10 - 20 μm thick sections of bovine and human dentine are described. The sections were optically thin, *i.e.* caused single scattering. All measurements were performed at the 633 nm HeNe-laser wavelength. After some corrections the asymmetry parameters for scattering processes parallel to the tubules were determined as $g = 0.36$ for bovine dentine, and $g = 0.44$ for human dentine. First-order maxima in the angular intensity functions of scattering processes perpendicular to the tubules are measured at 4° (bovine dentine) and 5° (human dentine). The linear scattering coefficient was determined as 200 mm^{-1} (bovine dentine) and 120 mm^{-1} (human dentine), the linear absorption coefficients were 0.35 mm^{-1} (bovine dentine) and 0.60 mm^{-1} (human dentine).

A theoretical model for the scattering of light by dentine is described in Chapter 5. The model that results is a superposition of several scattering contributions, *i.e.*, scattering by mineral crystals, collagenfibrils and dentinal tubules. These tubules are oriented so that they cause an anisotrope scattering process. The angular intensity functions are calculated for planes that are parallel or perpendicular to the plane of the tubules. The shape of the measured intensity function in the plane perpendicular to the tubules and the values of the scattering coefficient can be explained by the presented model. It is pointed out that the tubules are the most important scatterers. The collagen fibrils play a minor role. Scattering by the mineral crystals is negligible. The role of peritubular dentine is not clear from these calculations.

Chapter 6 describes HeNe-laser light scattering by 80 - 100 μm thick human dental enamel slabs. The angular intensity functions were measured, and compared with calculated intensity functions. From these intensity functions the asymmetry parameter was calculated as $g = 0.68$. The linear scattering coefficient was calculated from a model, and measured with collimated transmission. Correspondence between the calculated and measured scattering coefficient of $s = 6.6\ mm^{-1}$ at 633 nm was found. The prisms are the dominant scatterers when scattering is measured by collimated transmission. From the forwardly scattered pattern the interprismatic distance was calculated as 5.4 ± 1.0 μm and the angular distribution of the prisms as 74 ± 11°.
Chapter 7 deals with the measurements on carious bovine enamel. From bovine incisors 300 μm thick slabs were cut parallel to the labial surface. The slabs were diffusely illuminated and the reflections against black and a white backgrounds were measured at visible wavelengths. From these measurements the scattering coefficient for fluxes were calculated. The slabs were demineralised in a lactic acid containing gel. During this process they were removed from the gel several times and their reflectances were measured in the same way as for the sound case. Using Kubelka-Munk theory for a two-layer structure, the Kubelka-Munk coefficients were calculated for carious bovine enamel. From wavelength dependence of the scattering coefficient *S* it is shown that small structures are the dominant scatterers in both the sound and the carious enamel. *S* for carious enamel is about a factor 3 higher than *S* for sound enamel. The absorption coefficient of carious enamel is also increased with respect to the sound tissue.
Chapter 8 is a general discussion on the results and contains proposals for further research. It is concluded that for dentine the tubules are the dominant scatterers. In transmission measurements of thin enamel slabs the prisms are the most important scatterers. In sound and carious enamel the mineral crystals are the dominant scatterers, when backscattered light is observed.

Chapter 10 **Achtergrond en samenvatting**

10.1 ACHTERGROND VAN HET ONDERZOEK

In de westerse wereld is de rol van het individu belangrijk. Mensen willen zelfstandig en onafhankelijk zijn en zich onderscheiden van anderen. Dit staat in schril contrast met de sommige tendensen om uniformiteit en perfectie na te streven. Een van de meest opmerkelijke voorbeelden is de enorme toename van het aantal adolescenten dat de orthodontist bezoekt en beugels draagt teneinde een perfect gebit te verkrijgen. Het lijkt ook steeds minder acceptabel dat mensen verkleurde tanden hebben, of een tandheelkundige restauratie die een andere kleur heeft dan de naast gelegen tanden. Onze aandacht wordt nu eenmaal gevestigd op kleur verschillen, zoals kleurverschillen in het gebit van een gesprekspartner wiens gebit gerestaureerd is na verlies van een tand, bijvoorbeeld na een ongeluk of een caféruzie. Onopvallende restauratie of vervanging is wenselijk, vooral wanneer het de voortanden betreft. Het totale uiterlijk van de restauratie is belangrijk. Dit uiterlijk wordt bepaald door een aantal factoren zoals kleur, doorschijnendheid, vorm en ruwheid van het oppervlak. De ontwikkeling van materialen die kunnen worden gebruikt voor onzichtbare restauraties vereist de kennis van de optische eigenschappen van de natuurlijke tandmaterialen.

Als we naar een voorwerp kijken, zien we meestal een samenspel lichtverstrooiing en -absorptie. Verstrooiing is het fenomeen dat licht van richting verandert. Een glas melk wordt als wit gezien omdat het licht dat op de melk valt in alle richtingen verstrooid wordt en de melk zonder absorptie verlaat. Een glas thee verstrooit geen licht, het licht gaat recht door de vloeistof en daardoor kunnen we er doorheen kijken, we noemen het transparant. Het ziet er bruin uit doordat er absorptie plaats vindt van vooral blauw en groen licht. Doen we melk in de thee dan neemt de verstrooiing toe en verandert de kleur, afhankelijk van hoeveel melk we erbij doen. Kleur is dus een samenspel tussen verstrooiing en absorptie. In de natuurkunde onderscheiden we verstrooiing en absorptie als twee materiaaleigenschappen. Eigenschappen die verantwoordelijk zijn voor hoe wij dingen zien, en dus eigenschappen die bepalen hoe wij onze tanden zien.

In de natuurkunde wordt de kleur van spectraal licht meestal aangeduid met de golflengte. Met behulp van Figuur 10.1 krijgen we een idee van het verband tussen kleur en golflengte. Het aangeven van de golflengte kan belangrijk zijn omdat absorptie en verstrooiing golflengte afhankelijke processen zijn. Dit kunnen we bijvoorbeeld zien in de Figuren 7.2 en 7.3.

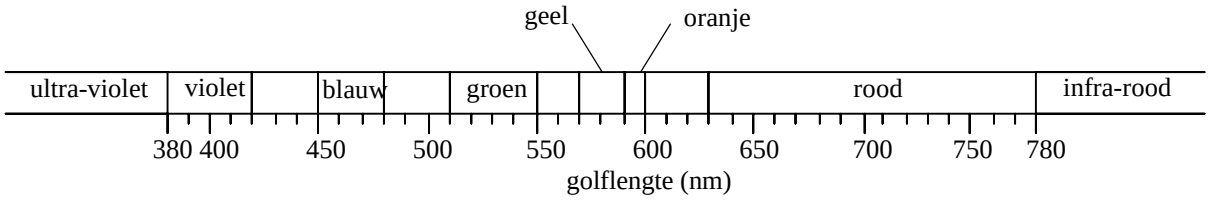

Figuur 10.1 Spectrum van licht en kleuren van spectraallicht. Licht is met een golflengte tussen 380 nm en 780 nm is zichtbaar.

Erg kleine deeltjes, zoals bijvoorbeeld moleculen, verstrooien blauw licht meer dan rood licht. Dit kunnen we dagelijks zien aan de 'blauwe lucht', het blauwe deel van het zonlicht dat de

dampkring binnen treedt wordt verstrooid, terwijl het rode licht meer rechtdoor gaat (Figuur 10.2a). Als we in een vliegtuig op grote hoogte naar boven kijken zien we een diep donker blauwe, bijna zwarte, lucht. Boven ons zijn er dan maar weinig luchtmoleculen die het blauwe licht kunnen verstrooien in de richting van ons oog. Bij een zonsopgang en een zonsondergang legt het licht een grote afstand af door de atmosfeer. Op deze lange weg wordt het blauwe licht verstrooid en het rode licht blijft over, daardoor zien wij zon als rood (Figuur 10.2b).

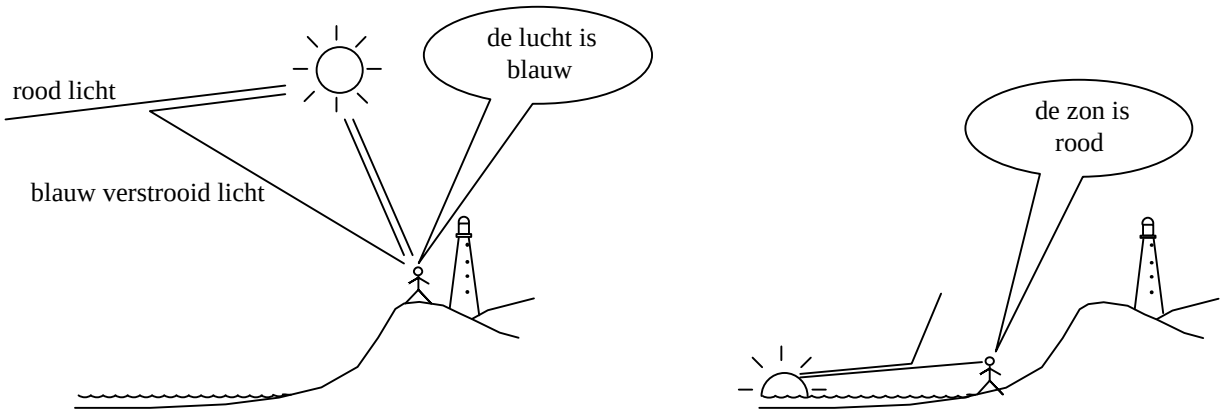

Figuur 10.2 (a) De lucht 'is blauw' doordat de lucht moleculen blauw licht meer verstrooien dan rood licht. (b) Als het licht een lange weg door de atmosfeer aflegt blijft het rode licht over, daardoor zien we een opkomende of ondergaande zon als rood.

Bij grotere deeltjes is het zo dat de verstrooiing niet zo erg afhangt van de golflengte. Mist bestaat uit grotere deeltjes, water druppeltjes, en is daardoor wit.
In tandglazuur wordt blauw licht meer verstrooid dan rood licht. In Figuur 7.3 is dit te zien, de verstrooiings coëfficiënt *S* is bij 380 nm veel groter dan bij 780 nm. Hieruit concluderen we dat het kleine deeltjes zijn die de lichtverstrooiing veroorzaken, de mineraalkristallen in glazuur zijn zulke kleine deeltjes.
Fluorescentie is ook een optisch fenomeen dat we dagelijks zien. Fluorescentie is het fenomeen dat bijvoorbeeld ultraviolet-licht wordt omgezet in zichtbaar licht. Dit zien we optreden in de opvallend oranje strepen op de motoren van de veel gevreesde motoragenten. In discotheken waar 'blacklights' aanwezig zijn lichten witte T-shirts door fluorescentie op, hier wordt ultraviolet-licht omgezet in blauw-paars licht. Ook tanden fluoresceren, het gebit licht in een donker gele kleur onder 'blacklight'-verlichting. Daglicht bevat ook ultraviolet licht, daardoor draagt fluorescentie ook bij tot de kleur van tanden.
We kunnen ons vele dingen afvragen met betrekking tot kleur en uiterlijk van tanden.
Waardoor hebben kinderen met een melkgebit wittere tanden dan volwassenen? Het is bekend dat glazuur van melktanden een lager mineraal gehalte heeft dan het glazuur van het permanente gebit. Misschien dragen poriën in het melktandglazuur bij tot een hogere verstrooiing, waardoor het uiterlijk witter wordt.

Het uiterlijk van voortanden verandert met de tijd. Na het doorbreken is de snijrand erg transparant, het lijkt donker met de donkere mondholte als achtergrond. Na slijtage kijken we tegen een dikkere rand aan die witter lijkt. Verdere slijtage kan eventueel zo'n dikke laag glazuur doen verdwijnen, dat het dentine bloot komt te liggen. Dit dentine is zo poreus dat er kleurstoffen uit voeding, dranken en tabak kunnen binnen dringen. Dit veroorzaakt een verkleuring van de tand.
Tandverkleuring is een algemeen bekend probleem in de tandheelkunde. Vele oorzaken van verkleuring zijn bekend, zoals bacteriegroei, het achterblijven van kleurstoffen uit voedsel, dranken en genotmiddelen, en het gebruik van antibacteriële agentia zoals chloorhexidine en tinfluoride. Het gebruik van tetracycline (dit is een bepaald antibioticum) tijdens de aanleg van dentine kan leiden tot grijze tot zwarte verkleuringen.
Ongelukken kunnen ook een oorzaak van tandverkleuring zijn. Na een ongeluk kunnen tanden dood gaan door beschadiging van de wortelpunt. Bloedresten in de pulpakamer worden afgebroken en onder andere zwart ijzersulfide vormen. Dit diffundeert in het dentine en de tand krijgt een grijze kleur. Avitaal bleken van de pulpakamer met natriumperboraat kan erg effectief werken. Een kleine beschadiging of een lesie die tot vlakbij het dentine reikt kan de aanmaak van extra dentine in gang zetten, de pulpakamer kan zo dichtgroeien, dit heet obliteratie. Deze obliteratie veroorzaakt een verhoogde verstrooiing in de tandkroon, en dus een afname van de doorschijnendheid. Bruine tot gele verkleuringen zijn het gevolg.
Sommige verkleuringen kunnen gedeeltelijk teniet gedaan worden door vitaal bleken. Voor bleken bij de tandarts wordt het tandglazuur eerst aangeëtst, vervolgens wordt een blekende gel, die waterstofperoxide bevat, aangebracht. Het tandvlees moet beschermd worden tegen de hoge concentratie van waterstofperoxide, daardoor is bleken vlakbij het tandvlees met deze methode niet mogelijk. Op deze plaatsen kan de tand eventueel bedekt worden met een troebel materiaal om het geheel een witter uiterlijk te geven. Voor het thuis bleken wordt een milder carbamideperoxide bevattende gel gebruikt. We weten niet precies hoe deze bleekprocessen werken.
Als tanden ouder worden worden ze in het algemeen ook geler. Waarschijnlijk wordt het glazuur minder troebel, dus de lichtverstrooiing neemt af in de tijd. Het licht dat wij zien heeft een langere weg door de tand afgelegd, en daardoor is een groter deel van dat licht geabsorbeerd.Dit geeft een donkerder kleur, maar ook een andere totaalindruk.
Tanden in de mond staan bloot aan een steeds wisselende chemische omgeving. Tijdens een maaltijd zal het gebruik van zuur voedsel en drinken de zuurgraad in de mond verhogen. Dit veroorzaakt het oplossen van een beetje mineraal aan de buitenkant van de tand (demineralisatie). Na de maaltijd zullen de chemische condities zo veranderen dat er weer mineraal neerslaat in de buitenkant van de tand (remineralisatie). Deze processen van de- en remineralisatie gaan altijd door, dag in dag uit, jaar in jaar uit.
Op sommige plaatsen kunnen de zure omstandigheden aanhouden, vooral op die plaatsen waar bacterie adhesie en -groei lijdt tot een biofilm (tandplak) en waar de tandenborstel moeilijk kan komen. De groeven in de tandoppervlakken (fissuren) en vlakken tussen de tanden zijn zulke plaatsen. Op deze plekken zijn zuur producerende bacteriën aanwezig die bij voldoende aanvoer van voedsel (koolhydraten) tot langdurige zure condities aanleiding geven. Daar kan cariës ontstaan, dit is het netto verlies van mineraal uit het glazuur, met als gevolg cariës laesies. In het beginstadium is zo'n carieuze plek te zien als een witte vlek. Sinds het begin van de tandheelkundige zorg wordt deze eigenschap gebruikt om cariës vast te stellen en de ernst ervan te schatten. We denken dat de verhoogde witheid het gevolg is van verhoogde lichtverstrooiing. De oorzaak van deze verhoogde verstrooiing is niet precies bekend.

De carieuze plek kan ook worden bestudeerd met het doorschijnen van licht door de gehele tand, dit heet transilluminatie. Transilluminatie is een veelbelovende techniek voor de detectie en meting van de ernst van carës. Door de verhoogde verstrooiing is de carieuze plek minder transparant, en kan deze gezien worden door een verminderde lichttransmissie. We kunnen deze effecten begrijpen als we de totale lichtverstrooiingsprocessen in gezonde en carieuze tandweefsels kennen.
Een aantal van deze vragen kunnen we oplossen als we meer weten over de optische eigenschappen van tandweefsels. En daar gaat dit proefschrift over.

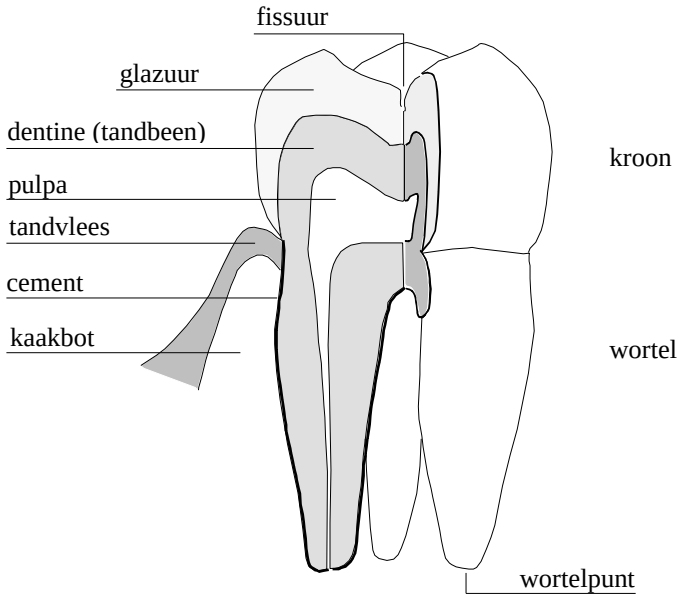

Figuur 10.3 Menselijke kies. De weefsels glazuur en dentine zijn de harde tandweefsels waarvan de optische eigenschappen in dit proefschrift worden behandeld.

Vele kleurverschillen en kleurveranderingen zijn aanwezig of doen zich voor in het gebit dat in de mond zit. De meeste van deze verschijnselen zijn niet volledig bekend. Waardoor is er een systematisch kleurverschil tussen de tanden? Hoektanden zijn bijvoorbeeld geler and de andere voortanden. Wellicht komt dit doordat de dentine laag in hoektanden dikker is dan die in andere tanden. Waardoor wordt de kleur van tanden sterker en geler bij een stijgende leeftijd? Misschien wordt het glazuur homogener door de continue de- en remineralisatie en daalt daardoor de licht verstrooiing en wordt de kleur meer verzadigd. Waardoor hebben oude tanden soms transparant dentine, vooral vlak bij de wortelpunt? Misschien zorgt het continue neerslaan van mineraal in de dentinekanaaltjes er voor dat de kanaaltjes kleiner worden, en dat daardoor hun bijdrage aan lichtverstrooiing afneemt. Waardoor veroorzaakt fluorose verkleuring van het gebit? Milde fluorose kunnen we zien als witte strepen op de tanden, het komt voor bij mensen in gebieden waar het drinkwater een hoog fluoride halte heeft, en bij mensen die teveel fluoridebevattende gebitsbeschermingsmiddelen gebruiken, bijvoorbeeld fluoride-pilletjes èn fluoride tandpasta.

De buitenkant van de tandkroon bestaat uit tandglazuur (Figuur 10.3). De glazuurlaag (1 - 2 mm dik) is het enige deel van een gezonde tand dat in kontakt is met de mondholte. Daardoor ontstaat cariës meestal in het glazuur. Tandglazuur is het hardste weefsel dat in de natuur groeit. Het bevat ongeveer 87 vol% hydroxiapatiet-achtig kristallijn materiaal, 2 vol% organisch materiaal en 11 vol% water. Gezond glazuur is redelijk transparant.
Een tand bestaat voor het grootste gedeelte uit dentine, ook wel tandbeen genoemd. Het is een beenachtig materiaal en bevat ongeveer 48 vol% mineraal, 28 vol% organisch materiaal en 24 vol% water. In het dentine zijn kanaaltjes aanwezig die lopen van de pulpa (tandholte) naar de glazuur-dentinegrens. Hun diameter en aantal hangt af van de plaats in de tand.
De fissuren zijn groeven in de tand oppervlakken. Op het kauwvlak van kiezen komen ze bijelkaar en zit vaak een diepe holte. Deze holte is moeilijk schoon te houden en daardoor ontstaat daar gemakkelijk cariës.
De wortel is bedekt met cement. Als terugtrekking van het tandvlees plaatsvindt komt de cementlaag bloot te liggen. Het cement is vrij zacht en kan gemakkelijk oplossen of weggepoetst worden. Er kan dan gemakkelijk wortelcariës ontstaan.

10.2 SAMENVATTING

Hoofdstuk 1 geeft een inleiding in het belang van de optische eigenschappen van tandweefsels en tandmaterialen voor wat wij dagelijks zien, en het belang van optische eigenschappen die kunnen worden gemeten in de tandheelkundige praktijk. Het bevat tevens een overzicht van eerder gedaan onderzoek en onderzoek dat gelijk tijdig werd uitgevoerd door andere onderzoekers. Onderlinge relaties tussen de gevonden data worden behandeld.
Het eerste deel van Hoofdstuk 2 beschrijft de instrumenten die werden gebruikt voor de metingen van de optische eigenschapppen van de diverse tandmaterialen. Het al of niet gebruiken van bepaalde technieken voor bepaalde metingen wordt beschouwd. Het tweede deel beschrijft de berekeningen van de hoekafhankelijke intensiteitsfuncties voor licht dat verstrooid wordt door bolletjes of cylinders bij loodrechte inval. Dit deel is bedoeld voor diegenen die exact willen weten welke formules werden gebruikt in de daarop volgende hoofdstukken.
Hoofdstuk 3 gaat over de optische eigenschappen van tandbeen (dentine) in de tandkroon. De luminiscentiespectra in de literatuur werden bestudeerd. De Kubelka-Munk absorptiecoëfficiënt (hier aangeduid met *A*, maar *K* is meer gebruikelijk) en de Kubelka-Munk verstrooiingscoëfficiënt *S* werden gemeten aan natte 170 μm dikke plakjes. Rundersnijtanden en menselijke halve kiezen werden gebruikt. Uit elke tand werden werden een aantal plakjes parallel aan het wangvlak gezaagd. De diffuse reflectie en transmissie van de plakjes werd gemeten voor zichtbaar licht. De Kubelka-Munk theorie werd gebruikt. Transversale microradiografie werd gebruikt voor de bepaling van het mineraalgehalte van elk plakje. Voor menselijke halve kiezen bleek de absorptiecoëfficiënt voor lichtflux *A* afhankelijk te zijn van de golflengte met een minimum rond 550 nm. In het materiaal neemt *A* toe van de wangzijde naar de tongzijde. De verstrooiingscoëfficiënt voor lichtflux *S* daalt licht met toenemende golflengte. *S* heeft een maximum boven de tandholte, dit komt waarschijnlijk door de hogere dichtheid aan dentinekanaaltjes op deze plaats in het tandbeen. Er wordt aangetoond dat er geen relatie bestaat tussen de verstrooiingscoëfficiënt en de mineraalconcentratie in het dentine. De literatuur over fluorescentie-eigenschappen vermeld emissie banden bij 350 nm, 400 nm, 450 nm en 520 nm. De chromoforen van de eerste twee banden zijn geïdentificeerd, de andere niet.

In Hoofdstuk 4 worden de hoekafhankelijke intensiteitsfuncties van 10 - 20 μm dikke plakjes runder- en mensdentine beschreven. Deze plakjes waren zo dun dat ze enkelvoudige lichtverstrooiing teweeg brachten. Alle metingen werden uitgevoerd bij met 633 nm HeNe-laserlicht. Na enige correcties werden de asymmetrieparameters voor het verstrooiingsproces parallel aan de kanaaltjes bepaald op $g = 0.36$ voor runderdentine en $g = 0.44$ voor mensdentine. Eerste-orde maxima in de hoekafhankelijke intensiteitsfuncties werden gemeten bij 5° (runderdentine) en 4° (mensdentine). De lineïke verstrooiings coëfficiënt werd bepaald op 200 mm^{-1} (runderdentine) en 120 mm^{-1} (mensdentine), de lineïke absorptiecoëfficiënten waren respectivelijk 0,35 mm^{-1} en 0,60mm^{-1}.
Een theoretisch model voor de lichtverstrooiing aan dentine wordt beschreven in Hoofdstuk 5. Het resulterende model is een superpositie van verschillende verstrooiingsbijdragen, zoals verstrooiing door mineraalkristallen, collageenfibrillen en dentinekanaaltjes. De oriëntatie van deze kanaaltjes veroorzaakt een anisotroop verstrooiingsproces. De hoekafhankelijke intensiteitsfuncties worden berekend in de vlakken parallel aan en loodrecht op de kanaaltjes. De vorm van de gemeten intensiteitsfunctie in het vlak loodrecht op de kanaaltjes en de waarden van de vestrooiingscoëfficiënt kunnen worden verklaard met het model. Er wordt op gewezen dat de kanaaltjes de belangrijkste verstrooiers zijn. De collageenfibrillen zijn minder belangrijke verstrooiers, de verstrooiing door de minerale kristallen is verwaarloosbaar. De rol van peritubulair dentine komt uit deze berekeningen niet naar voren.
Hoofdstuk 6 beschrijft de HeNe-laserlicht verstrooiing door 80 - 100 μm dikke plakjes menselijk tandglazuur. De hoekafhankelijke intensiteitsfuncties werden gemeten en vergeleken met berekende functies, de berekende en gemeten verstrooiingscoefficienten stemden overeen. De asymmetrieparameter werd bepaald op $g = 0,68$. De lineïke verstrooiingscoëfficiënt werd berekend met het model en gemeten door gecollimeerde transmissie. Er werd overeenstemming gevonden tussen de berekende en de gemeten waarde van 6,6 mm^{-1}. De prismata zijn de belangrijktse verstrooiers bij de meting van gecollimeerde transmissie. Uit het voorwaarts verstrooide lichtpatroon werd de hart-op-hart afstand tussen de prismata geschat op 5,4 ± 1,0 μm. De prismata liggen niet allemaal in dezelfde richting, ze zijn verdeeld over hoeken van 74 ± 11°.
Hoofdstuk 7 behandelt de metingen aan gezond en carieus runderglazuur. Van rundersnijtanden werden 300 μm dikke plakjes gezaagd, parallel aan het lipvlak. De plakjes werden diffuus belicht. De reflectanties met witte en zwarte achtergronden werden gemeten voor zichtbaar licht. Met Kubelka-Munk theorie werden de verstrooiings coëfficiënten voor lichtflux berekend. De plakjes werden gedemineraliseerd in een melkzuur bevattende gel. Gedurende dit proces werden ze enkele malen uit de gel gehaald en werden de reflectanties gemeten op dezelfde manier als bij gezond glazuur. Gebruikmakend van de Kubelka-Munk theorie voor een dubbellaag werden de absorptie en verstrooiingscoeffiënten van het carieus glazuur bepaald. Uit de golflengteafhankelijkheid van S werd aangetoond dat kleine structuren de belangrijkste lichtverstrooiers zijn, in zowel gezond als carieus glazuur. De verstrooiingscoëfficiënt voor carieus glazuur ligt een factor 3 hoger dan die voor gezond glazuur. De absorptie coëfficiënt is ook hoger in vergelijking met gezond glauur.
Hoofstuk 8 is een algemene beschouwing over het hier gepresenteerde werk en bevat aanbevelingen voor verder onderzoek. We concluderen dat voor dentine de dentinekanaaltjes de belangrijkste verstrooiers zijn. In transmissie metingen van dunne plakjes glazuur zijn de prismata de belangrijkste verstrooiers. In gezond en carieus glazuur zijn de mineraalkristallen de belangrijkste verstrooiers wanneer terugverstrooid licht wordt waargenomen.

List of publications

Publications (first author)

Angular dependence of HeNe-laser light scattering by dentine - J.R. Zijp and J.J. ten Bosch. Archives of Oral Biology, Vol. 34, 283-289, (1991).

Theoretical model for the scattering of light by dentin and comparison with measurements - J.R. Zijp and J.J. ten Bosch. Applied Optics, Vol. 32**,** 411-415, (1993).

Pascal program to perform Mie calculations - J.R. Zijp and J.J. ten Bosch. Optical Engineering, Vol. 32, 1691-1695, (1993).

Angular dependence of HeNe-laser light scattering by dentine, a comparison of experiment and theory - J.R. Zijp and J.J. ten Bosch. In: *Optics in Medicine, Biology and Environmental Research*. G. von Bally and S. Khanna eds. (Elsevier, Amsterdam) 143-145, (1993).

Use of tabulated cumulative density functions to generate pseudorandom numbers obeying specific distributions for Monte Carlo simulations (Techn. Note) - J.R.Zijp and J.J. ten Bosch. Applied Optics, 33**,** 533-534, (1994).

HeNe-Laser light scattering by human dental enamel - J.R. Zijp, J.J. ten Bosch and R.A.J. Groenhuis. Journal of Dental Research, Vol. 74**,** 1891-1898, (1995).

Two dimensional patterns of Fraunhofer diffraction - J.R. Zijp and J.J. ten Bosch. In: *Photon Propagation in Tissues*. B. Chance, D.T. Delpy and G.J. Müller eds. SPIE 2626**,** 113-120, (1996).

Anisotropy of volume-backscattered light - J.R. Zijp and J.J. ten Bosch. Applied Optics, Vol. 36, 1671-1680, (1997).

Light scattering properties of bovine muscle tissue *in vitro*, a comparison of methods - J.R. Zijp and J.J ten Bosch. In: *Photon Propagation in Tissues IV*. D.A. Benabaron, B. Chance, M. Ferrari and M. Kohl eds. SPIE 3566, 143-150, (1998).

Optical properties of bovine muscle tissue *in vitro*; a comparison of methods - J.R. Zijp and J.J. ten Bosch. Physics in Medicine and Biology, Vol. 43, 3065-3081, (1998).

Publications (co-author)

Optical properties of dentin - J.J. ten Bosch and J.R. Zijp, In: *Dentine and dentine reactions in the oral cavity*. A. Thylstrup, S.A. Leach and V. Qvist eds. (IRL Press Ltd, Oxford), 59-65, (1987).

Measurement of color and scattering phenomena of translucent materials - J. Sjollema, Th. den Exter, J.R. Zijp and J.J. ten Bosch. In: *Innovative Optics and Phase Conjugate Optics*. R. Ahlers and T.T. Tschudi, eds. SPIE, Vol. 1500, 177-188, (1991).

Reduced light-scattering properties for mixtures of spherical particles: a simple approximation derived from Mie calculations - R. Graaff, J.G. Aarnoudse, J.R. Zijp, P.M.A. Sloot, F.F.M. de Mul, J. Greve and M.H. Koelink, Applied Optics, Vol. 31, 1370-1376, (1992).

The determination of Kubelka-Munk scattering and absorption coefficients using diffuse illumination - R. Molenaar, J.J. ten Bosch and J.R. Zijp, Applied Optics, Vol. 38, 2068-2077 (1999).

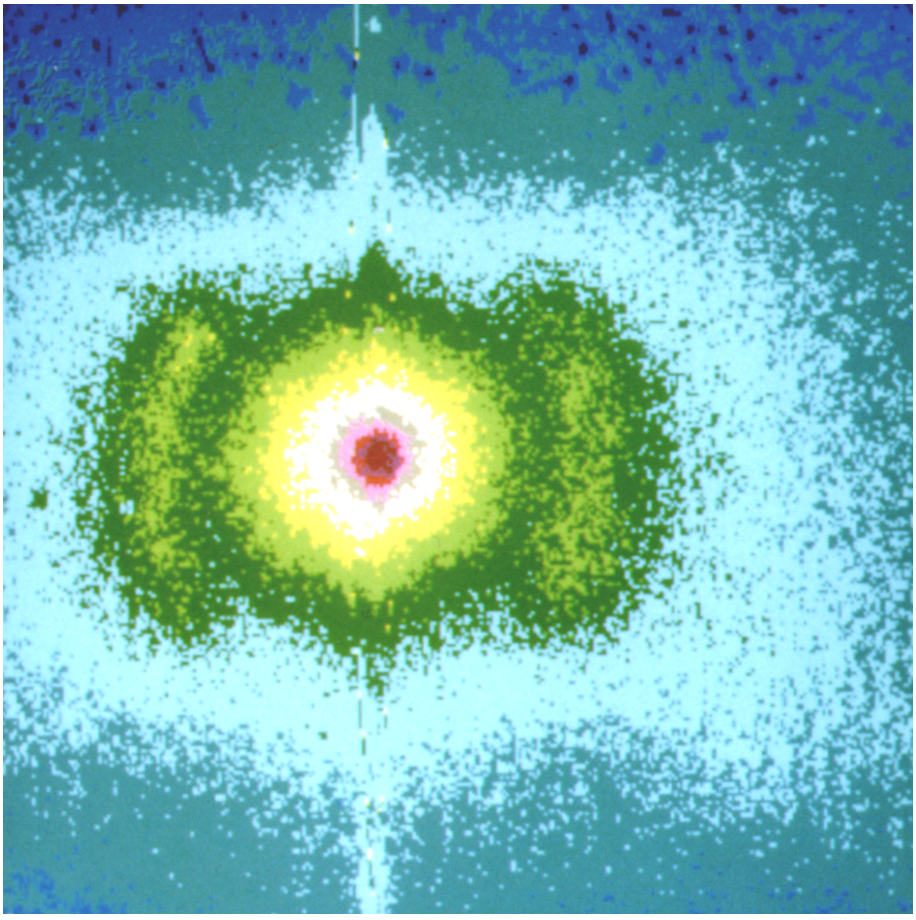

J.R. Zijp **Optical properties of dental hard tissues** 2001